SYNOPTIC CASE STUDY

OF A

WARM CORE TROPICAL DEPRESSION

by

COLLEEN ANN LEARY

S. B., Massachusetts Institute of Technology
1970

SUBMITTED IN PARTIAL FULFILLMENT

OF THE REQUIREMENTS FOR THE

DEGREE OF MASTER OF

SCIENCE

at the

MASSACHUSETTS INSTITUTE OF

TECHNOLOGY

November, 1972 (i.e. Feb. 1973)

Signature of Author .....
Department of Meteorology
November 3, 1972

Certified by .....
Thesis Supervisor

Accepted by .....
Chairman, Departmental Committee
on Graduate Students

Abstract

SYNOPTIC CASE STUDY OF A WARM CORE TROPICAL DEPRESSION

by

Colleen Ann Leary

Submitted to the Department of Meteorology on November 3, 1972 in partial fulfillment of the requirements for the degree of Master of Science.

This thesis is a case study of a warm core tropical depression which passed through the BOMEX data network during the period from July 24 to 26, 1969. Time compositing was selected as the best method of studying the available data. Flow charts, satellite cloud mappings, relative flow charts, humidity charts, and vertical wind shear analyses illustrate the structure of the depression on July 25 and 26. Calculations of divergence and vorticity about the vortex show strong circulation and convergence in the boundary layer. Although the depression possessed a warm core, strong vertical wind shear near the depression and developing anticyclonic flow behind it inhibited further intensification.

Thesis Supervisor: Frederick Sanders
Title: Professor of Meteorology

Table of Contents

1. Introduction

During July 1969, the fourth phase of the Barbados Oceanographic and Meteorological Experiment (BOMEX) collected data with the particular aim of studying tropical convection. Of the storms which passed through the data network, one grew sufficiently intense to be regarded as a tropical depression (Frank, 1970).

This thesis is a case study of that tropical depression, which passed through the network during the period from July 24 to 26. It was chosen for three reasons. First, the storm is perhaps the first tropical depression to be so well observed, on both synoptic and smaller scales. Second, it is an interesting example of a tropical disturbance with a distinct warm core which nevertheless (Palmén and Newton, 1969) did not develop into a hurricane. Third, this storm formed in the ITCZ (intertropical convergence zone) during an unusual northward penetration of the ITCZ.

2. Organization of the case study

The organization and methods of analysis used in this synoptic case study depended upon the types, coverage, and reliability of the meteorological observations. Currently the most complete description and inventory of the BOMEX data is a technical report by de la Moriniere (1972). Although voluminous, the data were

not uniformly distributed with respect to space, time, or quality. Time compositing was selected as the best method of combining the available data so as to minimize limitations of both quality and quantity.

Charts were prepared for the 25th and 26th of July, each with a nominal time of 1200GMT (0800AST). Data taken as far as 12 hours from the nominal time were plotted on the composites, with positions corrected for the movement of the storm. A preliminary examination of aircraft and radiosonde wind data yielded a model of the depression upon which to base the composites. This model consists of a wind shift line separating northeasterly winds to the west from southeasterly winds to the east. The line has an orientation from northeast (035°) to southwest (215°). The wind shift line moves perpendicular to its orientation, from southwest (125°) to northwest (305°) at a constant speed of 10 knots. Observations for other than the nominal times were displaced along a line parallel to the motion of the wind shift line, by an amount proportional to the deviation of the time from 1200GMT and the speed of the storm.

The 25th and 26th of July were chosen because on those days the storm passed through the data network, and appeared most intense on satellite pictures. The region of interest, determined by the position of the storm and the data coverage, extended from 5°N to

20°N, and from 45°W to 70°W.

Data from a variety of sources, all time-composited by this method, form the basis of this study.

3. The flow field in the vicinity of the depression

Tropical pressure gradients are characteristically small, except in intense storms. In particular, this depression never developed an intense low pressure center near the surface, even though it did possess a warm core. The weakness of the pressure gradient and the closeness of the system to the equator made the wind field seem the best representative of the atmospheric flow field. Flow charts were prepared for both the 25th and 26th of July, at four levels: 950mb (figures 1 and 2), 850mb (figures 3 and 4), 700mb (figures 5 and 6), and the upper troposphere (figures 7 and 8). Differences in the sources and formats of observations required a variety of data processing techniques.

Data processing for the 950-mb flow charts

The 950-mb level was chosen as the optimum level to depict the planetary boundary layer. To supplement the available 950-mb wind observations, surface data were included at those locations and times for which surface data, but not 950-mb data, were available. The main source of data was radiosonde winds from the BOMEX ship array, composed of the Oceanographer, Rainier, Rockaway, Mt. Mitchell, and Discoverer (figure 9).

These data came in one or both of two formats. Standard teletype reports of some of the radiosonde launches were transmitted in real time from all of the ships except Mt. Mitchell. From these data, the reported wind nearest the 950-mb level was used. Usually 2000 feet was the closest level. Analog data received and recorded from the radiosonde launches were processed (de la Moriniere, 1972) at 5-second intervals for many of the launches, and were called A_o data. Where both data sets were available, teletype-reported winds were preferred, because they incorporated in real time corrections for ship motion. A_o data contain no such corrections because the ships' logs did not contain accurate navigational information. This shortcoming in seamanship was particularly disastrous because the deep sea anchors, supposed to keep the ships on station, had failed, and the ships were drifting when they were not steaming (de la Moriniere, 1972). Where only A_o data were available, no corrections could be made, and it can only be hoped that the motions were small enough so that the radiosonde winds were not greatly affected. When only A_o winds were available, the 5-second values of the u (west-east) and v (south-north) wind components closest to 950mb were utilized. The winds were converted from components to direction and speed by use of a nomograph.

Soundings were to be taken at the ships every

three hours. Many launches were missed, and surface data, where available, were used to fill the gaps. These were transmitted in the surface ship synoptic code over teletype, or, when a sounding was taken, but winds were not measured, the surface wind was reported with the sounding. On July 25, soundings at the Discoverer showed strong frictional veering at low levels. Between such soundings were times for which only surface winds were available. These were corrected to represent the 950-mb level by comparison with the flanking soundings.

Where neither radiosonde nor surface ship synoptic data were available, boom data were sometimes available. The boom extended 10m beyond the bow of the ship at a height of about 10m, and supported instruments which continuously recorded meteorological and oceanographic parameters, including wind direction and speed. Processed boom data in the form of the 10-minute averages nearest in time to the nominal times for the radiosonde ascents were utilized for the 950-mb flow chart in the absence of other ship wind data. Like the A_o soundings, these data are uncorrected for ship motion.

Surface winds measured by ships not participating in the BOMEX experiment were available from two sources. Working charts, plotted in real time during the BOMEX project, contained some wind reports from ships in the area of interest. These reports suffered from the lack

of a written wind direction and speed, so the direction and speed were subject to errors in plotting. The other source of ship synoptic data was the Northern Hemisphere Data Tabulations, which contain wind observations from surface ships at 1200GMT. These were utilized for the ships in the area of interest.

The Northern Hemisphere Data Tabulations contained another set of useful data. Radiosonde launches at island stations in the Caribbean are tabulated there, and winds are listed at 50-mb intervals, including 950mb.

Special soundings were taken at Barbados at 0600GMT, 1500GMT, 1800GMT, and 2100GMT during the fourth phase of BOMEX. These were transmitted by teletype, and were utilized like the teletyped ship radiosonde reports. Twice daily soundings at Kourou, French Guiana, not reported in the Northern Hemisphere Data Tabulations, were made available by the Environmental Technical Applications Center of the United States Air Force. These also were obtained in the teletype format.

Several aircraft flights through the storm were made in the boundary layer on July 25 and 26. Table 1 lists all the aircraft flights which obtained data used in this study. The NOAA Research Flight Facility "A" plane, flying at an altitude of 1500ft, took measurements of wind speed and direction every second during its flight on July 25 (Friedman, Michie, and McFadden, 1970). Data processed by and obtained from the National Hurricane

Research Laboratory contain averaged winds at 10-second intervals. In this study, averages every 15 minutes were computed from the NHRL data. The procedure consisted of making a 3-minute, 19-point average of the 10-second values, each average centered on a 15-minute value where possible. Sometimes data gaps necessitated a slight departure from the nominal 15-minute intervals. Wind direction and speed were averaged separately. The arithmetic mean of the wind speed values was considered to be the average wind value. For the wind direction, the 19 point values of direction were plotted, and a curve drawn through them. The most representative wind direction was selected by averaging the curve by eye. These 15-minute averages, like the soundings, were corrected in position to correspond to a nominal time of 1200GMT.

Also on July 25, the Woods Hole Oceanographic Institution's C-54Q flew a boundary layer flight at 973mb through the depression (Bunker and Chafee, 1970), measuring meteorological parameters once every minute. For the 950-mb flow chart on July 25, three readings of wind speed and direction at 1-minute intervals were averaged arithmetically at 15-minute intervals of flight time. Wind speed and direction were averaged separately. These, as were all other aircraft observations, were corrected to a nominal time of 1200GMT.

On July 26 the Queenair, a research aircraft from

the National Center for Atmospheric Research, penetrated the storm at a height of 500ft, and collected readings of meteorological parameters every second. These observations were processed and computer-plotted by NCAR. For this study, every 15 minutes a 3-minute centered average was estimated by eye from the plots of wind direction and speed.

Data processing for the 850-mb flow charts

Ship radiosonde observations were treated similarly at 850mb as at 950mb. For the A_o data, the 5-second values of wind components closest to 850mb were converted to wind direction and speed. From the teletype messages, either the 850-mb mandatory level or the closest height level (usually 5000ft) was utilized. When necessary, an observation above 850mb and one below this level were averaged to give a representative wind. Island data from the North American Data Tabulations at the 850-mb level were also used. Island data from Kourou and at non-synoptic times from Barbados were treated the same way as the ship data received in teletype format. On July 26, the RFF "B" plane flew at the 5000-ft level, and the "A" plane flew at the 4000-ft level in the region of interest. Data from these flights was included on the 850-mb chart for July 26. It was processed in the same way as data from the RFF "A" flight at 950mb on July 25.

Data processing for the 700-mb flow charts

At the 700-mb level, data from the North American Data Tabulations, the ship radiosondes, and island data were processed in a manner analogous to that described for the 950-mb and 850-mb flow charts. Aircraft data were available on the 26th, when the RFF "E" plane penetrated the depression at 10,000ft. These data were processed like the other RFF data.

Data processing for the upper tropospheric flow charts

The upper tropospheric flow charts contain data from several levels. This was necessary on account of the scarcity of upper atmospheric data, and because of the rapid changes of wind direction and speed with height in the tropical upper atmosphere, which make information at any one level unrepresentative. Island data came from the North American Data Tabulations and from teletype messages from Kourou and Barbados. Plotted on figures 7 and 8 are winds at the 250-mb and 300-mb levels. Ship radiosonde data often were either not recorded or not processed above 400mb. In some cases, where the A_o data was processed to a level close to but not reaching 300mb, the highest wind observation was plotted on the upper tropospheric flow chart. When available, 250-mb and 300-mb data were both plotted.

On July 25, the Colorado State University Convair 990, flying at about 31,000ft, recorded weather observations

and navigational data. Complete navigational information was tabulated (Cole et al., 1969) at intervals of about 2 minutes. Using an E-6B flight computer, we computed winds graphically from the true air speed, ground speed, ground track, and true heading. Winds were computed at each time when the location of the aircraft, true air speed, ground speed, true heading, and ground track were all available simultaneously. When more than one reading of a parameter was taken during the interval, the average was used. Winds were also computed in real time by Kroupa, the flight navigator, and usually agreed within 30° and 5kt with the computations described above. Our winds were used in preference to Kroupa's because ours matched the navigational information better, and were computed at more frequent intervals of flight time. Since the plane made two nearly parallel traverses of the ITCZ region, winds on the two legs of the flight served as a comparison test for the accuracy of the navigational data. Unfortunately, there existed on both flight legs (flown in nearly opposite directions) an average headwind of 17 knots. It seemed most natural to attribute this headwind to errors in measurement of the true air speed indicator, rather than to a real change in the wind direction and speed from the first to the second flight leg. So further processing of the data was necessary. The fictitious head wind of 17 knots was subtracted from

each of the wind observations. These corrected winds resulted in a much more consistent flow pattern, although some noise was still present in the data, probably due to inaccurate readings of navigational parameters.

Analysis of the flow charts

After the wind directions and speeds were plotted, the fields of motion were analyzed. At the three lower levels, the procedure was straightforward. Isogons were drawn at intervals of 30° in wind direction. Auxiliary line segments of the proper orientation were drawn on the isogons. Streamlines were then drawn parallel to the wind directions of the observations and the isogons. The streamlines on figures 1 through 8 are not intended to depict a mathematical streamfunction, but merely to indicate the wind direction. Isotachs were also drawn, at intervals of 5 knots. At the 950-mb level, the combination of data from a variety of altitudes, including the surface, and the unreliability of some of the surface data, precluded drawing isotachs at distances far from the center of the depression.

In the upper troposphere the procedure was slightly different. Isogons and streamlines were drawn for wind directions which represented a compromise between the 250-mb and 300-mb data, when both were available. Similarly, isotachs were drawn for the average of the 250-mb and 300-mb wind speeds. Otherwise, the analysis

was the same as for the lower levels.

Interpretation of the flow charts

The flow charts in figures 1 through 8 show something of the structure of the depression. The flow at 950mb is important because it is representative of the planetary boundary layer. On both the 25th and 26th of July, the data coverage at 950mb was extensive, especially when supplemented by information at lower levels. Gaps in the data do exist, making some comparisons between the two days difficult or impossible.

On both days the region ahead (west) of the depression experienced relatively undisturbed northeasterly flow. Behind (east of) the depression, the flow patterns show more character, with both northeasterly and southeasterly flow. The depression itself contains a vortex, substantiated on both days by aircraft flights in the boundary layer, in which the winds shifted from northeasterly to southeasterly through west. On neither day were the data sufficient to locate the vortex center more accurately than about one-half degree latitude (30 nautical miles). (In these discussions, distances are often expressed in degrees latitude for convenience in referring to the figures.) One degree of latitude is equivalent to 60 nautical miles or 111 kilometers.

Although the flow patterns, especially in the vicinity of the vortex, are quite similar on the 25th and the 26th,

some features are peculiar to one day or the other. These differences have two possible causes. First, real changes in the flow pattern would produce differences in the analyses. Second, variations in the data coverage could lead to different analyses, depending upon what assumptions are made regarding the regions for which there is no data.

On the 26th, when the data coverage at 950mb was particularly good in the vicinity of the vortex, a wind maximum of 31 knots is located about 1^{o} northeast of the vortex. This is the maximum wind observed in the immediate vicinity of the depression on any of the flow charts. Ahead of the vortex, the flow is somewhat more zonal on the 26th. Real differences between the two flow patterns occur behind the depression. On the 25th, a line of strong confluence extends from slightly north of west to somewhat south of east behind the depression. It does not appear on the analysis of the 26th. Instead, the flow pattern in figure 2 shows anticyclonic curvature of the flow behind the depression. The confluence line of the day before has disappeared, although the streamlines do converge somewhat at the rear of the depression. The anticyclonic curvature has the appearance of a ridge in a wave in the easterly flow. This difference in the nature of the flow patterns is striking, because in the vicinity of the vortex the two patterns can be superposed with amazing consistency. On the

26th, the line connecting the vortex center to the col to the south has inclined to a more east-west orientation, but this may be a figment of the analysis, because there are few observations in this region.

Had the boundary layer data from both days been analyzed together, with the vortex centers superposed, a quite different analysis east of the depression would have resulted. The confluence line observed behind the storm on the 25th would be supported by the northeasterly winds at the Discoverer and Rockaway between 12°N and 15°N on the 26th. A new feature, a line of diffluence, would appear south of the confluence line from the contrast of easterly and slightly southeasterly winds at the Mt. Mitchell and Oceanographer between 5°N and 11°N on the 26th with the much stronger southerly component of the aircraft winds about 2° to the north on the 25th. These two features would dominate the circulation behind the depression, eliminating the anticyclonic ridge in figure 2.

The existence of this alternate interpretation raises an important question about the compositing procedure. That compositing 24 hours of data on one chart works is shown by the ability of the analysis to produce a coherent, relatively simple, flow field. The difficulty arises when comparing two such composites, if they are similar in some respects. When the two data sets considered together produce a different, but

still realistic, flow pattern for the disturbance, one or the other of the interpretations (or perhaps both) must be incorrect. One way to resolve such differences is to compare the implications of the interpretations with the patterns of other features, like cloudiness. Another is to examine the flow at other levels in order to arrive at the most consistent three-dimensional picture of the depression. Combined, these two methods should yield the most reliable explanation.

The flow field at 850mb (figures 3 and 4) represents the flow at a layer somewhat above the atmospheric boundary layer, but still in the lower troposphere. Frictional influences have diminished greatly by this level. A vortex is analyzed on both 850-mb charts. On July 26 this analysis is substantiated by the RFF "B" aircraft flight. Comparable data are not available on the 25th, but since the cyclonic character of the available wind observations in the vicinity of the depression is comparable at 950mb on both days, one can infer that the vortex exists on the 25th at 850mb also. Data coverage on the 25th is sparse in the immediate vicinity of the vortex, and in the region about 3° to 7° behind the vortex, on account of the lack of aircraft flights near this level. In contrast, the data coverage for July 26 at 850mb was particularly good, due to two RFF flights near that level. This was fortunate, in that it provided data in a region of

particular interest, the area east of the depression.

The two days were similar at 850mb in two respects. First, relatively undisturbed flow occurs ahead of the depression from a nearly easterly direction. Second, in the immediate vicinity of the vortex the flow is quite comparable, although this may be due to lack of data on the 25th.

A feature of interest on the 26th, for which comparable data are not available on the 25th, is a wind maximum of 27kt located about one and one-half degrees northeast of the vortex center. This maximum is somewhat weaker than the maximum at 950mb. On the 26th, the analysis in front of the storm at 850mb is somewhat more zonal than on the 25th, but the data are insufficient to make a definite conclusion.

In the region behind the vortex, the aircraft flights on the 26th delineate a distinct anticyclonic ridge about 5° east of the vortex at 850mb. Farther east, about 10° east of the vortex, the wind shifts to west of north, giving the wind field a divergent character, with cyclonic circulation farther east. The anticyclonic circulation east of the trough is consistent with the similar feature observed in the boundary layer. Unfortunately, 850-mb data on the 25th are insufficient to establish a similar comparison for that day, although the observations at the Oceanographer between 6°N and 7°N strongly suggest anticyclonic flow. Ahead

and near the depression, the 850-mb and 950-mb patterns on the 25th are quite comparable. On the 26th, the same is the case, with the added observation that the anticyclonic curvature of the flow is more pronounced at 850mb than at 950mb.

The analysis at 850mb on the 26th lends credence to the idea that the anticyclonic circulation behind the trough is a real feature. Comparing the 950-mb flow on the 25th to the 850-mb flow on the 26th gives a poor match, especially east of the depression where the wind directions often differ by more than 90°. This supports the idea that the structure of the flow field has undergone a real change between the 25th and the 26th. The appearance of the anticyclonic flow east of the depression, with cyclonic flow still farther to the east, is consistent with the approach of a new system from the east, moving at a somewhat faster rate than the speed of the depression, and beginning to affect the circulation near the depression.

Referring to the satellite-observed cloud patterns in figures 10, 11, and 12, one notices that the band of cloudiness extending from west to east behind the vortex center on the 25th is located just north of the confluence line on the 950-mb flow chart for that day. By the 26th at 1246GMT, there is a great reduction of the extent of the cloud band, consistent with the absence of the confluence line in the analyses at 950mb

and 850mb on the 26th. A further clue that the flow field may really be changing with time is the satellite picture for 1600GMT on the 26th, which shows only remnants of the cloud band which was so prominent the day before. At this point it may be concluded that in the lowest levels the circulation changed but little between the 25th and the 26th ahead of and at the depression. Behind the disturbance, this was not the case, and there is strong reason to suspect that there the flow field changed significantly with time.

The flow patterns at 700mb shed further light on the structure of the storm. As at 850mb, the 700-mb chart on the 25th is limited to radiosonde data, and coverage does not extend east of 51°W. In contrast, an RFF flight on the 26th provides extensive coverage at 700mb to supplement the radiosondes. No vortex is analyzed at 700mb on either day. The 25th lacks data in the vicinity of the storm center, but the cyclonic character of the nearest observations is not so strong as at lower levels, so the continued presence of a vortex center to 700mb cannot be reliably assumed. On the 26th, when there was aircraft data in the vicinity of the storm center, the winds did not support the existence of a closed vortex, so no vortex was analyzed on this day either.

On the 25th, an undisturbed current precedes the depression. An interesting feature of the wind pattern

is the maximum wind velocity northwest of the storm, which extends further westward as a band of winds stronger than 25kts. These winds are stronger than the winds in the same region at lower levels. Little can be said about the flow behind the depression, except that observations at the Oceanographer and Kourou between 5°N and 9°N suggest anticyclonic flow there.

The flow pattern of the 26th is of a quite different character. Overall, in the vicinity of the disturbance, the winds are light and variable, particularly those that came from the RFF flight. The wind-measuring system on the aircraft during that flight (APN-153) was less reliable than the system used on the other flights (APN-82). This circumstance, combined with the light and variable nature of the winds, renders them rather noisy. Even with the noisy data, some basic features of the circulation remain. The depression is in an area of cyclonic circulation at 700mb. About 3° east of the depression, the flow is anticyclonic, in keeping with a similar feature at 850mb and 950mb on the same day. Ahead of the depression, there is an area of maximum wind in the northwest corner of figure 6, similar to the one observed at this level on the 25th. Because the winds at 700mb have weakened between the 25th and the 26th, some of the small-scale variability in the vicinity of the depression is probably real.

In the upper troposphere, the flow patterns are

quite different from those at lower levels. On both days, the area of interest is dominated by anticyclonic flow centered near but not on the vortex center. Winds on both days were relatively light (less than 10kt) over the center of the disturbance.

Some differences exist between the two upper tropospheric analyses. On the 25th, a double center of anticyclonic motion is analyzed, one of inflow and one of outflow. The double center is supported by only 2 or 3 observations, so is suspect. The 25th is fortunate for having aircraft data from the Colorado State University Convair 990. This noisy, unreliable, but abundant data set fits most of the radiosonde data. Interestingly, the most variability in this data occurs over the ITCZ, where the depression is located. Some diffluence is analyzed in the vicinity of the ITCZ, consistent both with the data and the notion of outflow at high levels over a tropical depression.

On the 26th, the outflow center has disappeared, and the inflow center is located about 2^{o} west of the 950-mb vortex. No aircraft flew in the upper troposphere on July 26 that produced usable winds, so no mesoscale information could be inferred.

Reservations must be made along with the interpretation of the upper tropospheric flow chart. It is possible that the compositing technique does not apply to the upper troposphere, where systems move somewhat independently

of those at lower altitudes. The general northwest-southeast elongation of the flow pattern may be more a reflection of the compositing technique than of the flow field. Another difficulty is the realization that the upper tropospheric flow charts, in an attempt to picture some average upper tropospheric flow, may be picturing something that doesn't exist at all, considering the great vertical variation in wind that exists at these levels in the tropics.

4. Satellite observations of the depression

During the BOMEX project, meteorological satellites provided photographic coverage of the data network. The ATS III, a synchronous satellite at an altitude of 35,800km, was moved to a subsatellite point of 10°N, 46°W, for the duration of the project. In addition, the ESSA 9, a polar-orbiting satellite, made one pass per day over the BOMEX area at an altitude of about 910 statute miles.

On the 25th, the ATS III provided several pictures, all of rather poor quality, because they were afflicted by a great deal of distortion. On the 26th, the ATS III produced pictures of much higher quality, at a nominal interval of about 13 minutes.

Satellite pictures can be used in two ways. They can be merely looked at to get a general idea of the cloud patterns. This mode requires no processing, and

provides little information. Any more detailed analysis involves accurate mapping of the cloud formations. For this, accurate gridding of the satellite pictures is necessary. BOMAP (Barbados Oceanographic and Meteorological Analysis Project) supplied a set of transparent overlays with a latitude and longitude grid at 5^{o} intervals, along with continental outlines, so that the best match could be determined by aligning the continental boundaries on the grid with the boundaries on the satellite pictures. For the high quality pictures of the 26th, this was possible with a tolerable degree of accuracy, to about 10 nautical miles. On the 25th, the distortion made this procedure impossible. Fortunately, the ESSA 9 pass over the region of interest occurred within minutes of the ATS III photograph at 1803GMT. A recognizable cloud feature, the center of the brightest cloud area, was chosen for reference, and its position accurately determined from the Catalog of Meteorological Satellite Data--ESSA 9 Television Cloud Photography (National Oceanic and Atmospheric Administration, 1969). Then the transparent grid overlay was placed on the ATS III satellite photograph, using this feature as the reference point.

A serious limitation of the BOMAP transparent overlays is the grid size of 5^{o} of latitude and longitude. For an accurate mapping of cloud features, it is necessary to be able to estimate distances as small

as 0.1°. To solve this problem, another grid was constructed. This was an acetate overlay, etched by razor at intervals of 1° of latitude and longitude. Once the BOMAP grid was correctly positioned, this second grid was superposed.

The cloud mappings were constructed by making a free hand rendering of the cloud patterns on a base map, referring to the gridded satellite picture for guidance. The BOMAP grid overlays had a systematic error in the placement of the geographic outlines of about 20 nautical miles. The cloud mappings on the 26th were corrected for this error. On the 25th, when the positioning of the grid was determined relative to the storm, this correction was unnecessary. The cloud mappings were then corrected in position to correspond to the nominal time of 1200GMT, so that they would be compatible with the other data. Three mappings were made, each for a time chosen as characteristic of the depression at an important stage in its development: 1803GMT on July 25, and 1246GMT and 1600GMT on July 26. They are shown in figures 10, 11, and 12, respectively.

The mappings of the satellite cloud pictures are subject to several uncertainties. Because the three pictures mapped were so different in photographic quality, lighting, time, and types of cloud present, they are not, strictly speaking, comparable. Determining the boundary of the cloud was a very subjective process,

and varied even within the same photograph. Also, after all the corrections, some small gridding errors may still be present, although they are probably smaller than 10 nautical miles.

In spite of the difficulties, the three cloud mappings show some interesting features of the storm's development. On the 25th, the ITCZ is displaced northward from its average position, and consists of two connected lines of cloudiness. One is aligned with the 950-mb flow for the same day, along the shear line which contains the vortex. The other extends from northwest to southeast behind the shear line. As discussed above, it is located slightly north of a confluence line at 950mb in the flow field.

On the 26th at 1246GMT the cloud pattern is quite different. Only a suggestion remains of the northwest-southeast cloud band, so prominent the day before. Substantial cloudiness exists along and behind the wind shift line. Much of the cloudiness in the southeast portion of the cloud mass was not present the day before. This is not a solid cloud mass, but is so drawn because the original photograph was not of sufficient quality to resolve the component cloud masses.

By 1600GMT on the 26th, more changes occurred. Figure 12 shows a striking reduction in the cloudy area which appeared on the 1246GMT photograph to the southeast of the vortex center. At the same time,

the northwest-southeast cloud band has all but disappeared. The cloud pattern has several sizeable cloud masses surrounded by regions having little or no cloudiness. About 1° northeast of the vortex center is the center of a bright cloud area which expands greatly later on in the day and becomes the dominant visual feature of the circulation. As discussed earlier, the time evolution of the satellite pictures suggests an evolution of the storm which is corroborated by the differences in the flow fields behind the depression between the 25th and the 26th.

5. The flow field relative to the depression

It is of interest to know the motion of air relative to the storm. Under the assumptions that the storm is a steady state, that it moves with a constant velocity, and that the air motion is horizontal, an analysis of the flow field relative to the storm is also an analysis of the air particle trajectories. So relative motion charts were constructed for the three lowest levels, 950mb, 850mb, and 700mb, on both the 25th and the 26th. In each case, a vector wind from 305° at 10 knots was graphically added to each vector wind observation on the corresponding flow chart. The wind vectors on the resulting six charts were converted to values of wind direction and speed, also graphically. All measurements of wind speed were made to the nearest knot, and wind

directions were measured to the nearest degree. The charts were then analyzed in the same format as shown in the flow charts. The relative flow charts are shown in figures 13 through 18. The flow relative to the storm at 950mb, in figures 13 and 14, is dominated by a cyclonic inflow center less than 1° northeast of the 950-mb vortex on the flow charts in figures 1 and 2. North of the inflow center the relative flow comes from the northeast on both the 25th and the 26th. This flow covers a wide area north of the inflow center from 49°W to 70°W. One portion of this current curves cyclonically as it travels southward and joins the inflow, while about 8° ahead of the depression there is a separation, east of which the air executes an anticyclonic curve. The other current affecting the depression is a southerly one, located to the south of the storm. On the 25th, this flow occupies the area south and west of the storm, from about 50°W to 55°W. On the 26th, the pattern is more complicated, because the northeasterly flow in the region behind the storm acquires a large anticyclonic curvature as it nears the storm, forming a ridge in the relative flow pattern about 3° behind the storm. This feature is not present on the 25th. Much of the southerly inflow on the 25th is part of the southerly current, while on the 26th the southerly inflow has its origin in the northeasterly, anticyclonically curving current. That part of the southerly flow on the 26th due to the southerly current

is confined to a narrow area between 58°W and 61°W, about 10° south of the inflow center. This contrast between the relative flow for the two days is a reflection of the differences in the data and analyses of the 950-mb flow charts in figures 1 and 2.

The patterns of convergence and vorticity must be the same for the relative flow charts as for the flow charts, because the storm's motion was treated as a constant. With the storm's motion eliminated, some features in the divergence and vorticity field stand out more clearly, so are more visible on the relative flow charts. On the 25th, a confluence line extends eastward from the inflow center to about 45°W. This line corresponts almost exactly with the band of cloudiness observed on the satellite cloud photograph for the 25th. The strongest convergence appears to be at the inflow center, with some additional convergence about 2° south of this center.

On the 26th, the anticyclonic ridge behind the depression limits the extent of the convergence there. The convergence line extends only about 3° east of the inflow center. This agrees well with the more limited extent of cloudiness in the area on the satellite pictures of the 26th. Other areas of convergence on the 26th agree well with the cloud representations. A line directed northwest to southeast, about 3° long, is present about 3° west of the inflow center. Another

is located ahead and to the south of the depression. This corresponds particularly well to the satellite observations of extensive cloudiness south of the center of the circulation system at 1600GMT.

At 850mb, the two days show quite similar relative flow patterns in the region for which data exists for both days. As at 950mb, there is an inflow center northeast of the center of the depression surrounded by cyclonic flow. Again, northeasterly flow to the north of the center curves cyclonically and joins the inflow. To the south, there is some contribution to the inflow from a southerly current.

On the 25th, the relative flow at 850mb is remarkably similar to that at 950mb. The sole exception is a marked veering of the wind with height from 950mb to 850mb in the region slightly northeast of the inflow center. The shift in wind direction here is about 90°, and geostrophically would indicate the advection of warm air. This strong veering with height occurs in the cloudy area of the satellite picture in figure 10, and is centered almost exactly on the center of the brightest cloud area, which was used for reference in locating the satellite cloud pattern. It is of interest that the quasi-geostrophic concept of wind veering with height accompanying warm air advection, inferring upward vertical velocity, can find application in a depression so close to the equator.

The 26th had an additional area of data behind the depression. The relative flow behind the storm at 850mb is dominated by a large anticyclone southeast of the main center of inflow. Surprisingly, the anticyclone surrounds a center of inflow. Comparing this picture with that of the 25th, we see a slight suggestion of anticyclonic curvature on that day at about 7°N, 52°W. By the 26th, this tendency is so pronounced that the anticyclonic circulation at 850mb behind the depression is comparable in size to the cyclonic circulation of the storm itself.

Comparing the relative flow at 950mb and 850mb on the 26th produces both similarities and differences. Ahead of the disturbance the northeasterly current is similar on both charts. Behind the inflow center the relative flows are quite different. At 950mb the air entering the center was once part of the northeasterlies, while at 850mb, the inflowing air was part of a southwesterly flow relative to the storm. This difference in origin of air is interesting, because the change takes place within a layer of only 100mb, and represents one of the more radical changes found in this data set that cannot be easily explained by insufficient or incomparable observations.

There are several areas of marked convergence in the relative flow fields at 850mb. On the 25th, the inflow center dominates, along with the area just east

and southeast of it. Two lines of convergence also appear, both oriented from southwest to northeast. One intersects 7°N, 53°W, and the other intersects 12°N, 55°W. On the 26th, the convergence appears to be concentrated along the wind shift line and at the inflow center. The streamlines also converge along a line parallel to the wind shift line and about 2° east of it. The second inflow center is also the scene of convergence. Behind it is a region where the confluence is not great, but the wind speed decreases drastically, causing convergence.

At 700mb, the main similarity of the relative flow charts with each other, and with those at lower levels, is the northeasterly relative flow ahead of the vortex in the undisturbed area. Other than that the patterns are quite different. On the 25th, the inflow center in the relative wind field is located southwest of the vortex center. As at the other levels, the northeasterly current north and ahead of the storm curves cyclonically and enters the inflow center from nearly every direction. A southerly current also supplies cyclonic inflow and circulation around the storm.

On the 26th, the only undisturbed flow is located ahead of the depression. An inflow center is located about 2° northeast of the 950-mb vortex. Surrounding and feeding it is cyclonically curving air. Behind and south of the depression, the flow is anticyclonic. There is marked convergence along a line which extends

from northwest to southeast and changes direction at about 8°N, 55°W to north-south. At this location there is an area of convergence. Interestingly, this is almost directly over the inflow center at 850mb. Perhaps this convergence in the lower troposphere but not the boundary layer accounts for the transient cloudiness on the 26th which disappears by 1603GMT aftering covering a rather extensive area earlier in the day, at 1246GMT.

6. The moisture field in the vicinity of the depression

Processing of relative humidity data

In a warm core tropical depression, latent heat release is a factor of great importance, so it is necessary to keep track of the moisture supply in the storm. Relative humidity charts are a useful way to do this, and are compatible with the format of the BOMEX data. Twelve composites were prepared--one for each day at each of six levels: 950mb, 850mb, 700mb, 500mb, 400mb, and 300mb. These are shown in figures 19 through 30. Each contains data taken over a period of 24 hours, composited with respect to a nominal time of 1200GMT. Data came from the same sources as for the flow charts--the ship and island radiosondes, and aircraft observations. As with the winds, the different data types were processed somewhat differently.

Island radiosonde data from the North American Data Tabulations contain relative humidities at 50-mb intervals. Relative humidities at the appropriate levels were inserted on the composite charts. Ship radiosonde data received in A_o format were processed by selecting the relative humidity value at the level closest to the nominal level. This was never more than 2mb away. Ship radiosonde data received in teletype format required conversion from dew point depression to relative humidity. This was computed for each observation from the temperature sounding plotted on a skew T--log p diagram.

Ship radiosonde data were corrected where necessary for known errors (de la Moriniere, 1972). One occurred whenever a radiometersonde was flown on the same balloon with the humidity sensor. It was corrected by looking at the humidity values nearest the nominal level which were unaffected by the error, and choosing the nearest one. Since the error occurred for only short periods of time, this substitute value appeared to be quite representative, especially if humidity values recorded before and after were consistent. Another error was called frequency doubling (de la Moriniere, 1972). Two methods of correction were possible. The first uses an empirical correction provided by BOMAP. The second, used most often in practice, is the procedure described above for

correcting humidity errors by inspection. All daytime (1200GMT to 2100GMT) radiosonde humidity measurements, from both the ship and island stations, were corrected for a daytime bias induced by the effects of solar radiation on the humidity sensor, which causes the measured relative humidity values to be lower than their real values. This error was corrected by using correction values attributed to Ostapoff (Janota, 1971). Where both A_o and teletype formatted data were available, both were included as a consistency check.

Aircraft data were processed according to the format in which they were received. For each flight, relative humidity data were assigned to the same level to which its wind data were assigned on the flow charts. Research Flight Facility relative humidity data took the form of averaged values once every 10 seconds of flight time. For each 15 minutes of flight time a 3-minute average relative humidity was computed by plotting the 19 10-second values centered on the time of the average and choosing a representative value. The NCAR Queenair flight measured temperature and dew point every second. For each 15 minutes of flight time a 3-minute average temperature and 3-minute average dew point were determined by inspection from the computer-plotted data. From these average values, an average dew point depression was computed, and then converted to a relative humidity by the use of the

skew T--log p diagram. On the WHOI flight, a spot value of relative humidity was read once every minute of flight time. Three consecutive 1-minute readings were averaged to produce a 3-minute average. This procedure was followed once every three minutes of flight time.

After plotting, the data were analyzed by contouring at rather large intervals of relative humidity. The contour intervals were different at the various levels, because their intent was to highlight particularly moist and particularly dry areas. Much more could not be expected from the data, for several reasons. Relative humidity, more than other meteorological parameters, is subject to rather large variations in the horizontal, the vertical, and in time. The averaging of the aircraft data tends to suppress unrepresentative or extreme values, while the spot values from the radiosondes tend to include such values. The differences in processing techniques, along with the varied instruments used, may make the data less consistent than desired, and the approximation of assigning aircraft data to the nearest level must introduce some error.

Interpretation of the relative humidity charts

The boundary layer relative humidity charts of figures 19 and 20 show that on both days the air is uniformly rather moist. The point values of relative humidity vary between 68% and 99%, a somewhat narrower

range than at other levels. Contours are drawn at 80% and 90%, so as to highlight the relatively moist and dry areas. The resulting pattern is mottled, probably reflecting the limits of the accuracy and compatibility of the data. A relatively dry area occurs about 5° behind the depression on both days. The data at this level are so uniform, within the limits of noise, that it would be impossible to delineate the structure of the depression on the basis of the 950-mb relative humidity charts.

By 850mb the picture has changed considerably. Relative humidities vary between 20% and 100% on figures 21 and 22, showing that some areas are markedly drier above the boundary layer. Some of these drier areas are quite close to the disturbance. On both days one dry area was located about 2° northwest of the storm center, and another about 5° southeast of the center. Contours are drawn for 25%, 50%, 75%, and 90% relative humidity. On both days the greatest moisture was observed somewhat northeast of the 950-mb vortex. This was also the case on July 26 at 950mb. From the flow charts, it appears that the region just northeast of the 950-mb vortex is an area of moisture convergence, as the streamlines are confluent and the wind speed decreases along them.

In contrast, the dry areas southeast of the vortex centers on both figures 21 and 22 coincide with

anticyclonic flow at 950mb and 850mb. The dry areas have relative humidities considerably below the average relative humidity of 74% determined by Jordon (1958) for the West Indies area in July at 850mb. Also, at 1803GMT on the 25th and 1600GMT on the 26th, these areas are a good match for the cloudless areas observed by satellite.

At 700mb the relative humidity varies from 10% to 100%, with the average relative humidity somewhat less than at 850mb. Contours are drawn at 25%, 50%, and 75%, delineating the moistest and driest areas. The moistest areas overlie those on the 850-mb charts. Moist bands are aligned with the depression. As at 850-mb, the moistest region lies northeast of the 950-mb vortex. Behind the depression the gradient of relative humidity at 700mb is large. On both days it coincides with the boundary between the cyclonic confluent flow behind the storm and the anticyclonic flow farther east. Between 850mb and 700mb, particularly on the 26th, the relative humidity over the vortex center has decreased, as the maximum has shifted farther behind the wind shift line.

By 500mb, although the relative humidity ranges from 7% to 97%, the background relative humidity has decreased greatly. Contours at 25%, 50%, and 75% outline the moist areas. There is a general increase in relative humidity from northeast to southwest on both charts. On the 25th, a moist band extends along

and somewhat behind the depression. By the 26th, the moist band has fallen farther behind the disturbance, continuing the trend observed at 700mb. In fact, the air at 500mb above the 950-mb vortex center appears to be quite dry. This is probably due to a lack of humidity data near the center, particularly northeast of it, where the most severe convection was reported by the aircraft flight logs. Southwest of the vortex center is another moist area on the 26th.

By 400mb, the drying trend has become considerable, as the contours, again at 25%, 50%, and 75%, show. The range of humidity is still great, from 8% to 95%. On the 25th, the moist band along and behind the depression, observed at lower levels, is still present. On the whole, the moisture pattern on the 25th shows a more pronounced alignment with the depression in the flow field than do the moisture patterns for the next day. On the 26th, the moist area associated with the depression has increased in size, but, like at 500mb and 700mb, has fallen behind the vortex center. Another feature in common with 500mb is the northeast to southwest overall increase in relative humidity.

At 300mb the air is quite dry. Contours are drawn at 25% and 50% relative humidity. Overall, the relative humidity at this level ranges from 10% to only 69%. Part of this apparent drying out from 400mb to 300mb is due to the convention of reporting mixing ratios

with respect to water saturation. At 300mb, where ice saturation is the appropriate consideration, a relative humidity of 69% is close to saturation with respect to ice, because temperatures at 300mb on these days were close to -34°C. On both days there is a fairly large band of moderate humidities located west of 65°W, too far from the depression to be associated with it. One lies to the east of the center, and the other lies to the northwest. On the 26th, a fairly well-defined band of moderate humidities is located about 3° east of the depression.

7. The wind-shear pattern in the vicinity of the depression

Preparation of the wind-shear charts

In addition to the wind field and the relative humidity field, it was desirable to obtain a picture of the temperature structure of the depression. The small magnitude of the temperature variations in the horizontal in the vicinity of the storm (about 3°C) was close to the noise level in the radiosonde data. This noise comes from diurnal variations, the differences between thermometers, and instrument errors. Only the aircraft could provide consistent temperature coverage in the horizontal, and the aircraft flights were not planned in such a way as to assist an analysis of the temperature structure of the storm. Therefore, there will be no mesostructure in any of the shear

charts used to define the temperature structure.

One indirect way of determing the temperature structure involves computing the thickness of the layer of air between two surfaces of constant pressure. Hydrostatically, the thickness of the layer is directly proportional to the mean temperature of the layer. Such thickness charts were constructed from ship and island radiosonde data on the 25th and 26th of July for the layer between 850mb and 300mb. Data were composited in time in the same way as on the flow charts. Unfortunately, these composites were all but useless on account of the inability of the radiosondes to measure temperature accurately enough. They did show an overall increase in thickness (and hence layer-mean temperature) from northeast to southwest in the vicinity of the depression.

Another, and more successful, way to obtain a picture of the depression's thermal structure was by constructing shear charts. The thermal wind relates the shear of the wind with height to the horizontal gradient of temperature. Shear charts were constructed graphically by using the same data analyzed in the flow charts. At each observation the wind vector at the lower level was subtracted from the wind vector at the upper level to provide a vector wind shear in the layer of interest. Three such layers were chosen: from 950mb to 700mb, from 700mb to the upper

troposphere, and from 950mb to the upper troposphere. The upper tropospheric winds were taken from the analyses in figures 7 and 8. The wind vectors were plotted in speed to the nearest knot and in direction to the nearest degree, then subtracted graphically. The shear vectors were then measured to the nearest knot in speed and the nearest degree in direction. This procedure was followed for each of the three layers on each of the two days, giving six time-composited shear charts in all, shown in figures 31 through 36. The justification of this method is the assumption that the wind measurements are more accurate and consistent than temperature measurements.

Interpretation of the wind shear charts

The analyses of wind shear from 950mb to the upper troposphere give some indication of the relative warmth of that entire tropospheric layer. On both days anticyclonic shear, indicating relative warmth, overlies the 950-mb vortex. On the 25th, a ridge of anticyclonic shear occupies the entire area of data coverage east of about 63°W. On the 26th the pattern is anticyclonic over the area of interest, except for west of 66°W and east of about 56°W, where the shear is cyclonic. A cyclonic trough of relative coldness on both days lies about 10° west of the vortex center.

The magnitude of the shear shows large variations from one place to another and from one day to the next. Over the 950-mb vortex center, a 15-knot shear was analyzed on July 25. On the 26th, the shear over the center had become reduced to about 2 knots, although it increases to 10kt within 1° of the center. These shear values are of interest because large shear values over tropical depressions have been claimed to hinder development (Gray, 1968). On July 25 the shear may have been sufficient to hinder development, but by the next day the surface vortex lay close to the location of minimum shear. North of the storm both days show a strong gradient of wind shear, with large values of westerly shear occupying the area between 15° and 20°N. Shear values in excess of 40 knots are observed on both days, with the maximum values to the north of the depression on the 25th, and to the northwest of the depression on the 26th. On the 26th, the direction of motion of the depression is nearly perpendicular to the isotachs of tropospheric wind shear, in the direction toward larger shear values. Since increased wind shear indicates increased ventilation, the storm on that day is moving toward a region possessing a factor which inhibits development. Perhaps this is one reason that the storm did not intensify further.

The wind shear in the lower troposphere is represented by the wind shear in the layer between 950mb and 700mb,

shown in figures 31 and 32. Superficially, the analyses of this shear are quite different on the two days. Upon closer inspection, though, the days are similar in several respects. Anticyclonic shear prevails over the 950mb vortex on both days. West of the depression there is cyclonic shear on both days, and in the extreme northwestern corner of both charts anticyclonic shear is observed. To the rear of the depression, the shear pattern is different on the two days. On the 25th the shear in that region is part of a large anticyclonic ridge in the shear pattern. On the 26th, the shear behind the depression has changed to predominantly cyclonic, indicating relative coolness. This change is consistent with the differences noted in the flow patterns on the two days, from which the shear charts were constructed. Here is another possible indication of the depression's failure to develop further. The narrowing in the lower troposphere of the region of relative warmth from the 25th to the 26th could indicate a change in the temperature field behind the depression acting to inhibit further intensification. On both days, the shear above the 950-mb vortex is about 10 knots, which is close to the overall average for both charts. It must be remembered that the shear data are derived solely from the same radiosonde observations which were inadequate to define, by themselves, a vortical circulation. So the shear

charts are in a sense unaware of the vortex, and cannot be expected to yield detailed information in its vicinity.

The shear in the upper troposphere is represented by the shear from 700mb to the mean upper tropospheric flow, and is shown in figures 33 and 34. As with the other shear charts, the shear on both days is anticyclonic over the 950-mb vortex. So, throughout the troposphere, on both days, relative warmth surrounds the 950-mb vortex center, supporting the assertion that it had a warm core on both days. On the 25th, anticyclonic shear prevails over the entire chart, except for the extreme northwestern corner. On the 26th, areas of cyclonic shear were observed not only in the northwest corner, but also in the southeastern corner of the chart and somewhat to the southwest of the depression. Over the 950-mb vortex center, the upper tropospheric shear was about 13kt on the 25th and about 6kt on the 26th. Large shears were observed north of the depression. Particularly impressive is a shear observation of 52kt on the 26th, in the northwest corner of the chart. On both days the shear increased markedly north of 15°N. The curvature of the shear flow, on the other hand, decreases northward, implying a more uniform and stronger north-south temperature gradient in the trade wind region than in the ITCZ region where the depression is located.

Direct evidence of the warm core nature of the depression is contained in figures 37 and 38. These contain data from the RFF "B" flight and "E" flight, respectively, on July 26. The temperatures plotted are 3-minute averages (19 data points) of 10-second averages. One such average was made every 15 minutes of flight time. The "B" flight flew at an altitude of 5000ft, and the "E" flight flew at an altitude of 10,000ft. The observations were corrected in position to a nominal time of 1200GMT. Both figures 37 and 38 support the existence of a warm core near the center of the circulation in the layer between 850mb and 700mb. An examination of the aircraft data on both the 25th and the 26th failed to reveal a warm core in the boundary layer on either day. This fact is not surprising, because convection would not be expected to enhance boundary layer temperatures.

8. Divergence and vorticity calculations

After the flow charts were made, it appeared desirable to measure the intensity of the storm in some quantitative way. Unfortunately, the limitations of data quality and coverage precluded all but the least refined calculations. Consequently, vorticity and divergence averages over circular areas of selected radius centered on the 950-mb vortex center were selected as the parameters which could be most reliably and most easily

calculated. The basic tools for the calculations were the analyzed flow charts. The computations were made separately for each level and for each day. On each of five circles, eight evenly spaced points were marked off. The circles had radii of 1°, 2°, 3°, 4°, and 5° of latitude at 10°N. At each point a wind vector was drawn, using the flow chart. Then the vectors were decomposed into outward radial and cyclonic tangential components relative to the vortex center. From these components the average vorticity and divergence were computed using the relations:

$$\overline{\nabla \cdot V} = \frac{1}{A}\oint_S V_r \, ds = \frac{2\overline{V_r}}{r} \qquad \overline{\nabla \times V} = \frac{1}{A}\oint_S V_t \, ds = \frac{2\overline{V_t}}{r}$$

where

$\overline{\nabla \cdot V}$	average divergence over the circle
$\overline{\nabla \times V}$	average vorticity over the circle
A	area of the circle
V_r	radial wind component
V_t	tangential wind component
$\overline{V_r}$	average radial wind component over the circle
$\overline{V_t}$	average tangential wind component over the circle.

The integration was performed by assuming that the wind components vary linearly between the selected points. So it was sufficient to obtain the arithmetic means of the components at adjacent points to get

values of $\overline{V_r}$ and $\overline{V_t}$. In order to check the procedure, the same calculations were repeated at a radius of 3° with eight points intermediate with respect to the eight points of the original calculations. The results were the same to within 10%, so it was decided that eight points were sufficient.

Similar computations were performed on wind shear charts for the layer between 950mb and the upper troposphere. The divergence of the wind shear in this layer represents the sum of the convergence in low levels and the divergence in high levels. The divergence of the wind shear gives an estimate of the vertical circulation in the layer. The results are plotted on figures 39, 40, and 41.

These computations were subject to several errors. Because each day and level has different data coverage, the results of different days and levels cannot in some cases be reliably compared. The analyses on the flow charts are highly dependent on the availability of data, so presumably any further analysis derived from them will also. Another liability is the accuracy of the wind measurements, especially when they are subject to uncertainties related to ship motion and aircraft navigation.

In spite of the limitations of the data, some information can be obtained from the calculations of divergence and vorticity. Most of the calculations

go out as far as 5°, but at 850mb and 700mb on July 25, the analysis, and hence the calculations, extended only as far as 4°. Figure 39 is a plot of the results.

Consistently on both days the convergence decreases from 950mb to 850mb, and from 850mb to 700mb, at all distances from the center of the vortex. While part of this decrease could be due to some tilt of the depression in the vertical, it is more likely merely an indication that the most important convergence occurs in the lowest levels, particularly the boundary layer. Variations between the two days in the numerical values are probably not significant, and can be explained by the simplifications of the computing method, and the great differences in data coverage on the two days.

At 950mb, the convergence drops by a factor of two between 1° and 2° distance from the center. It continues to drop out to 5° away from the center. This suggests that not only does most convergence occur at low levels, but that it also occurs rather close to the center of the depression. Above 950mb, the pattern is somewhat more confused, because of limited data coverage on the 25th for 700mb and 850mb, and the light, variable, and sometimes unreliable winds at 700mb on the 26th. At 850mb on the 26th, when the data coverage was good and also reliable, it is interesting to note that the divergence was close to zero at all distances. This

suggests that any important convergence on this day is accomplished in the boundary layer.

In the upper troposphere there is no marked convergence or divergence. This lack of an outflow layer here has several possible explanations. The outflow may occur at a level lower or higher than that represented by the analysis. Or, the analysis may be insufficiently representative of the 250-mb to 300-mb flow to detect a narrow outflow layer in that range. Alternatively, the storm may be insufficiently organized in the vertical to possess a concentrated upper tropospheric outflow layer at all, or it may only possess one on a scale smaller than that detectable with the sparse synoptic data available for this study. These all imply that the analyses of winds in the upper troposphere in figures 7 and 8 are unrepresentative. This observation recalls the diffluence detected in the detailed winds reported by the Convair 990 on July 25.

The divergences computed from the vertical shear in the layer from 950mb to the upper troposphere (figure 40) provide some measure of the vertical circulation over the depression. Convergence in low levels and divergence in the upper troposphere both contribute to positive divergence in the shear field. Positive divergence is measured on both days at all distances from the 950-mb vortex center. The divergence of the shear increases consistently at all distances from

the 25th to the 26th. The increase probably is not significant, due to data and analysis insufficiencies. In fact, it contradicts the divergence data obtained from the individual days in some respects. For example, at 3° from the depression's center, the flow at 950mb becomes more divergent from the 25th to the 26th, while the upper tropospheric flow becomes less divergent. If the shear divergence were an exact measure of this difference, there would be a decrease in the shear divergence at this distance. The opposite is observed, leading to the suspicion that the day-to-day differences are not significant.

Figures 39 and 40 are incompatible for another reason. The wind analyses used to derive figure 39 incorporate aircraft data, which delineate some of the mesoscale detail of the depression. Only radiosonde information was incorporated in the shear charts, from which figure 40 was derived. This difference points up the futility of attempting to study mesoscale structure with only synoptic observations, even in the relatively dense BOMEX network of stations. Aircraft traverses are essential if the mesoscale structure of a depression is to be reconstructed. This is especially important in cases like this one, where the essential nature of the circulation (i.e., the vortex) is mesoscale.

Some features of the vorticity pattern (figure 41) are also interesting to note. Consistently, on both

days and at all five distances from the center, the flow is cyclonic in the three lowest layers and anticyclonic in the upper troposphere. Here, as in the divergence calculations, the differences between days are probably not significant, owing to limitations in the data and technique.

At the three distances closest to the vortex center, the cyclonic circulation decreases with height in the three lower layers, on both days. This represents a decrease in the circulation of the storm, and presumably its intensity, with height. Beyond 3° latitude, as the cyclonic vorticity approaches zero, the differences between levels fall below the limits of accuracy of the computations. At 950mb, this dropoff of cyclonic vorticity with distance is particularly rapid between 1° and 2°, when it falls off by a factor of three. Between 2° and 3°, it falls off by a factor of two. By 5°, it is nearly zero. At 700mb on the 26th, there is almost no cyclonic circulation at any distance. This matches well the featureless divergence results from the same analysis.

At the 850-mb and 700-mb levels, the dropoff in cyclonic vorticity with distance is observed principally close to the storm. Because the vorticity is somewhat smaller to begin with, the values of vorticity approach the noise level more rapidly thanat 950mb.

9. Potential for development of the depression

In several respects, the depression looked like a potential hurricane. It had a warm core, a vortical circulation, and well organized convection. It is interesting then to inquire why the depression did not mature to become a hurricane. Since the theory of hurricane development is incomplete, one way to investigate the question is to compare the characteristics of the depression with empirically derived criteria for development, both as an attempt to discover where the depression fell short and as a test of the criteria.

One relatively complete set of criteria is used by the National Hurricane Center (Simpson, 1972). It consists of two decision ladders (figures 42 and 43), by which tropical disturbances can be tested for their development potential. One decision ladder is intended for tropical waves and weak depressions, called seedlings. The other is intended for strong depressions, storms, and hurricanes, and measures vortex development potential. This storm falls into the latter category, because it has a warm core and a vortical circulation. For completeness it will be tested by both sets of criteria. In comparing this storm to the criteria for development, some difficulties arise where the methods of analyzing the data were different. In some cases this meant that the criteria could not be tested, but in others a useful comparison still could be made.

The first criterion for vortex development potential is determined from a low level chart called an ATOLL chart. The 950-mb charts in figures 1 and 2 were considered equivalent. At this level, $\oint^{4^\circ} V_r \, \partial\theta < 0$ and $\frac{d}{dt} \oint^{4^\circ} V_r \, \partial\theta \leq 0$ are considered favorable conditions for development. From the computations from the determinations of vorticity and divergence, the first condition, that of inflow at a radius of 4° from the vortex center, was met on both days. The second condition, that of increased inflow with time, was also met, but the change was slight, well within the noise level of the computations. These low level observations then, on the whole, imply development.

The next criterion involves vorticity advection at 200mb. Data are insufficient to test it. Then follows a set of criteria concerned with the structure of the vortex. The 700-mb temperature gradient cannot be determined. Another criterion is a decreased radius of the maximum wind. At 950mb, where the depression appears most intense, this is the case when figures 1 and 2 are compared. A reservation must be made about this conclusion, because data on the 25th did not extend as close to the vortex center and its northeast quadrant as on the 26th. The other two criteria, concerned with the angular momentum flux and the gradient of equivalent potential temperature at 300mb, could not be evaluated.

The next set of criteria involve miscellaneous environmental factors. For a forecast of development, a mean mixing ratio of greater than 8 gm kg^{-1} in the layer between 1000mb and 600mb is required. The relative humidity data in figures 19 through 30 is not in a useful form to compare directly to mean mixing ratios, but a rough calculation from soundings and an examination of the relative humidity charts leads to the conclusion that in the vicinity of the vortex center, especially to the northeast of the center, this condition is met on both days. Sea surface temperatures were greater than 26°C in the vicinity of the disturbance on both days (Iwanchuk, 1972). Minimal ventilation can be tested by an examination of the vertical wind shear. Over the 950-mb vortex center, the condition is met on the 26th, with only 2kt of shear in the layer between 950mb and the upper troposphere, but is not met on the 25th, when there was a shear of 15kt. On both days, quite large shears were observed within a few degrees of the vortex center. The regions of large shear appeared to retreat at a speed comparable to the storm's, from the 25th to the 26th. Taken together, the environmental factors favor development.

Feeder bands were not observed on either day, a condition which is considered to hinder rapid development. All taken together, these criteria for development

would probably give the depression a coutious forecast for development. Since that was not the case, it is possible that the comparisons were incomplete. Particularly, the shear over the vortex center may be more unfavorable than appears at first, because the depression, even on the 26th, is quite close to the region of large shears.

The seedling development potential is measured by the other decision ladder, shown in figure 43. Many of the criteria for storm development are the same as those for the vortex development potential.

The first set of conditions deals with the state of the environment. On both days there is a cloud mass to the northeast of the depression center. Also, the mean shear, and therefore presumably the thickness, is above that of the surroundings on both days. So it can be assumed to be above normal, especially since the ITCZ is farther north than normal. As determined earlier, there are no feeder bands emanating from the depression. Similarly, the mean mixing ratio in the layer between 1000mb and 600mb can be assumed to be greater than 8 gm kg^{-1} somewhere in the vicinity of the disturbance, and the sea surface temperature is greater than 26°C. In total, four of the five environmental factors favor development. Only the feeder bands are absent.

The next condition involves the vertical wind

shear within 4° of the center of the depression. To favor development, the shear should be anticyclonic and average less than 10kt. On both days the shear is cyclonic at 4° from the vortex, but the average shear there is considerably larger than 10kt, as can be seen in figures 34 and 35. The failure of this criterion is sufficient to forecast no development on the seedling decision ladder.

The next set of conditions concerns the circulation and inflow characteristics of the storm at low levels. The first requires that $\frac{\partial V_\theta}{\partial r}$ in the direction of the pressure gradient is greater than zero at radii of 2° and 6°. The tangential wind component, calculated when the vorticities and divergences were determined, decreases monotonically from 1° to 5°, so $\frac{\partial V_\theta}{\partial r}$ is less than zero for the available measurements. It seems safe to assume that it will not suddenly increase at a radius of 6°. The alternative to this condition is radial inflow, increasing with time, at a distance of 2°, but it does not increase from the 25th to the 26th. Again, no development is indicated.

As before, there are insufficient data to determine vorticity advection at 200mb. The final condition, that of a cold trough in the mean shear 10° from the depression, is met on both days, as shown by the shear charts in figures 31 and 32. In spite of the fact that this condition favors development, several of the

other criteria are unfavorable, so as a seedling the storm would not be forecast to develop into a hurricane. It is interesting that as a whole the storm matches development criteria better as a vortex than as a seedling. Perhaps this is more a commentary on the structure of the decision ladders and the amount of data than of the storm. Large shear values in the vicinity of the depression appear to be an especially important factor in the failure of this depression to climb the seedling decision ladder.

10. Recommendations for future field experiments

Since BOMEX was the first in a series of large tropical experiments, it seems appropriate to suggest ways in which such a project could better contribute to the understanding of the development of tropical depressions. This study has brought to light several possibilities for improvement.

The upper troposphere is an important component of the atmosphere. During BOMEX, much of the collection and processing of data, particularly ship radiosondes, stopped at 400mb. This seriously limits any inferences about the three-dimensional structure of the storm, particularly the presence of an outflow layer in the upper troposphere.

Along with more complete radiosonde coverage in the vertical, more complete coverage in time is desirable.

As a synoptic framework into which mesoscale observations from aircraft can be integrated, a 3-hour interval between ship radiosonde launches is adequate. That this interval is operationally feasible is shown by some portions of the BOMEX data, where the radiosonde schedule was adhered to. But the BOMEX data set as a whole is remarkable for the volume of missing radiosonde data. Not only do missing observations destroy time continuity in the data, but they also seriously limit spatial coverage on time composites, like those on which this study is based.

Another important feature of radiosonde data is its quality. In middle latitudes, the radiosonde network has long been a mainstay in analysis and forecasting. This experience should be exploited by large tropical experiments to the point where radiosonde operations are of the same quality in the tropics as at weather ships in higher latitudes. Unfortunately, the BOMEX radiosonde operations were of much worse quality than those of the weather ships in middle latitudes. Contributing to the lack of wind data quality at the ships is insufficient navigational data. Since much of the derived information about a disturbance, like trajectories, shears, and computations of vorticity and divergence, comes from wind observations, it is especially important that the winds be determined accurately.

Navigation is also important on aircraft flights. Isolated weather and wind observations are of little use unless the aircraft's position is known. Accurate navigation is also important when it is used to determine winds, as on the Convair 990.

If the development of tropical disturbances is considered important enough to study, the data ought to be as comparable as possible when features at different times are compared. Airplanes flying consistently at the same levels in the same general region relative to the storm could contribute greatly to a consistent data set. Of course, this requires a capability for fast-response, real-time, mission planning. Matched data, in the sense of similar instruments calibrated for comparisons, would reduce the uncertainties of combining data from different flights. Comprehensive flight coverage is an absolute necessity for studying depressions like this one. For example, even if radiosonde launches had been made faithfully, they would have been insufficient to define and locate the vortical circulation this depression possessed.

Satellite pictures could, if processing improved, be more useful in delineating cloudy, and hence moist, areas. Enlargements and accurate gridding to small increments of distance could contribute to both synoptic and mesoscale analyses.

11. Conclusions

This case study has illustrated several features of interest about a tropical depression in the ITCZ. It would be interesting if further studies show to what extent they are typical of such depressions.

1. The depression has a distinct warm core, as evidenced by the aircraft temperature observations in figures 37 and 38, and the shear charts in figures 31 through 36.

2. It has its greatest intensity in the lowest layers of the atmosphere, showing a vortical circulation at both 950mb and 850mb on both days, with maximum winds in the boundary layer (figures 1 through 4, and 41)

3. By 700mb, the intensity of the storm has decreased markedly, especially on July 26 (figures 5, 6, and 41).

4. In the upper atmosphere, anticyclonic flow is present on both the 25th and the 26th (figures 7 and 8) in the vicinity of the depression.

5. By far the greatest convergence associated with the depression occurs in the boundary layer, close to the vortex center (figure 39).

6. In front (west) of the depression, relatively undisturbed northeasterly flow prevails (figures 1 through 6). Likewise, convection occurs mostly at and behind the wind shift line (figures 10 through 12).

7. By empirical standards (figures 42 and 43), and by its failure to produce a pronounced low-pressure center at the surface, the depression would not be forecast to intensify into a hurricane.

8. Large vertical wind shears were observed in the vicinity of the depression on both the 25th and the 26th (figures 31 through 36).

9. The character of the flow field behind (east) of the depression in the lower troposphere changed from the 25th to the 26th (figures 1 through 6, and 13 through 18), becoming markedly anticyclonic. This was reflected in the disappearance of the northwest-southeast cloud band on the 26th, and the presence of cyclonic shear in lower levels (figure 34) behind the depression on the 26th. These changes appear to be influences of a new system approaching the depression from the east, and inhibiting its development.

List of Table and Figures

Table

Figure

22. Relative humidity at 850mb, July 26

23. Relative humidity at 700mb, July 25

24. Relative humidity at 700mb, July 26

25. Relative humidity at 500mb, July 25

26. Relative humidity at 500mb, July 26

27. Relative humidity at 400mb, July 25

28. Relative humidity at 400mb, July 26

29. Relative humidity at 300mb, July 25

30. Relative humidity at 300mb, July 26

31. Wind shear in the layer between 950mb and the upper troposphere, July 25

32. Wind shear in the layer between 950mb and the upper troposphere, July 26

33. Wind shear in the layer between 950mb and 700mb, July 25

34. Wind shear in the layer between 950mb and 700mb, July 26

35. Wind shear in the layer between 700mb and the upper troposphere, July 25

36. Wind shear in the layer between 700mb and the upper troposphere, July 26

37. 5000ft temperatures, July 26

38. 10,000ft temperatures, July 26

39. Divergence profiles

40. Divergence of the shear in the layer between 950mb and the upper troposphere

41. Vorticity profiles

42. Vortex development potential decision ladder

43. Seedling development potential decision ladder

Date	Name	Flight Level
July 25	RFF "A"	1500ft
	WHOI C-54Q	973mb
	CSU Convair 990	31,000ft
July 26	NCAR Queenair	500ft
	RFF "A"	4000ft
	RFF "B"	5000ft
	RFF "E"	10,000ft

Table 1: Aircraft flights on July 25 and 26.

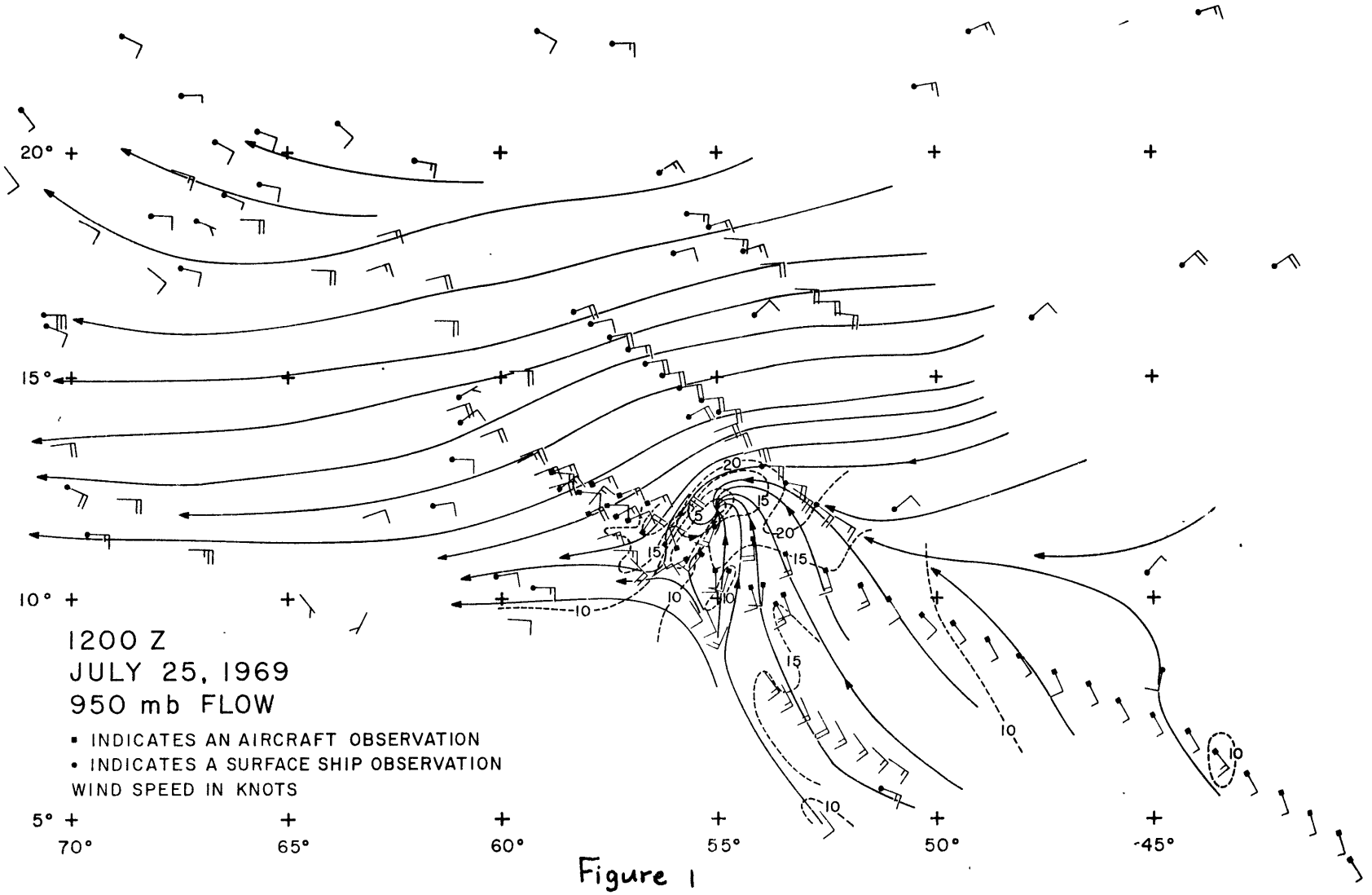
20°
15°
10°
5°
70°
65°
60°
55°
50°
45°
1200 Z
JULY 25, 1969
950 mb FLOW
▪ INDICATES AN AIRCRAFT OBSERVATION
• INDICATES A SURFACE SHIP OBSERVATION
WIND SPEED IN KNOTS

Figure 1

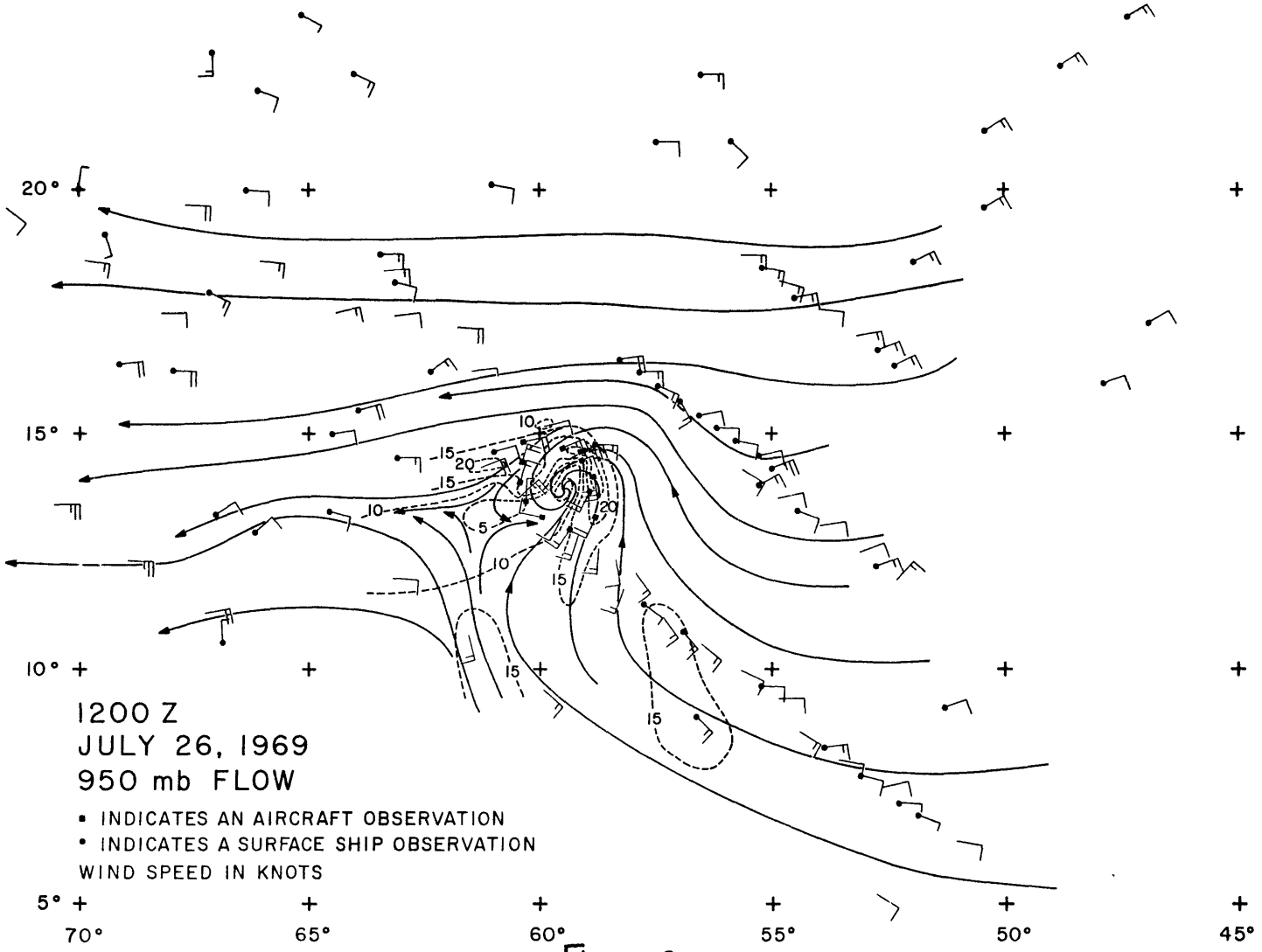
20°
15°
10°
5°
70°
65°
60°
55°
50°
45°
10
15
20
15
10
5
10
15
20
15
15
1200 Z
JULY 26, 1969
950 mb FLOW
▪ INDICATES AN AIRCRAFT OBSERVATION
• INDICATES A SURFACE SHIP OBSERVATION
WIND SPEED IN KNOTS

Figure 2

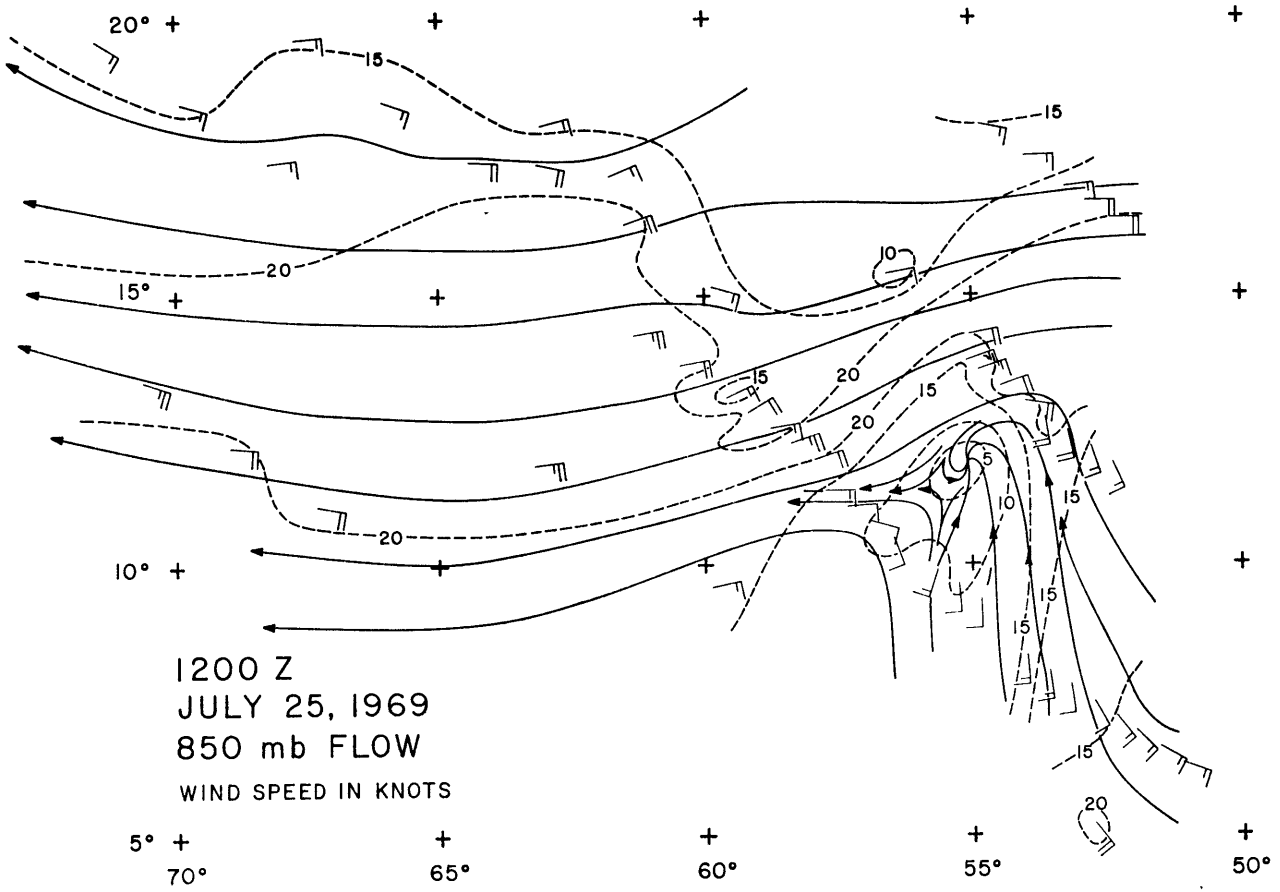
20°
15°
10°
5°
70°
65°
60°
55°
50°
1200 Z
JULY 25, 1969
850 mb FLOW
WIND SPEED IN KNOTS

Figure 3

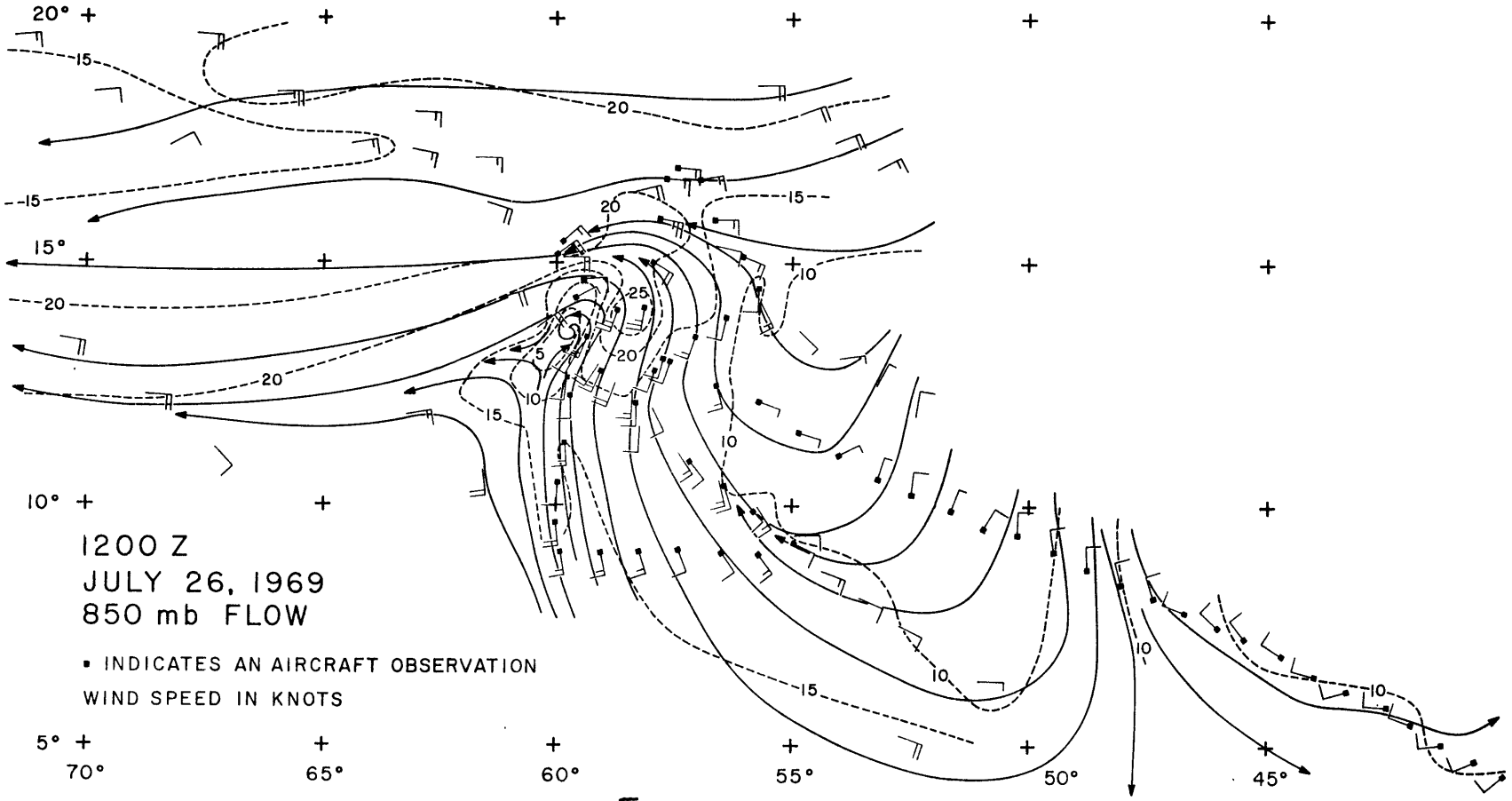
20° + + + + + +
15
20
15
15
20
15° + + + + +
20
25
5
20
20
10
15
10
10° + + + + + +
1200 Z
JULY 26, 1969
850 mb FLOW
• INDICATES AN AIRCRAFT OBSERVATION
WIND SPEED IN KNOTS
15
10
10
10
5° + + + + + +
70°
65°
60°
55°
50°
45°

Figure 4

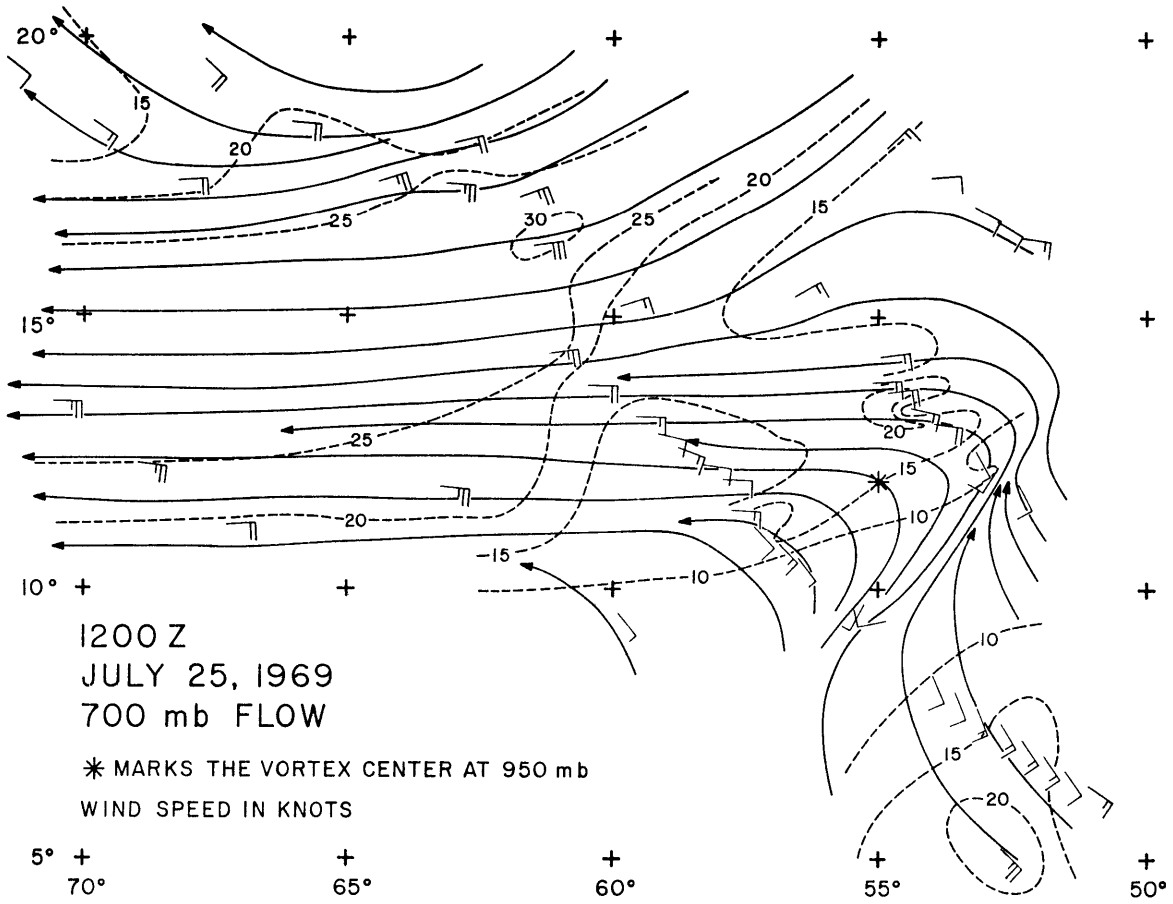
20°
15°
10°
5°
70°
65°
60°
55°
50°
15
20
25
30
1200 Z
JULY 25, 1969
700 mb FLOW
✳ MARKS THE VORTEX CENTER AT 950 mb
WIND SPEED IN KNOTS

Figure 5

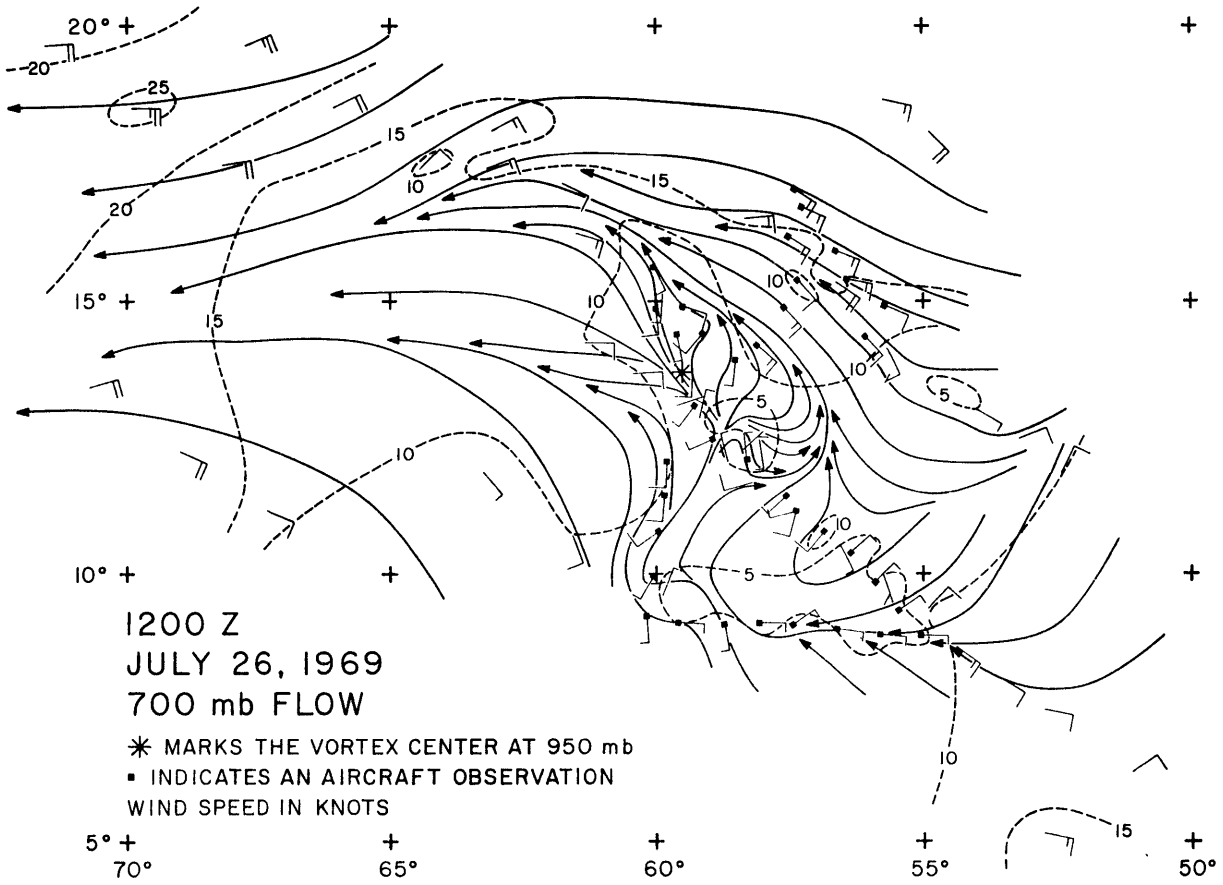
20° +
15° +
10° +
5° +
70°
65°
60°
55°
50°
1200 Z
JULY 26, 1969
700 mb FLOW
✳ MARKS THE VORTEX CENTER AT 950 mb
▪ INDICATES AN AIRCRAFT OBSERVATION
WIND SPEED IN KNOTS

Figure 6

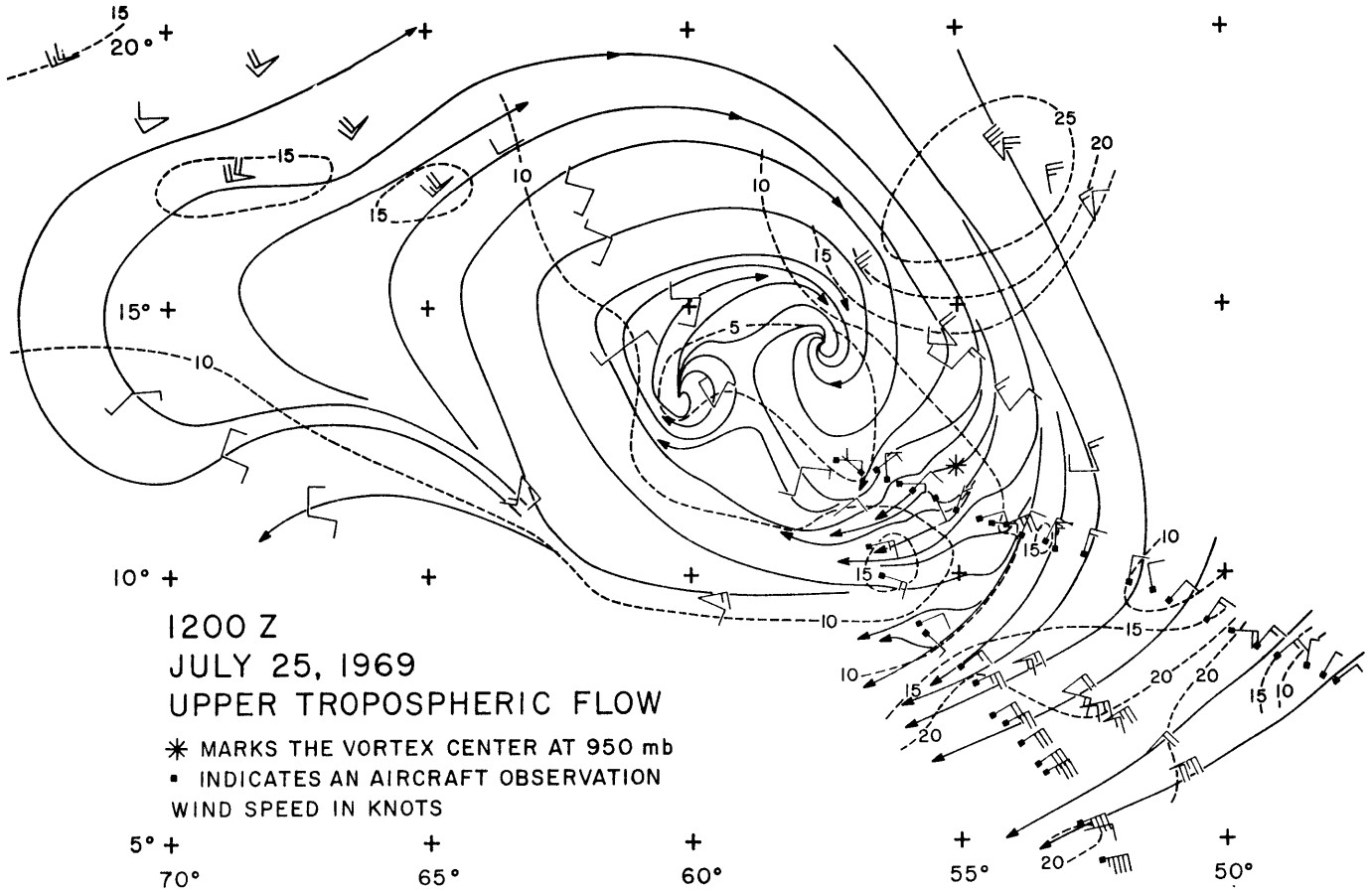
1200 Z
JULY 25, 1969
UPPER TROPOSPHERIC FLOW
✳ MARKS THE VORTEX CENTER AT 950 mb
• INDICATES AN AIRCRAFT OBSERVATION
WIND SPEED IN KNOTS
20°
15°
10°
5°
70°
65°
60°
55°
50°

Figure 7

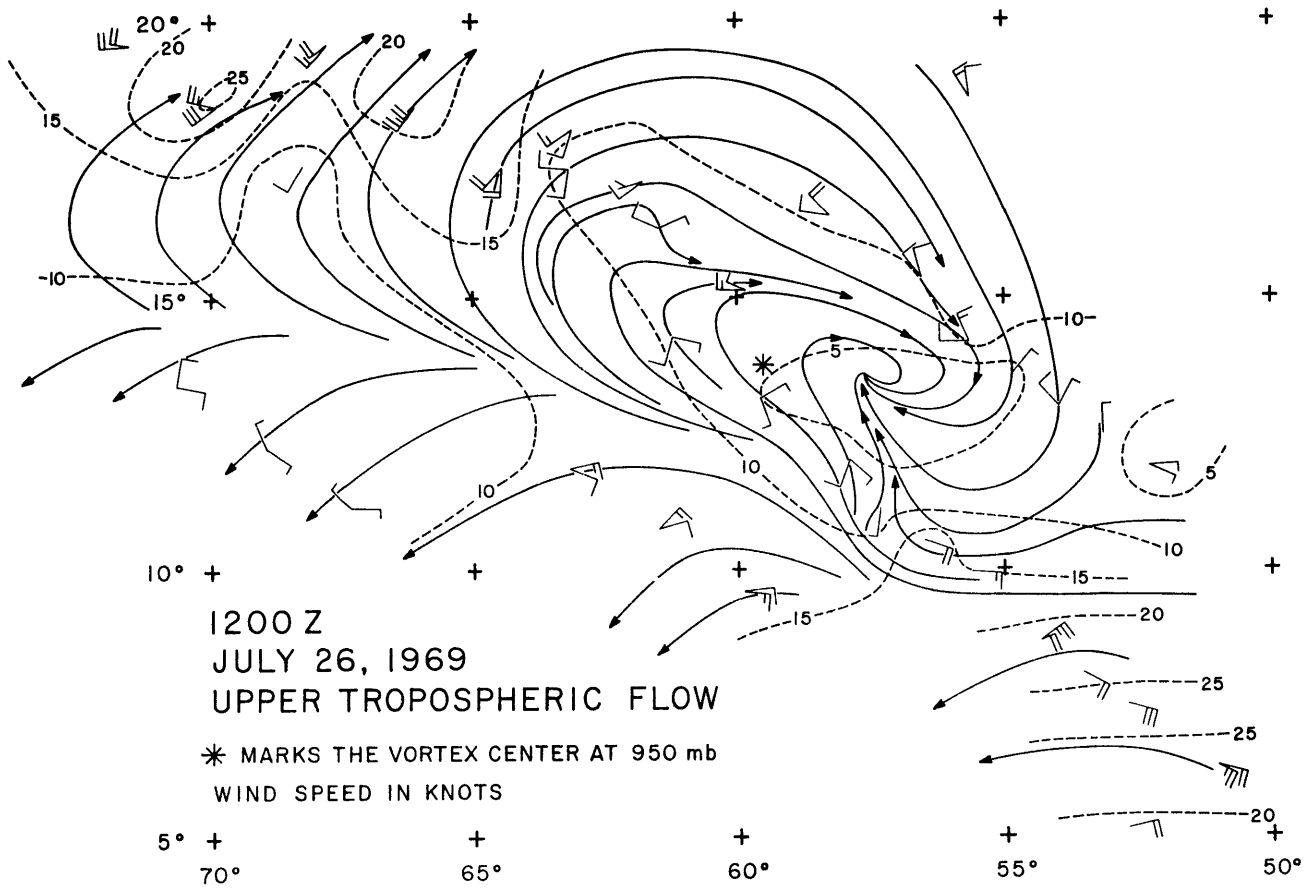
20°
20
20
25
15
15
-10
15°
10
10
5
-10-
10
5
10
15
15
20
25
25
20
10°
5°
70°
65°
60°
55°
50°
1200 Z
JULY 26, 1969
UPPER TROPOSPHERIC FLOW
✳ MARKS THE VORTEX CENTER AT 950 mb
WIND SPEED IN KNOTS

Figure 8

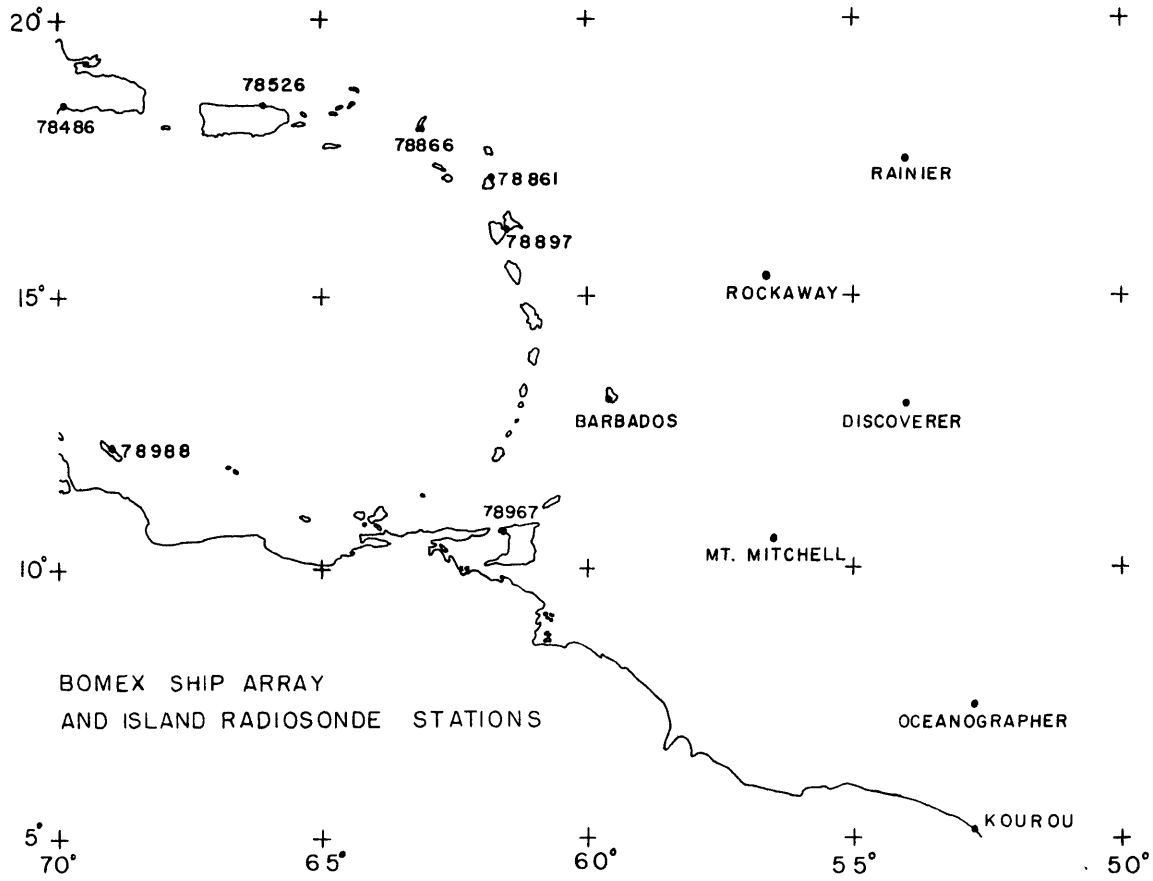
20°
15°
10°
5°
70°
65°
60°
55°
50°
78526
78486
78866
78861
78897
78988
78967
RAINIER
ROCKAWAY
BARBADOS
DISCOVERER
MT. MITCHELL
OCEANOGRAPHER
KOUROU
BOMEX SHIP ARRAY
AND ISLAND RADIOSONDE STATIONS

Figure 9

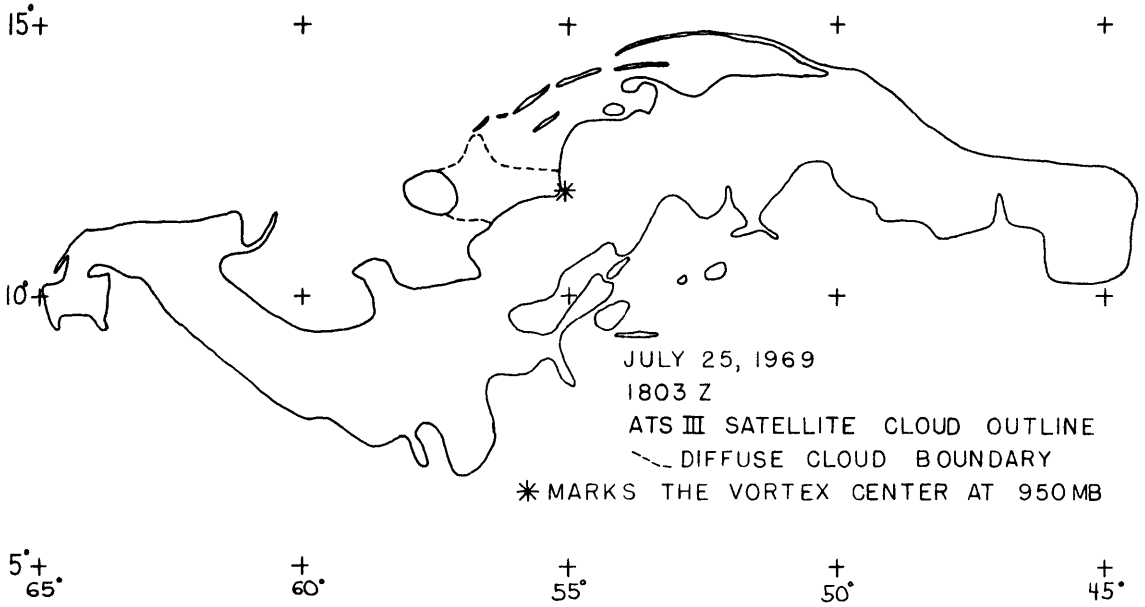
15°
10°
5°
65°
60°
55°
50°
45°
JULY 25, 1969
1803 Z
ATS III SATELLITE CLOUD OUTLINE
DIFFUSE CLOUD BOUNDARY
MARKS THE VORTEX CENTER AT 950MB

Figure 10

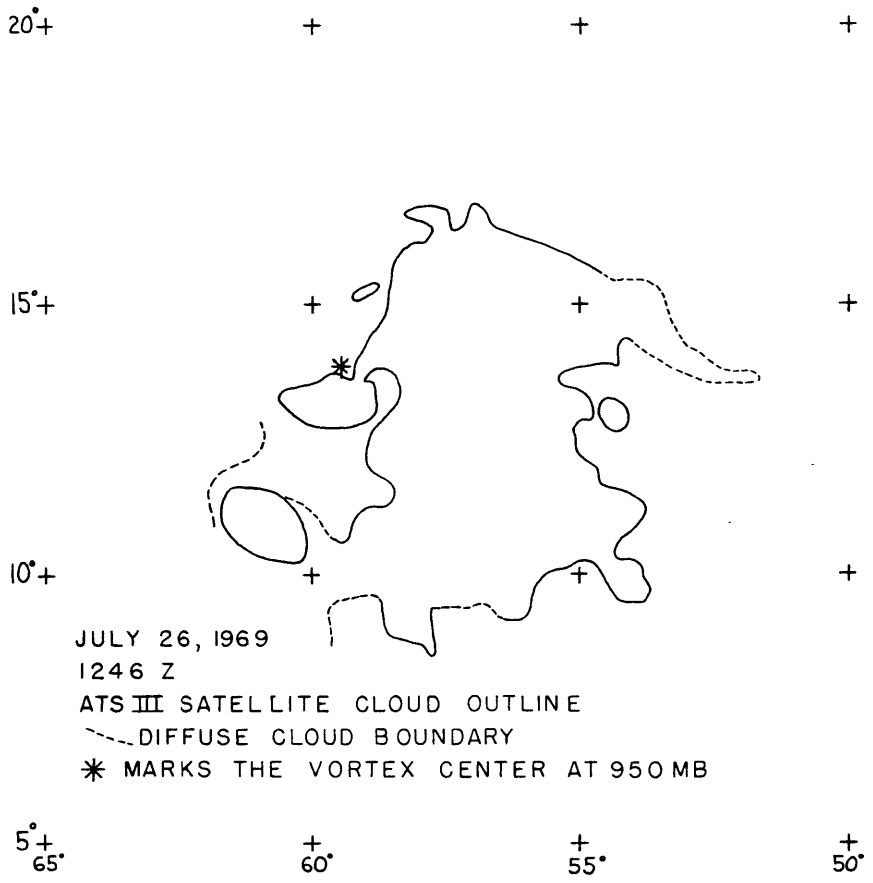
20°
15°
10°
5°
65°
60°
55°
50°
JULY 26, 1969
1246 Z
ATS III SATELLITE CLOUD OUTLINE
DIFFUSE CLOUD BOUNDARY
MARKS THE VORTEX CENTER AT 950 MB

Figure 11

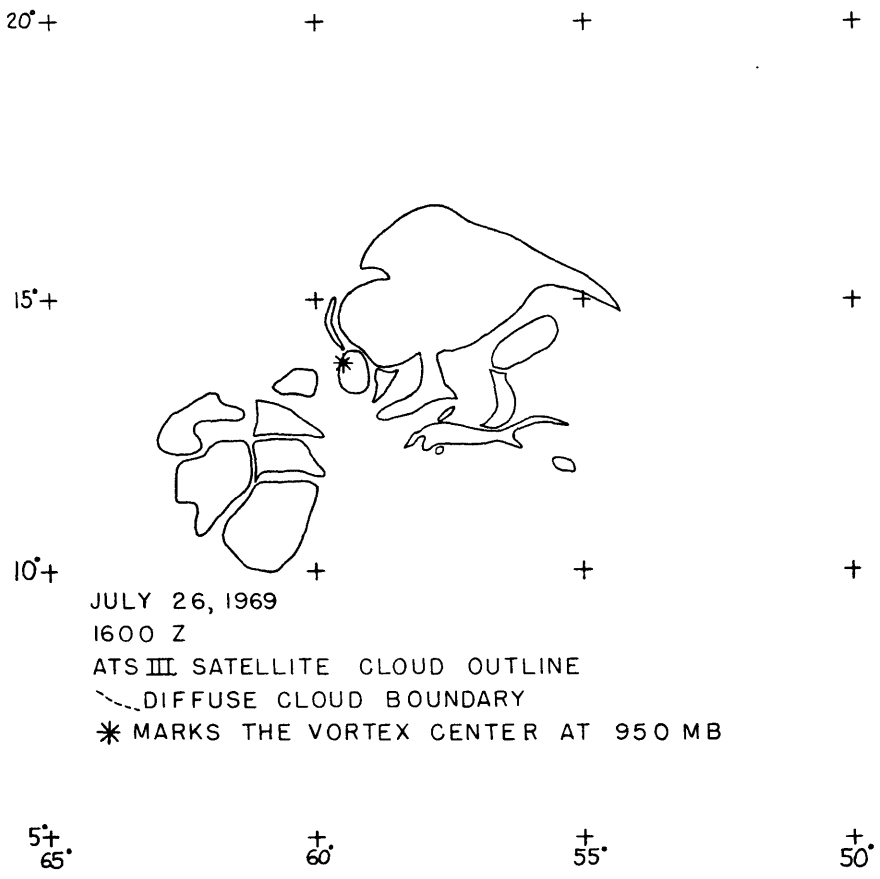
20°
15°
10°
5°
65°
60°
55°
50°
JULY 26, 1969
1600 Z
ATS III SATELLITE CLOUD OUTLINE
DIFFUSE CLOUD BOUNDARY
MARKS THE VORTEX CENTER AT 950 MB

Figure 12

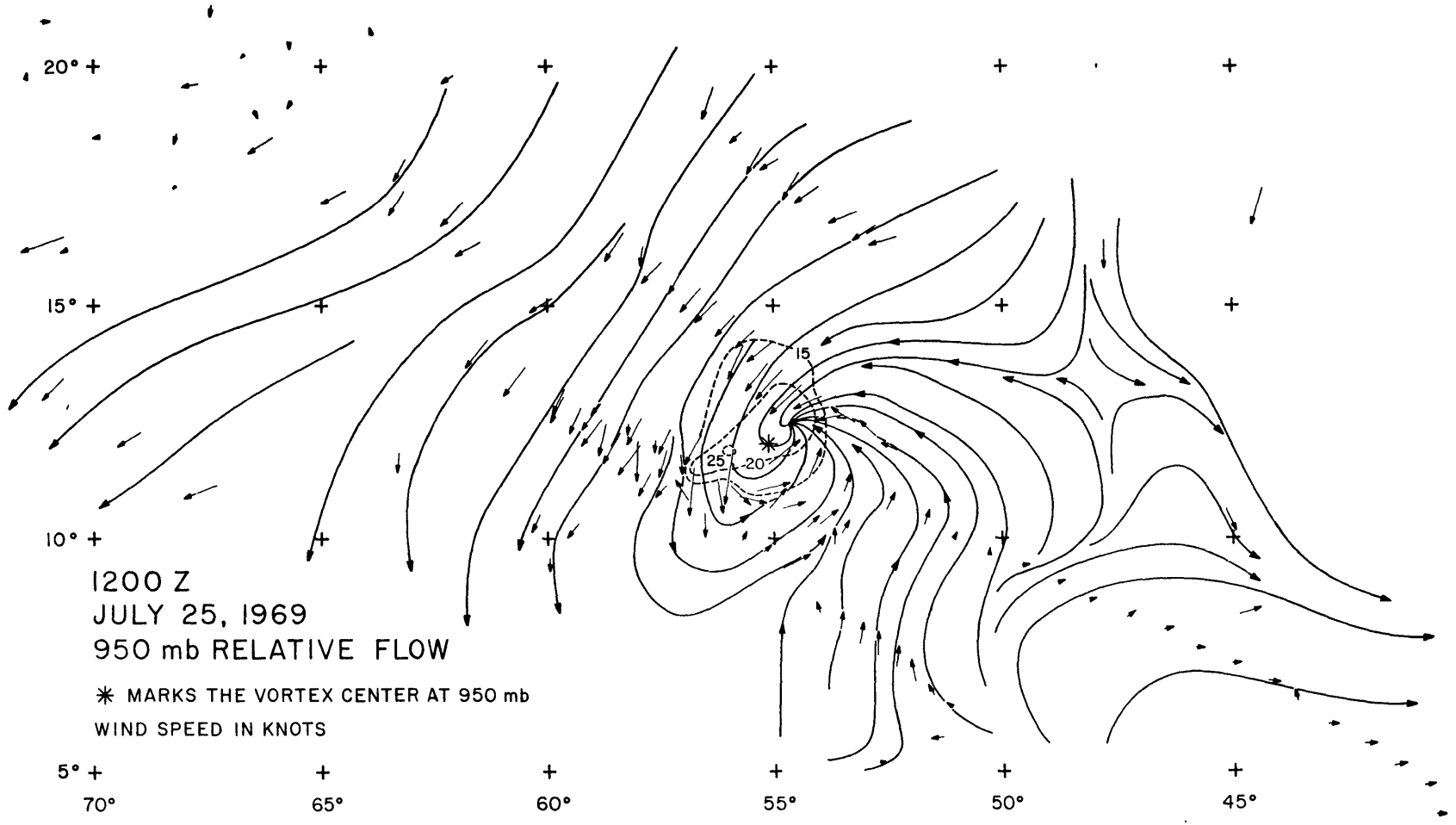
20° +
15° +
10° +
5° +
70°
65°
60°
55°
50°
45°
15
25
20
1200 Z
JULY 25, 1969
950 mb RELATIVE FLOW
✳ MARKS THE VORTEX CENTER AT 950 mb
WIND SPEED IN KNOTS

Figure 13

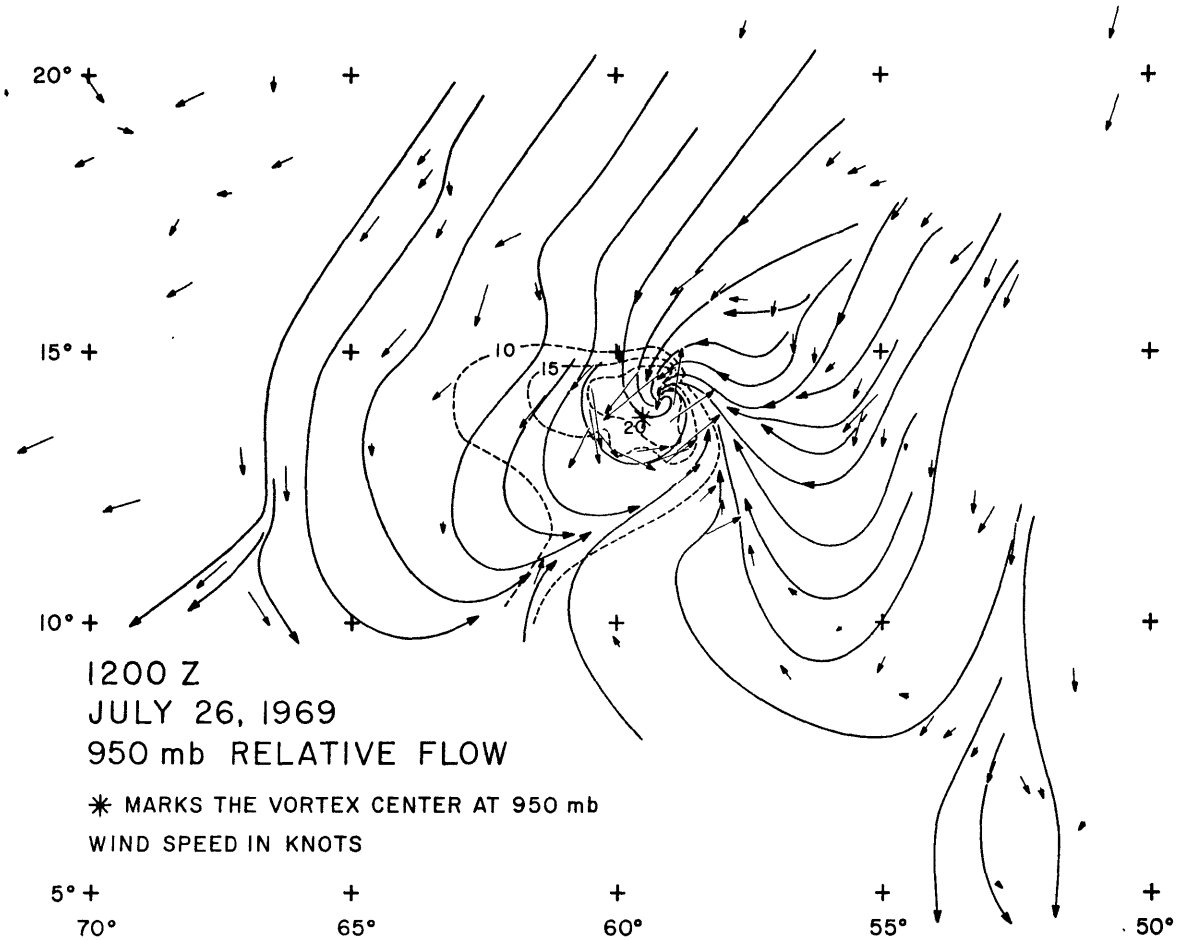
20°
15°
10°
5°
70°
65°
60°
55°
50°
10
15
20
1200 Z
JULY 26, 1969
950 mb RELATIVE FLOW
✳ MARKS THE VORTEX CENTER AT 950 mb
WIND SPEED IN KNOTS

Figure 14

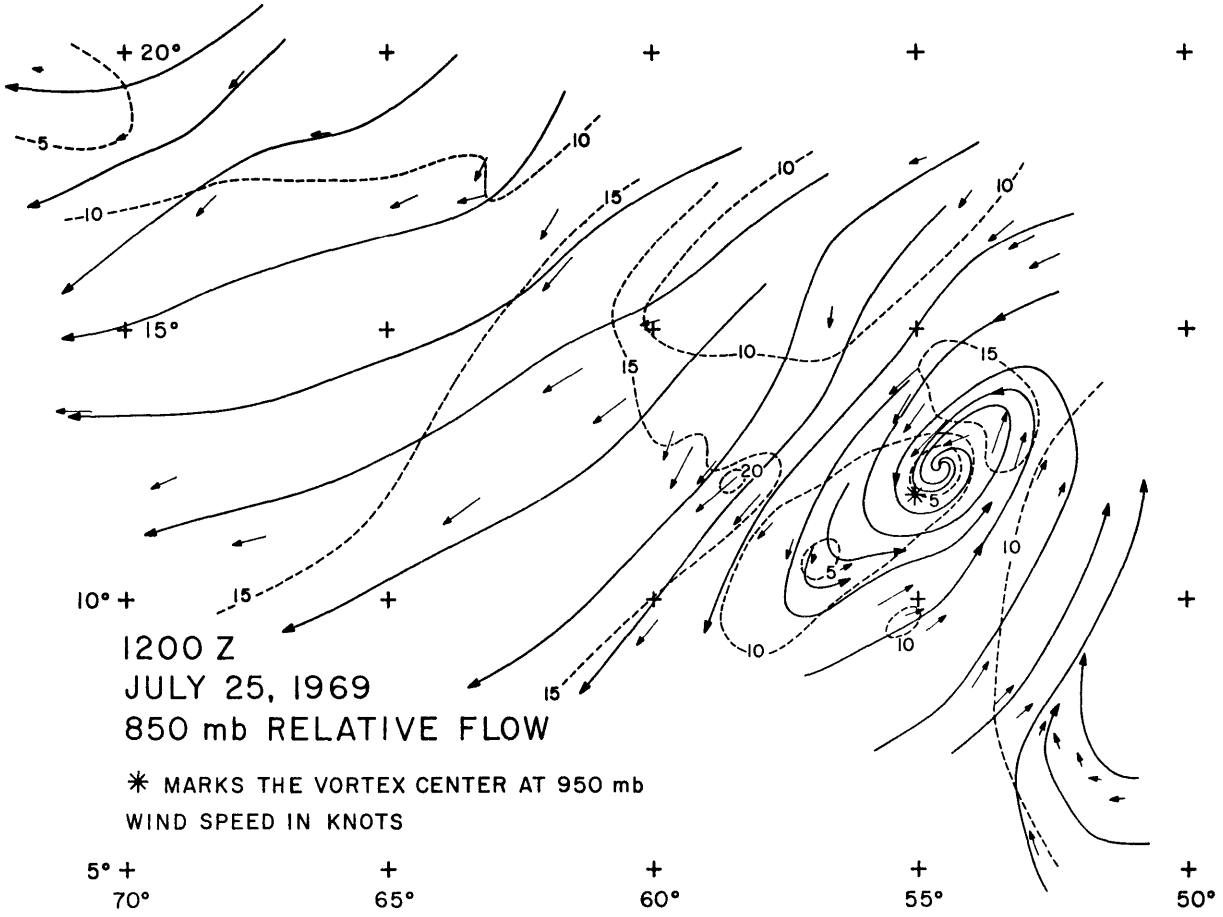
+ 20°
+ 15°
10° +
5° +
70°
65°
60°
55°
50°
1200 Z
JULY 25, 1969
850 mb RELATIVE FLOW
✳ MARKS THE VORTEX CENTER AT 950 mb
WIND SPEED IN KNOTS

Figure 15

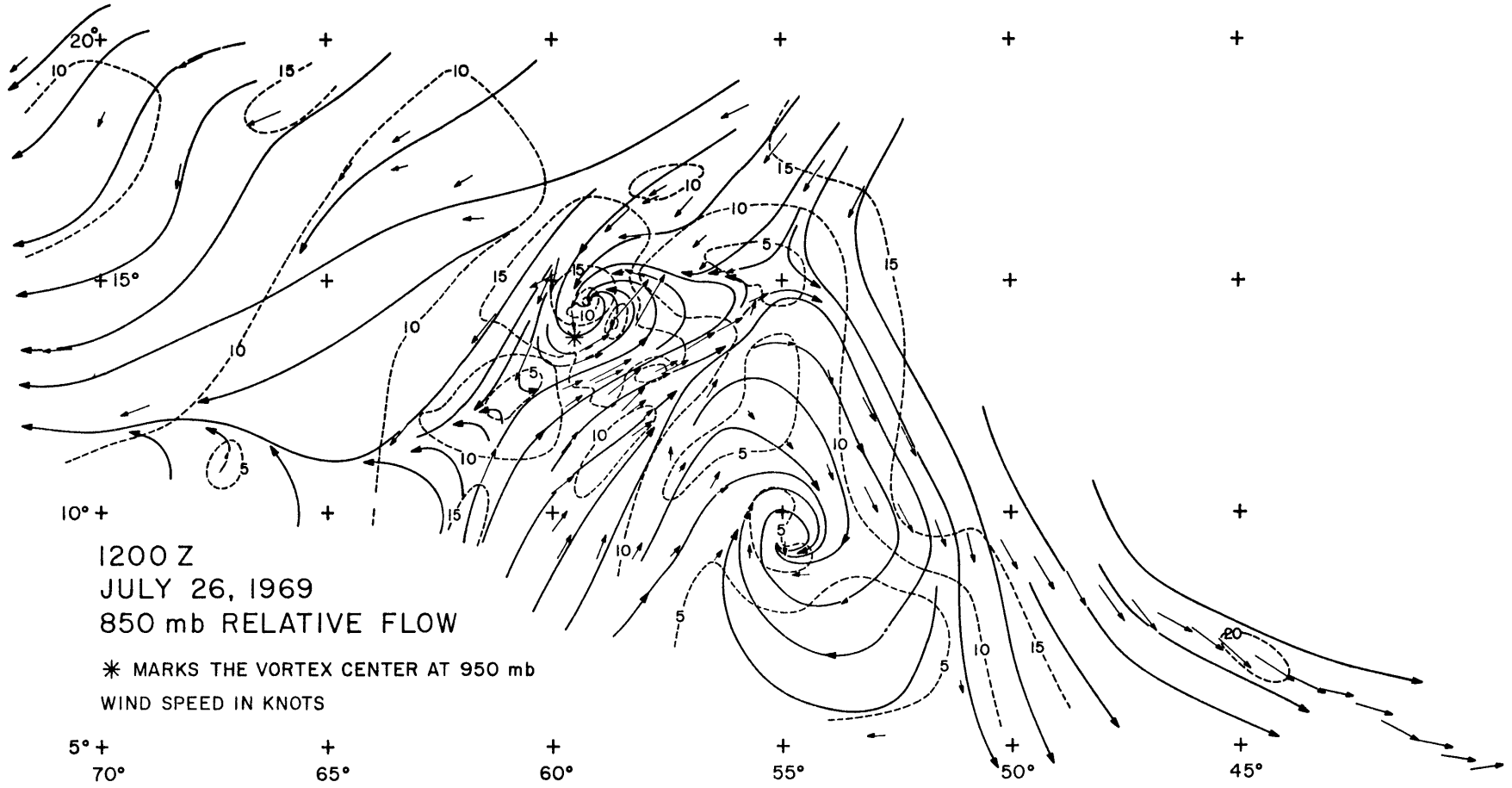
20°
15°
10°
1200 Z
JULY 26, 1969
850 mb RELATIVE FLOW
✳ MARKS THE VORTEX CENTER AT 950 mb
WIND SPEED IN KNOTS
5°
70°
65°
60°
55°
50°
45°

Figure 16

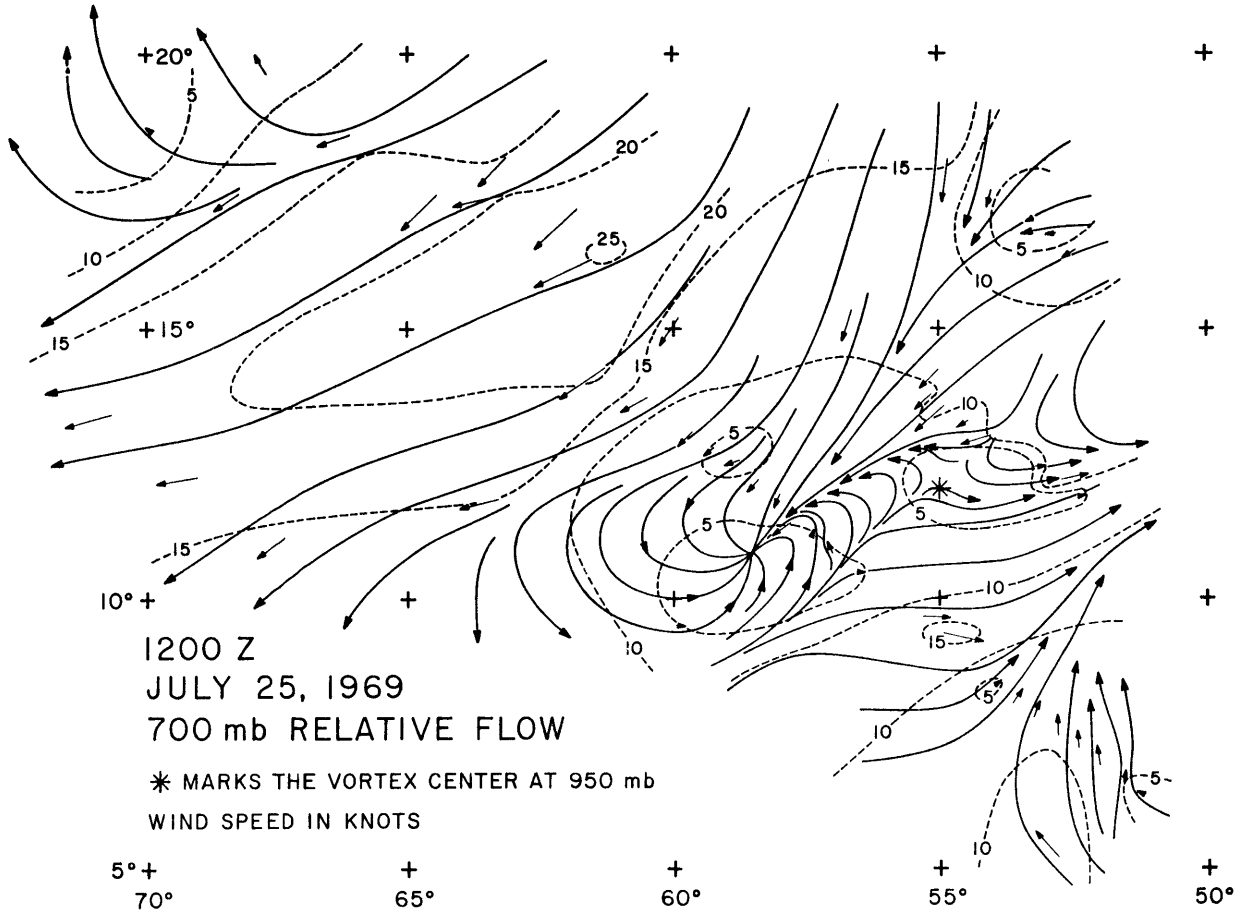
+20°
+15°
10°+
5°+
70°
65°
60°
55°
50°
1200 Z
JULY 25, 1969
700 mb RELATIVE FLOW
✳ MARKS THE VORTEX CENTER AT 950 mb
WIND SPEED IN KNOTS

Figure 17

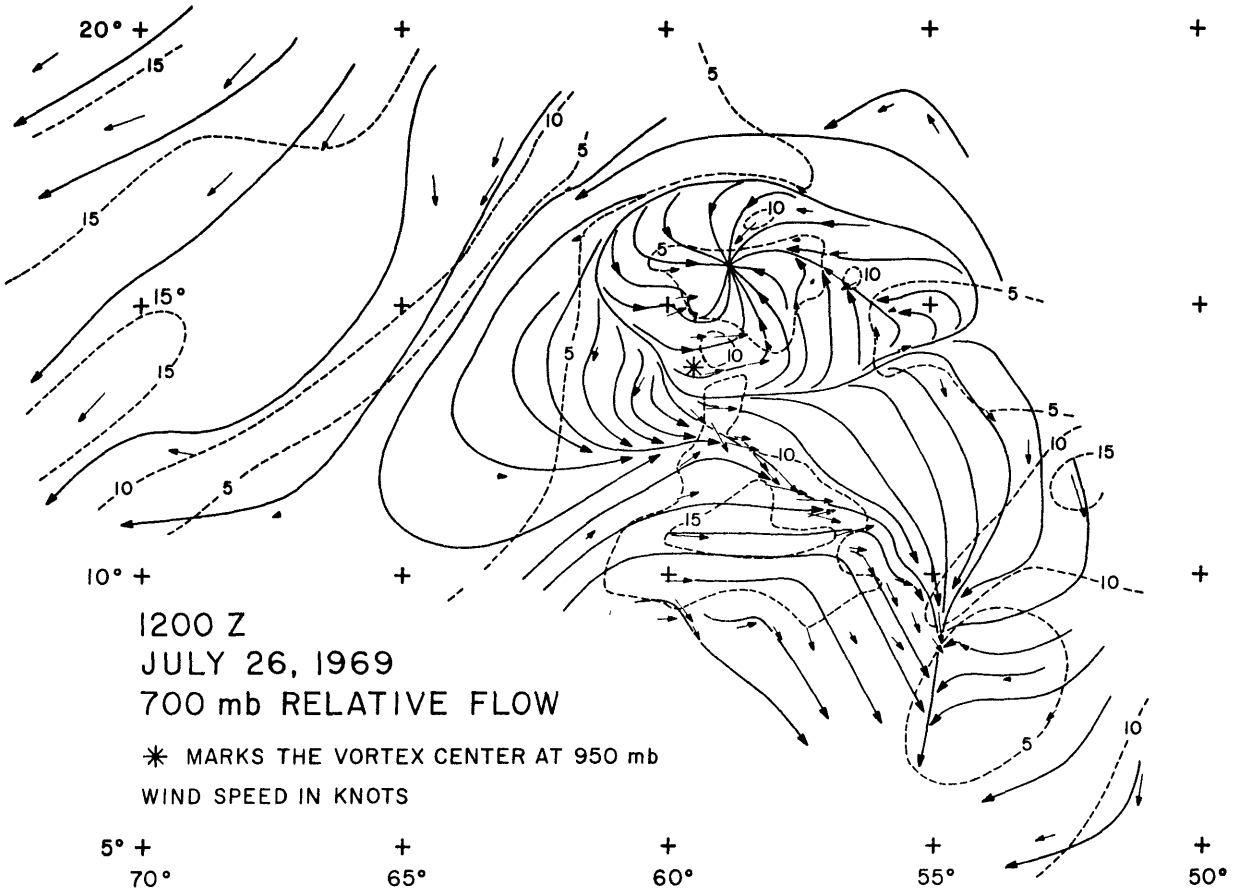
20° +
15
15
15°
15
10
5
10
5
5
10
5
10
5
5
10
15
10
15
10
5
10° +
1200 Z
JULY 26, 1969
700 mb RELATIVE FLOW
✳ MARKS THE VORTEX CENTER AT 950 mb
WIND SPEED IN KNOTS
5° +
70°
65°
60°
55°
50°

Figure 18

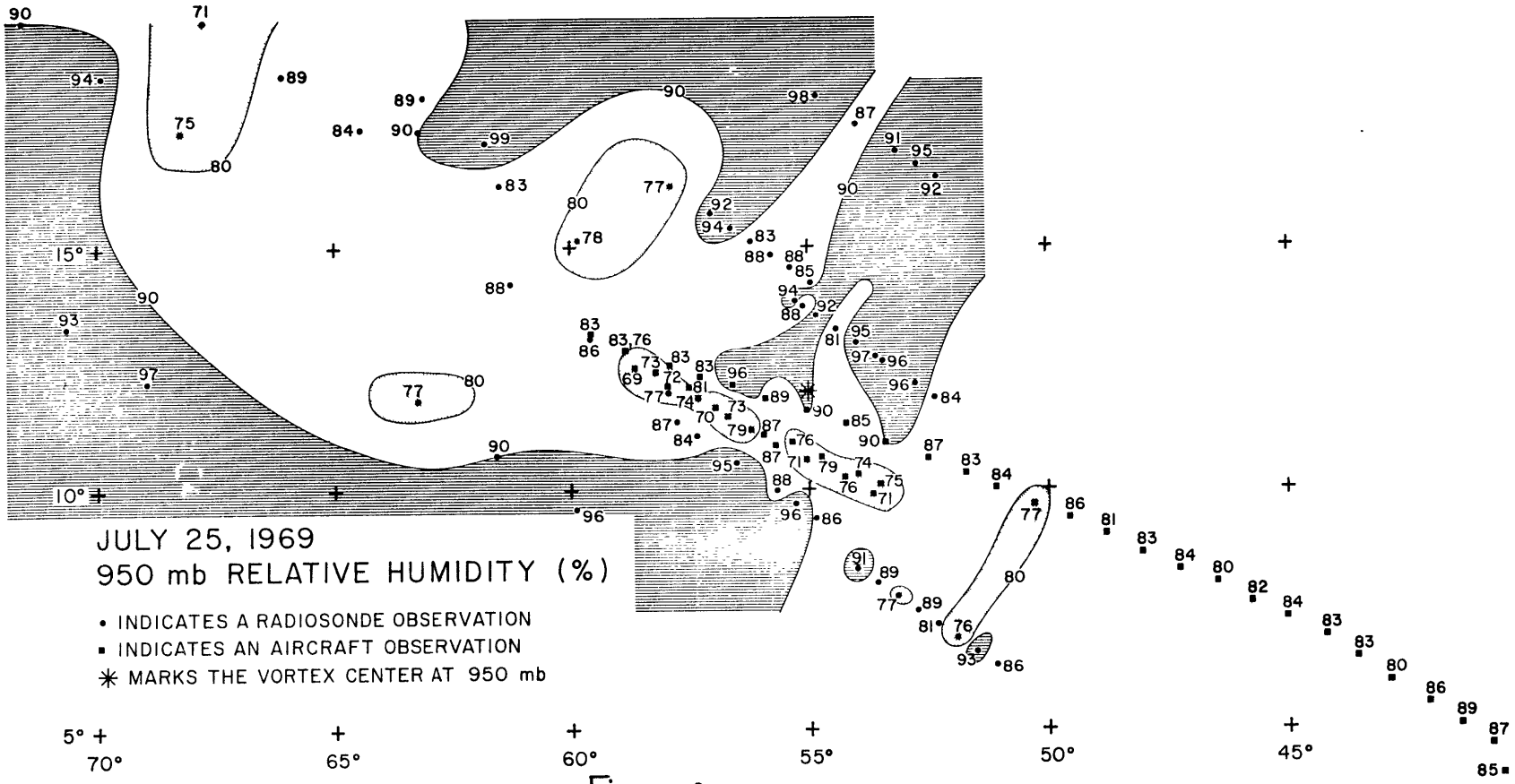
JULY 25, 1969
950 mb RELATIVE HUMIDITY (%)
• INDICATES A RADIOSONDE OBSERVATION
▪ INDICATES AN AIRCRAFT OBSERVATION
✳ MARKS THE VORTEX CENTER AT 950 mb
15°
10°
5°
70°
65°
60°
55°
50°
45°

Figure 19

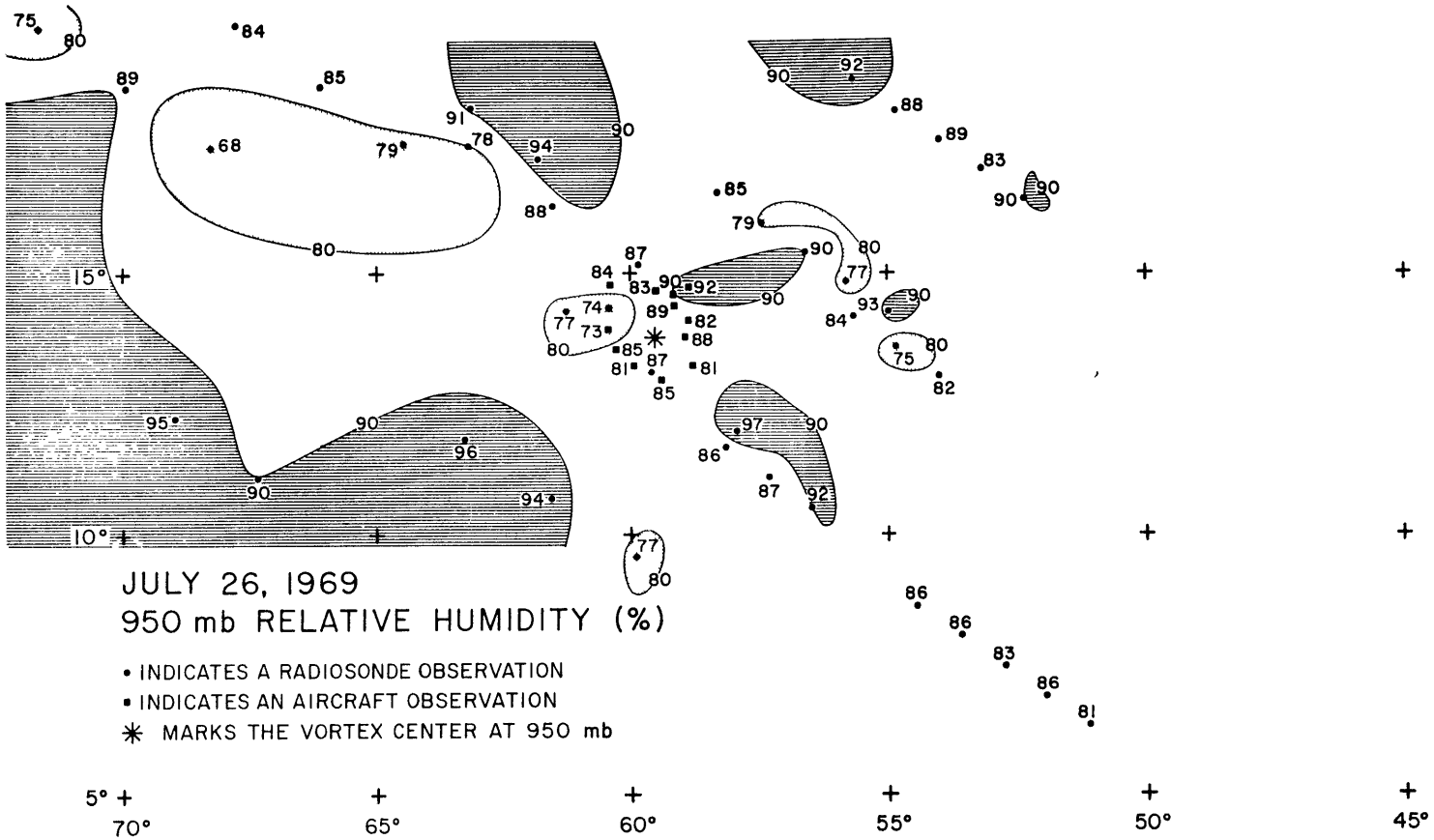
JULY 26, 1969
950 mb RELATIVE HUMIDITY (%)
• INDICATES A RADIOSONDE OBSERVATION
▪ INDICATES AN AIRCRAFT OBSERVATION
✳ MARKS THE VORTEX CENTER AT 950 mb
15°
10°
5°
70°
65°
60°
55°
50°
45°

Figure 20

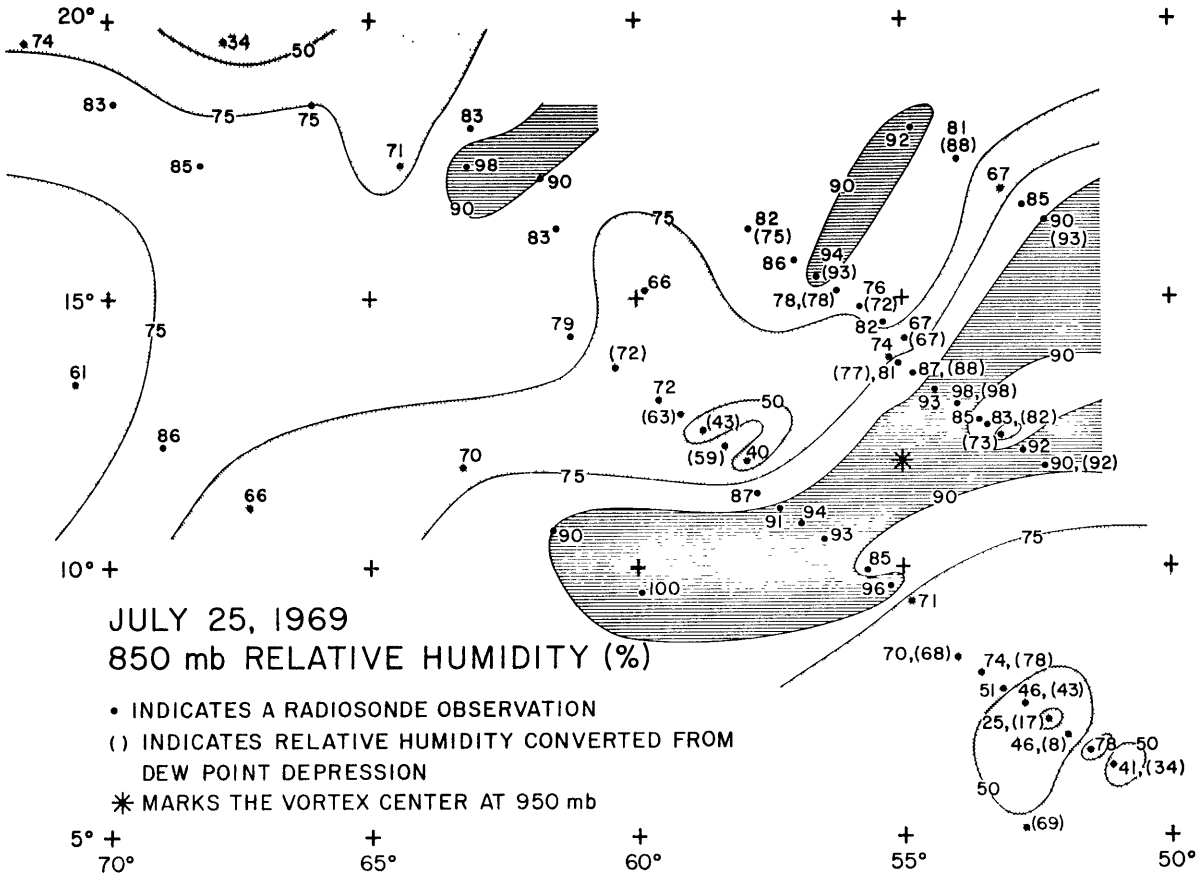
20°
15°
10°
5°
70°
65°
60°
55°
50°
JULY 25, 1969
850 mb RELATIVE HUMIDITY (%)
• INDICATES A RADIOSONDE OBSERVATION
( ) INDICATES RELATIVE HUMIDITY CONVERTED FROM DEW POINT DEPRESSION
✳ MARKS THE VORTEX CENTER AT 950 mb

Figure 21

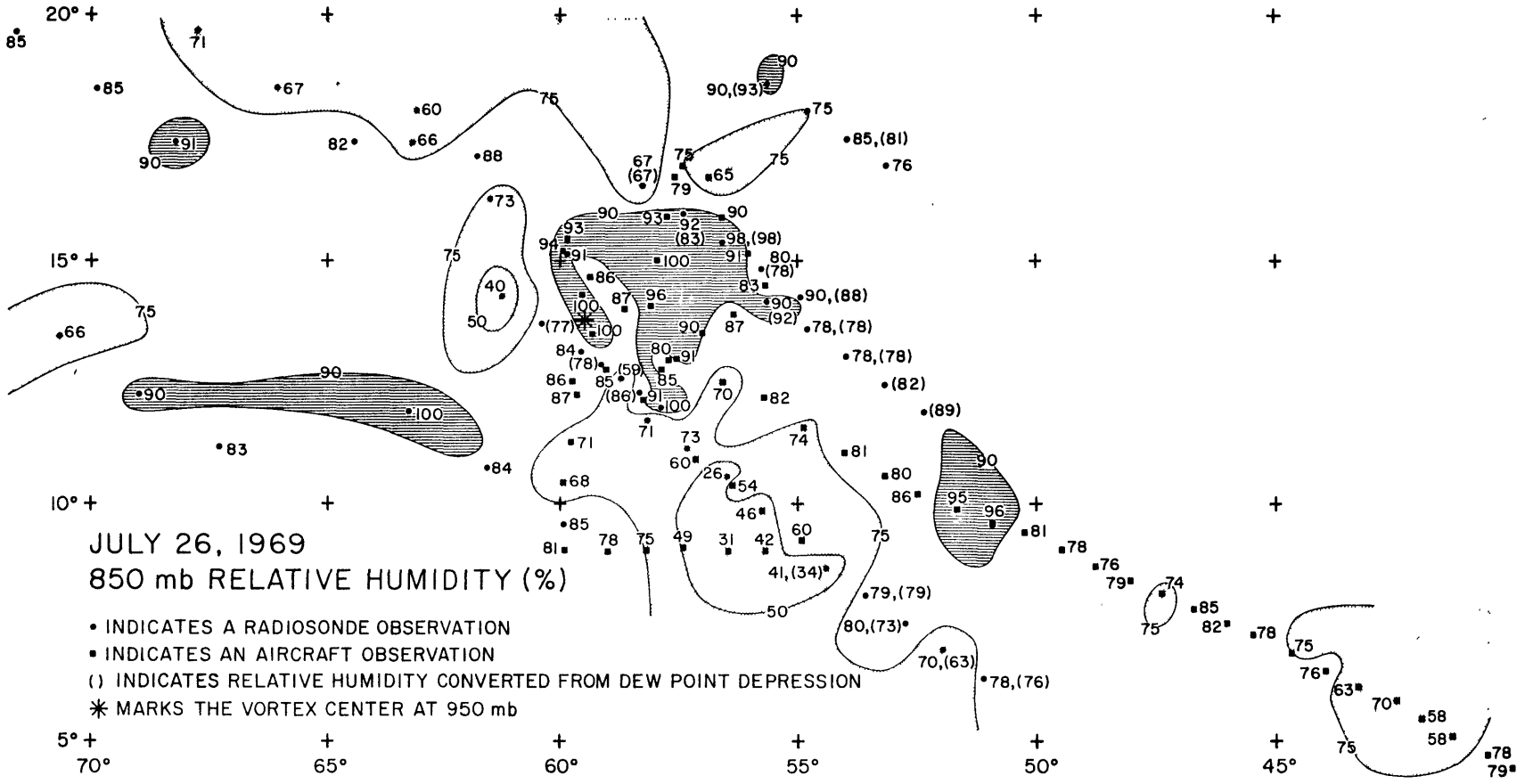
20° + + + + + +
15° + + + + + +
10° + + + + + +
5° + + + + + +
70° 65° 60° 55° 50° 45°
JULY 26, 1969
850 mb RELATIVE HUMIDITY (%)
• INDICATES A RADIOSONDE OBSERVATION
▪ INDICATES AN AIRCRAFT OBSERVATION
( ) INDICATES RELATIVE HUMIDITY CONVERTED FROM DEW POINT DEPRESSION
✳ MARKS THE VORTEX CENTER AT 950 mb

Figure 22

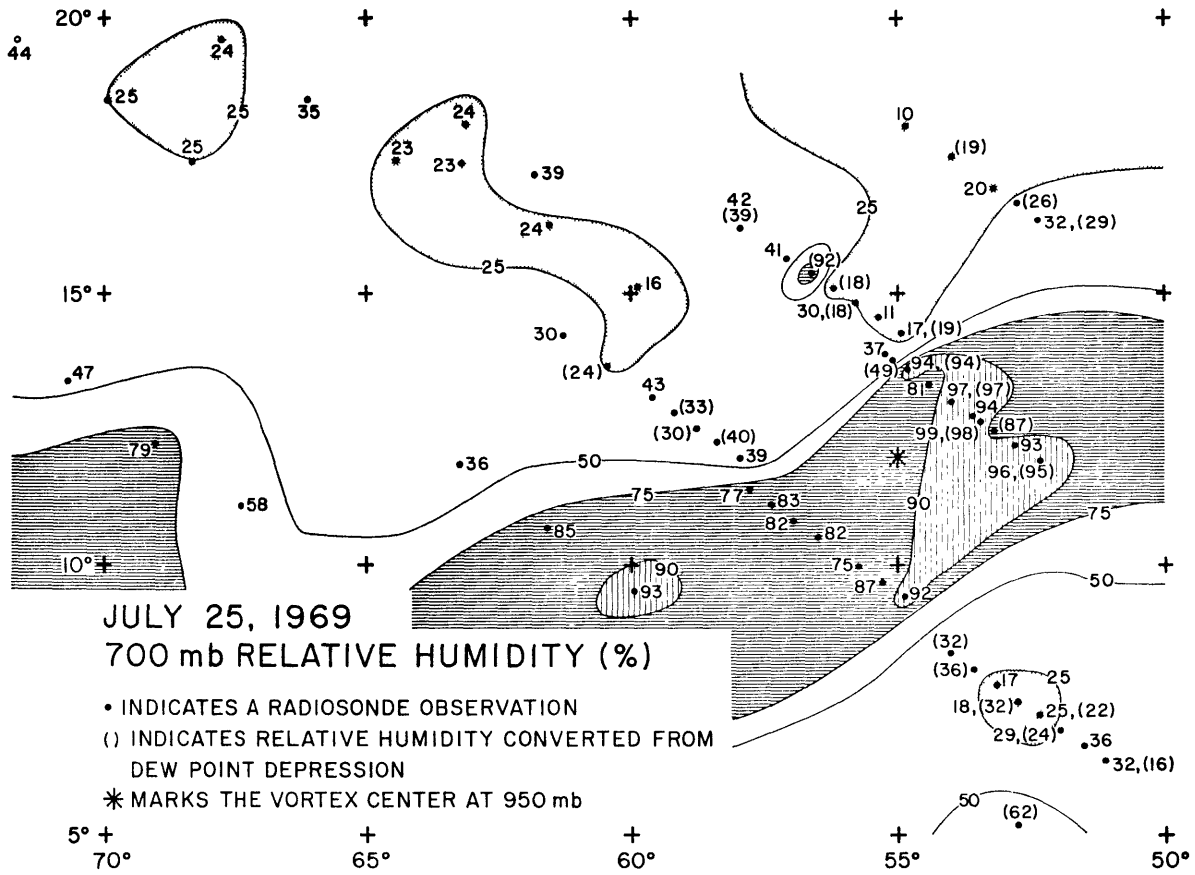
20°
15°
10°
5°
70°
65°
60°
55°
50°
JULY 25, 1969
700 mb RELATIVE HUMIDITY (%)
• INDICATES A RADIOSONDE OBSERVATION
() INDICATES RELATIVE HUMIDITY CONVERTED FROM DEW POINT DEPRESSION
✳ MARKS THE VORTEX CENTER AT 950 mb

Figure 23

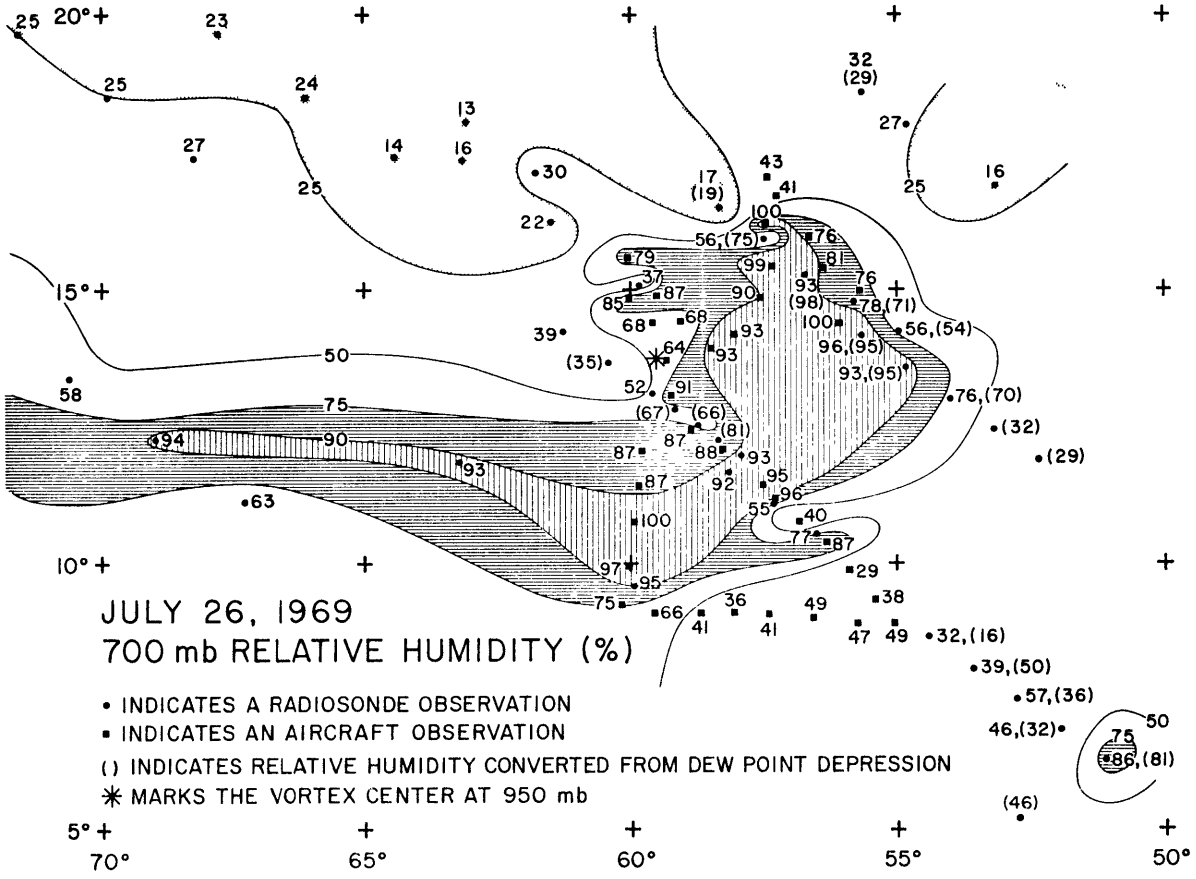
JULY 26, 1969
700 mb RELATIVE HUMIDITY (%)
• INDICATES A RADIOSONDE OBSERVATION
▪ INDICATES AN AIRCRAFT OBSERVATION
( ) INDICATES RELATIVE HUMIDITY CONVERTED FROM DEW POINT DEPRESSION
✳ MARKS THE VORTEX CENTER AT 950 mb
20°
15°
10°
5°
70°
65°
60°
55°
50°

Figure 24

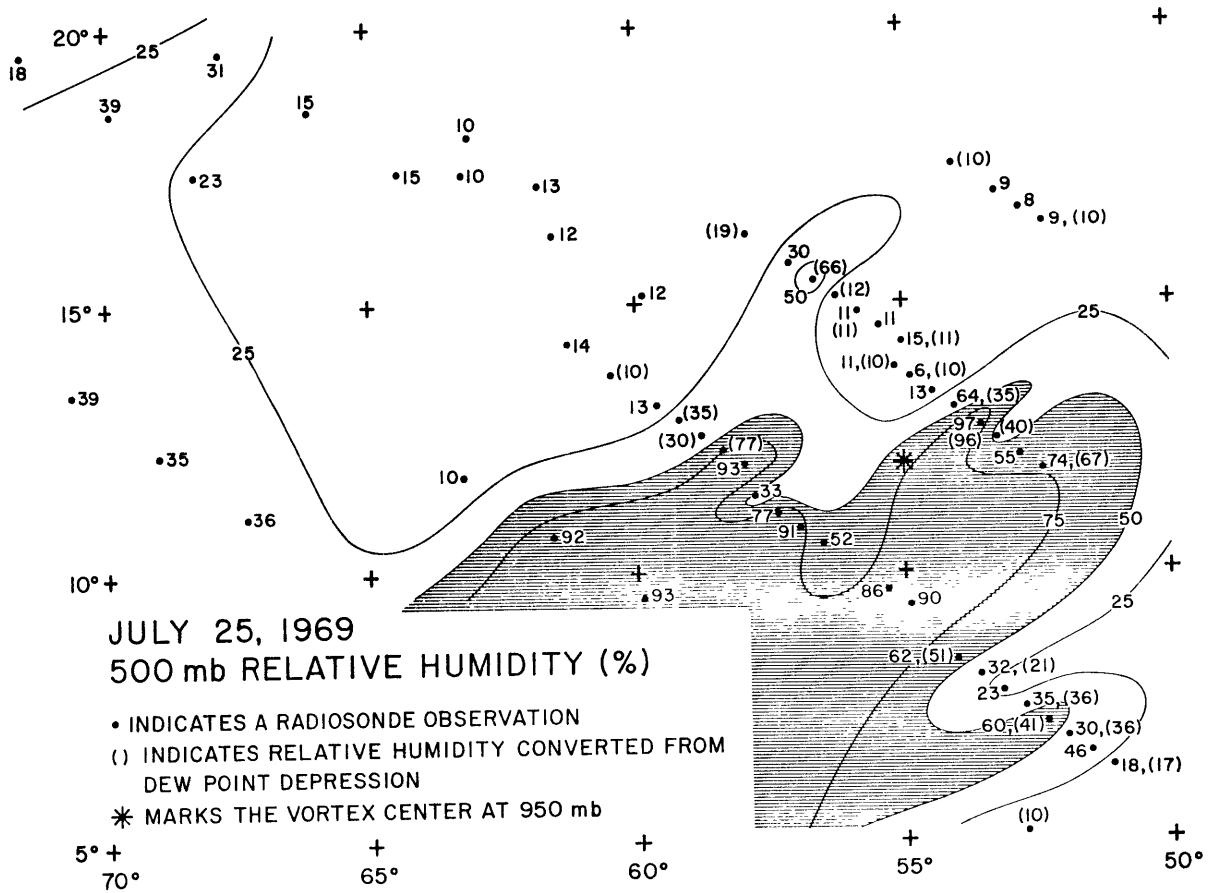
20°
15°
10°
5°
70°
65°
60°
55°
50°
JULY 25, 1969
500 mb RELATIVE HUMIDITY (%)
• INDICATES A RADIOSONDE OBSERVATION
( ) INDICATES RELATIVE HUMIDITY CONVERTED FROM DEW POINT DEPRESSION
✳ MARKS THE VORTEX CENTER AT 950 mb

Figure 25

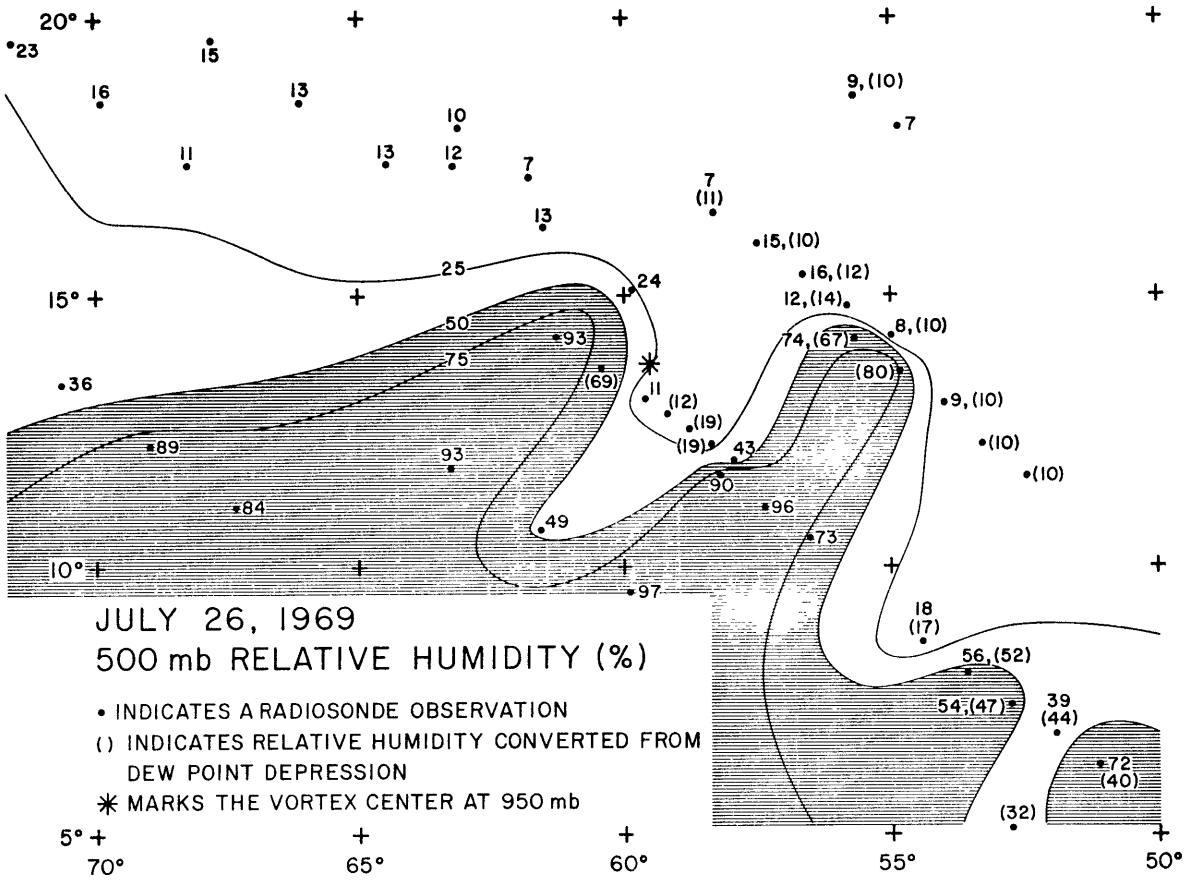

JULY 26, 1969
500 mb RELATIVE HUMIDITY (%)

• INDICATES A RADIOSONDE OBSERVATION
() INDICATES RELATIVE HUMIDITY CONVERTED FROM DEW POINT DEPRESSION
✳ MARKS THE VORTEX CENTER AT 950 mb

Figure 26

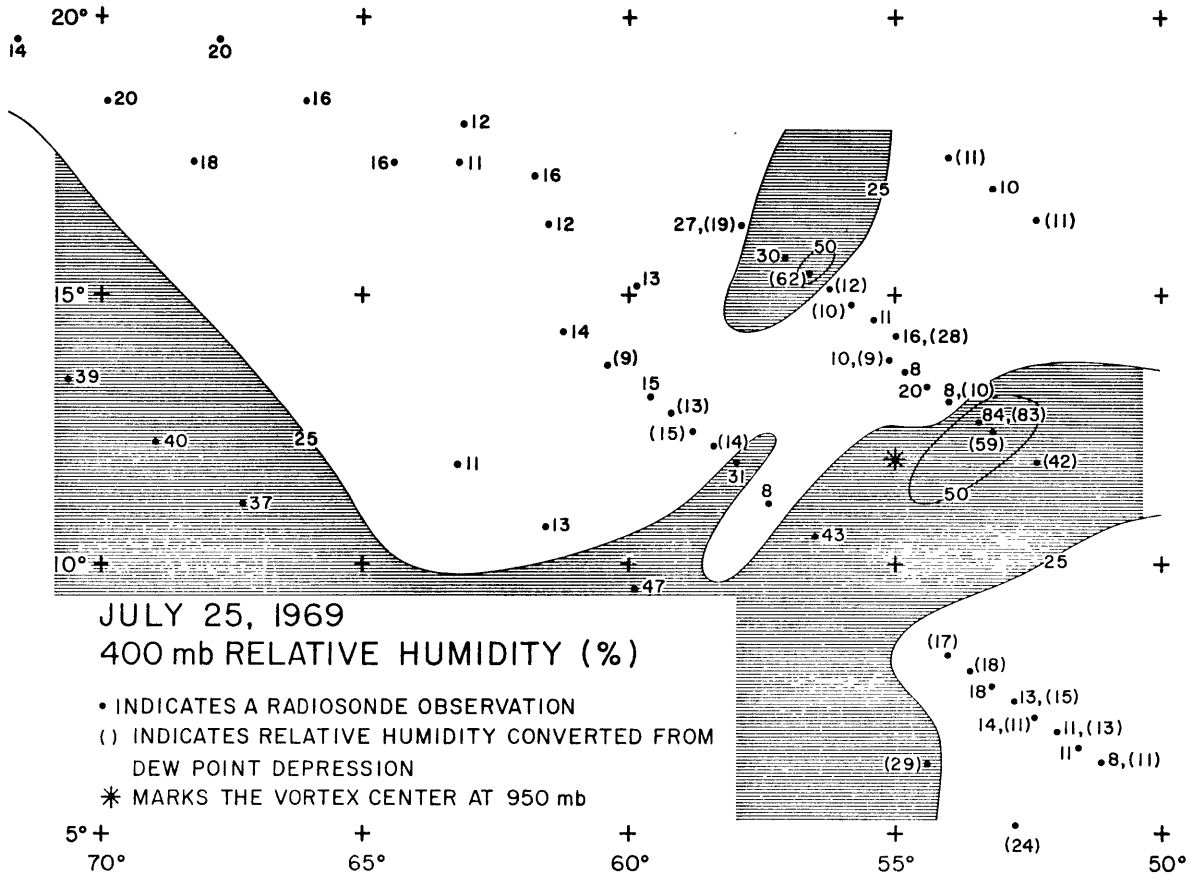
20°
15°
10°
5°
70°
65°
60°
55°
50°
JULY 25, 1969
400 mb RELATIVE HUMIDITY (%)
• INDICATES A RADIOSONDE OBSERVATION
( ) INDICATES RELATIVE HUMIDITY CONVERTED FROM DEW POINT DEPRESSION
✳ MARKS THE VORTEX CENTER AT 950 mb

Figure 27

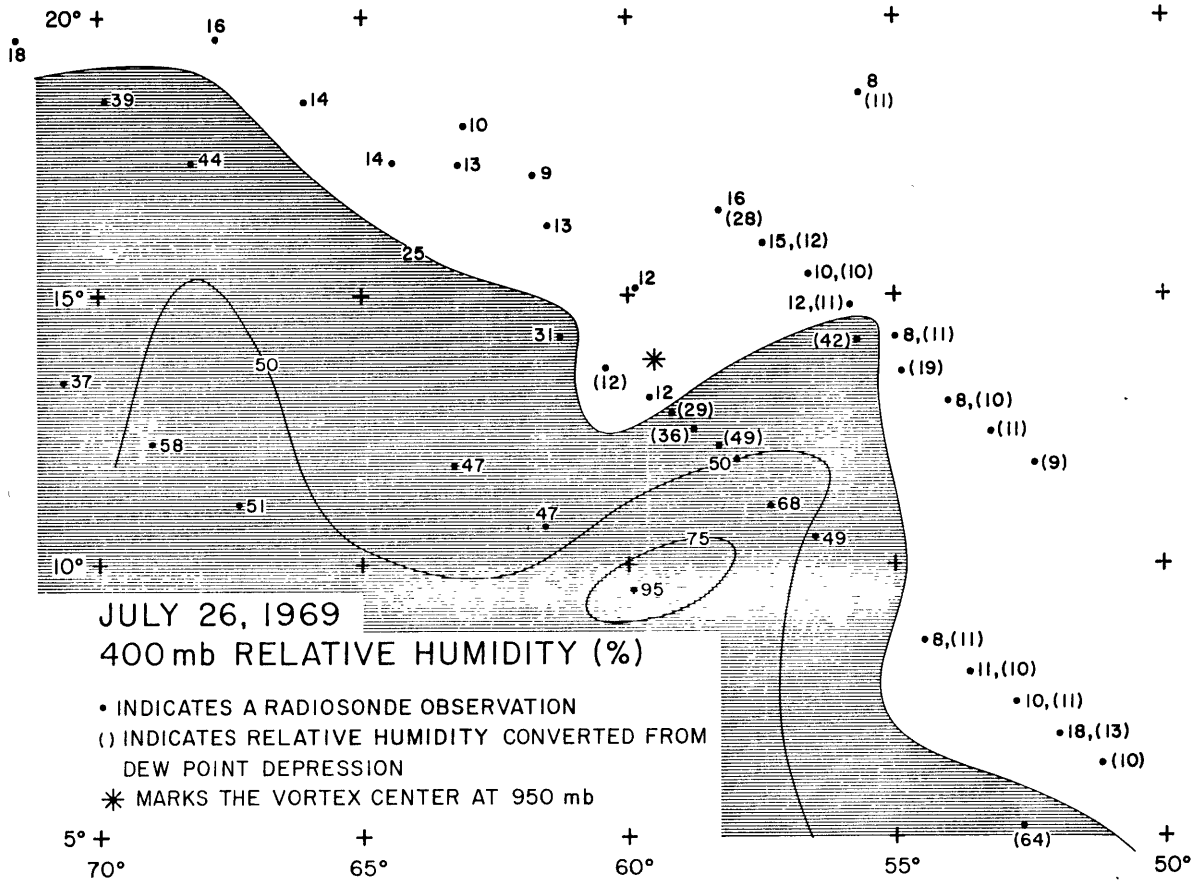
20°
15°
10°
5°
70°
65°
60°
55°
50°
JULY 26, 1969
400 mb RELATIVE HUMIDITY (%)
• INDICATES A RADIOSONDE OBSERVATION
( ) INDICATES RELATIVE HUMIDITY CONVERTED FROM DEW POINT DEPRESSION
✳ MARKS THE VORTEX CENTER AT 950 mb

Figure 28

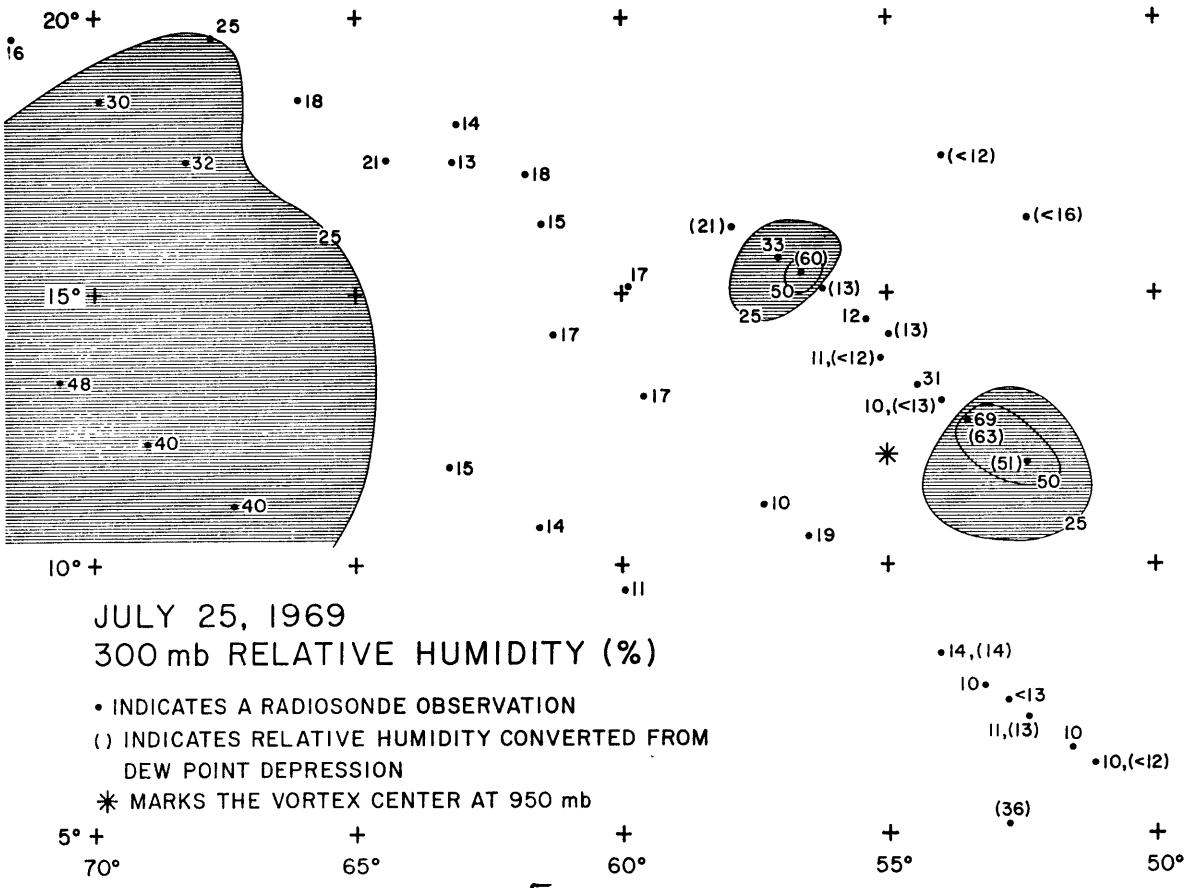
20° +
15° +
10° +
5° +
70°
65°
60°
55°
50°
25
16
30
18
14
32
21
13
18
15
25
17
48
40
40
15
14
11
(21)
33
(60)
50
(13)
25
12
(13)
11,(<12)
31
10,(<13)
69
(63)
(51)
50
25
10
19
(<12)
(<16)
14,(14)
10
<13
11,(13)
10
10,(<12)
(36)
JULY 25, 1969
300 mb RELATIVE HUMIDITY (%)
• INDICATES A RADIOSONDE OBSERVATION
( ) INDICATES RELATIVE HUMIDITY CONVERTED FROM DEW POINT DEPRESSION
✳ MARKS THE VORTEX CENTER AT 950 mb

Figure 29

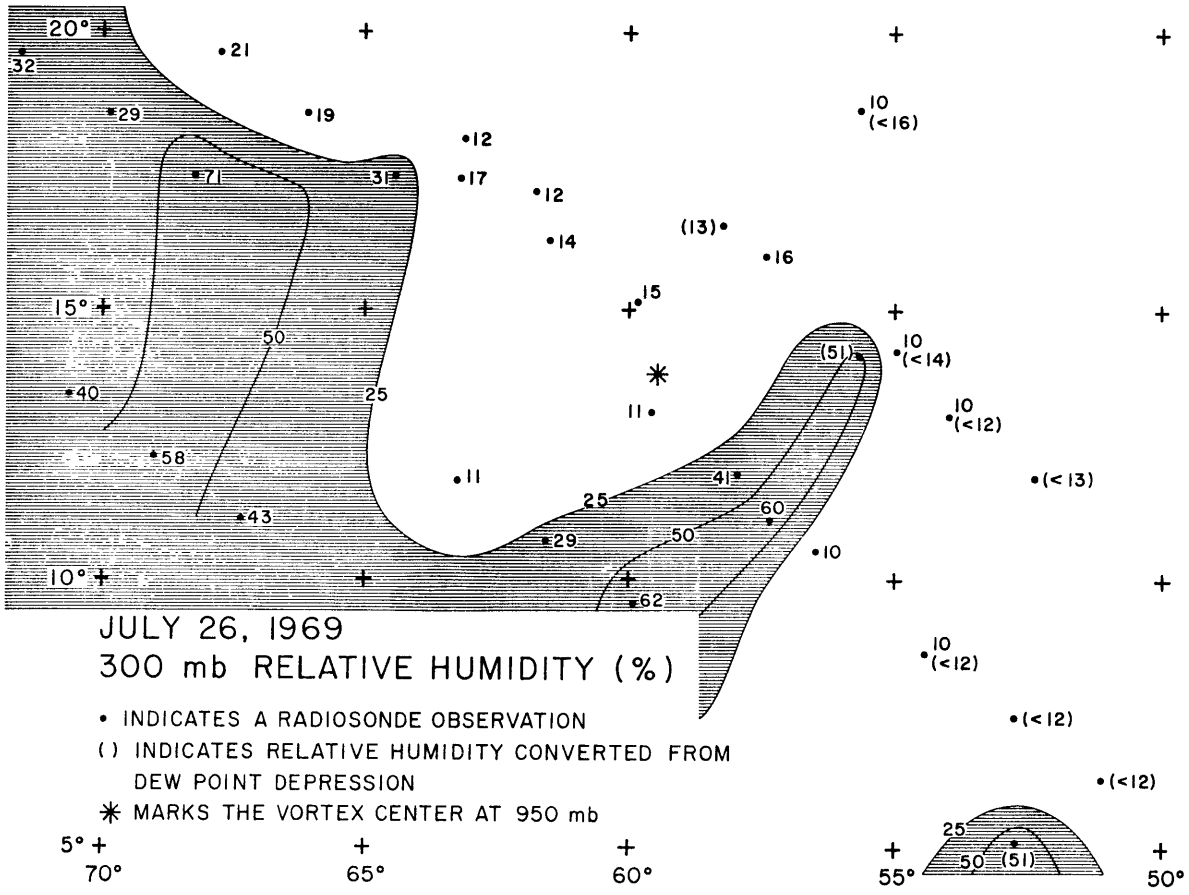
20°
15°
10°
5°
70°
65°
60°
55°
50°
JULY 26, 1969
300 mb RELATIVE HUMIDITY (%)
• INDICATES A RADIOSONDE OBSERVATION
( ) INDICATES RELATIVE HUMIDITY CONVERTED FROM DEW POINT DEPRESSION
✳ MARKS THE VORTEX CENTER AT 950 mb

Figure 30

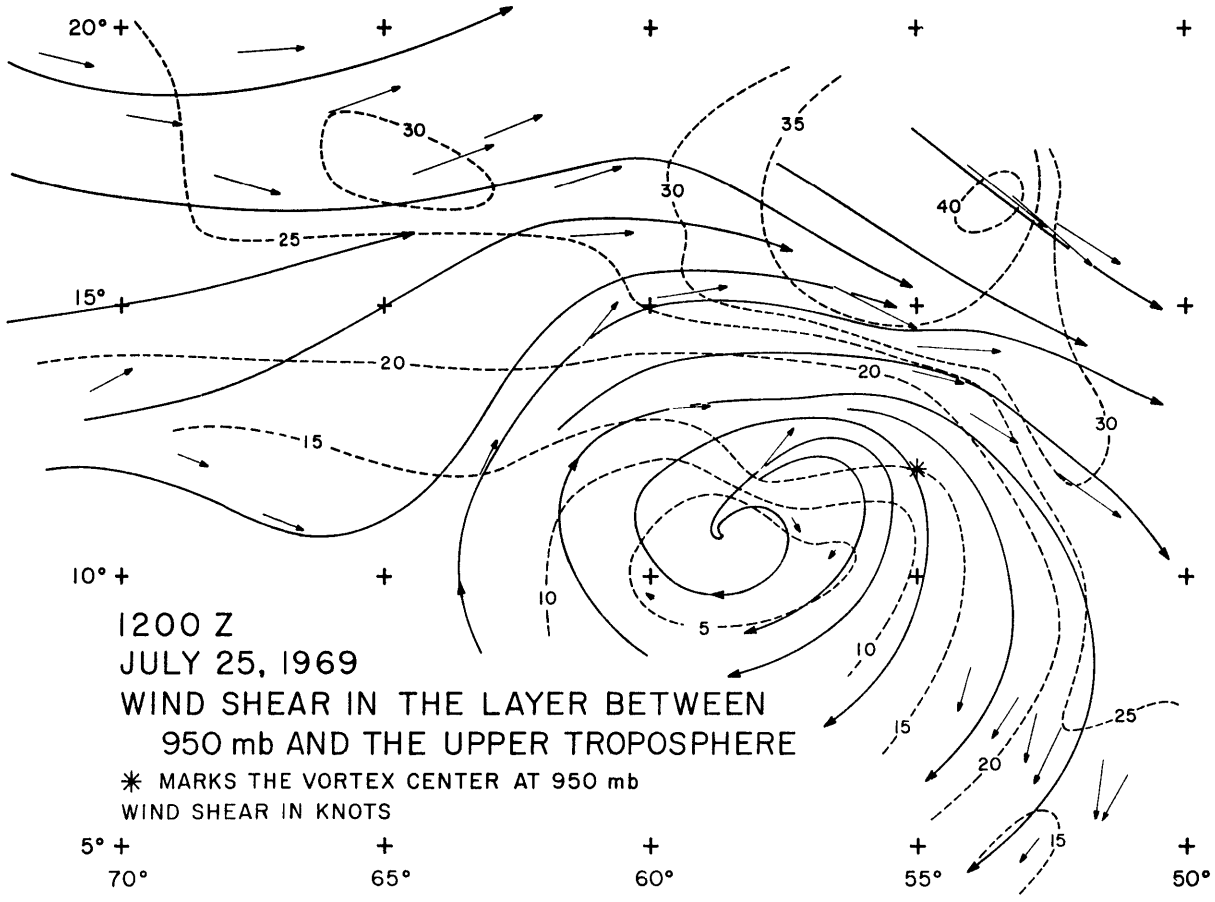
20°
15°
10°
5°
70°
65°
60°
55°
50°
30
25
35
30
40
20
20
15
30
10
5
10
15
20
25
15
1200 Z
JULY 25, 1969
WIND SHEAR IN THE LAYER BETWEEN
950 mb AND THE UPPER TROPOSPHERE
✳ MARKS THE VORTEX CENTER AT 950 mb
WIND SHEAR IN KNOTS

Figure 31

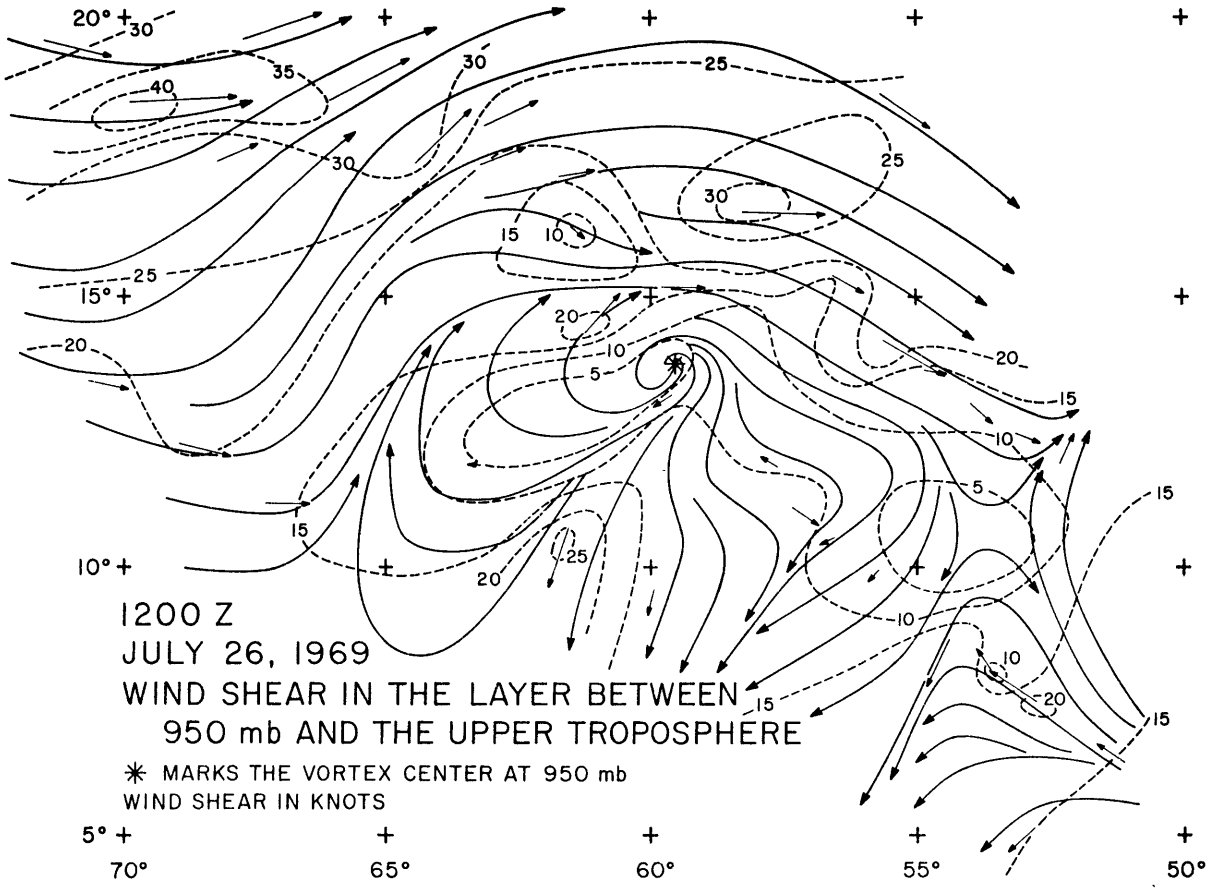
20° +
15° +
10° +
5° +
70°
65°
60°
55°
50°
1200 Z
JULY 26, 1969
WIND SHEAR IN THE LAYER BETWEEN
950 mb AND THE UPPER TROPOSPHERE
✳ MARKS THE VORTEX CENTER AT 950 mb
WIND SHEAR IN KNOTS

Figure 32

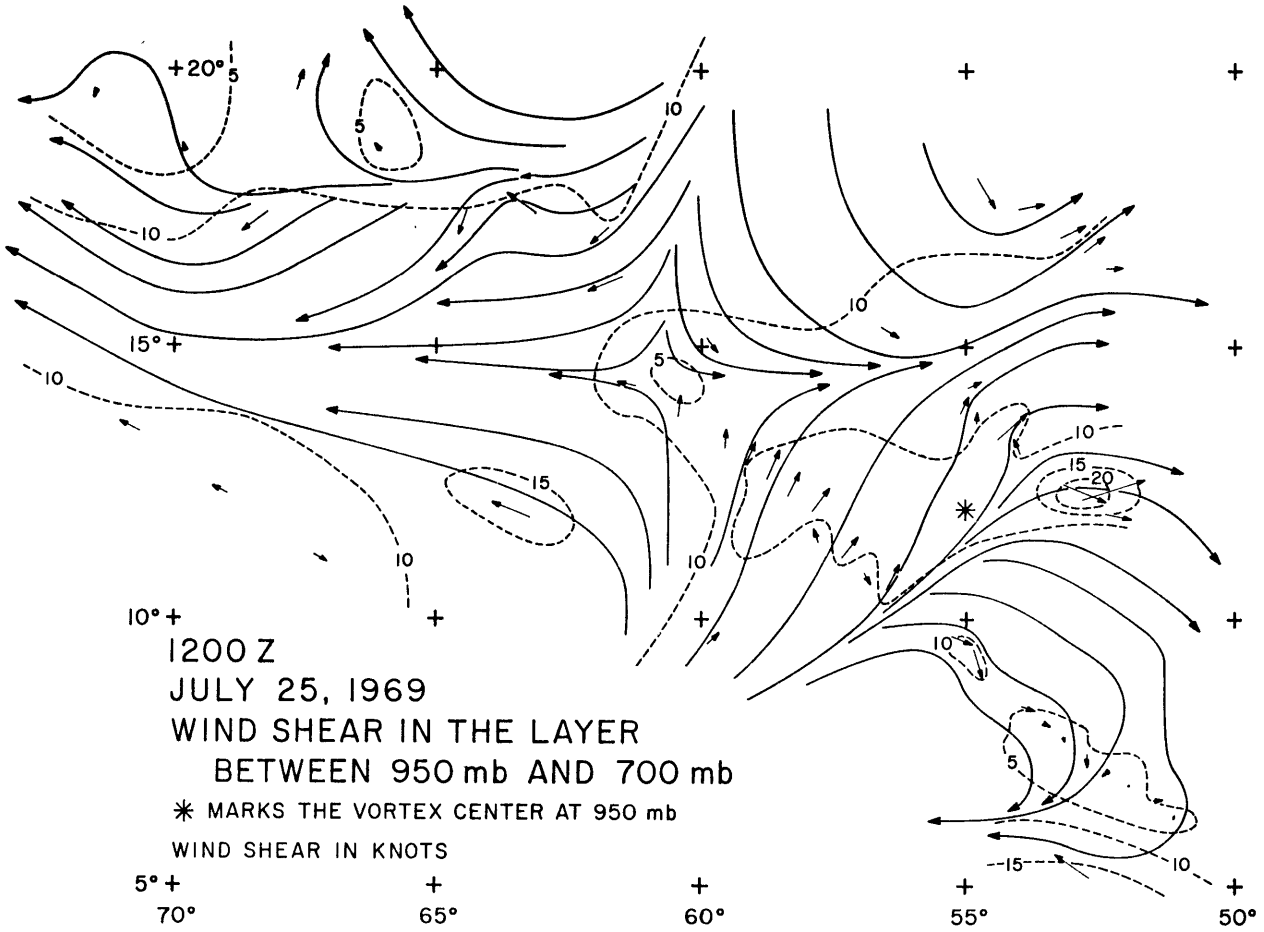
+20°
5
10
5
10
15°+
10
5
10
15
10
10
15
20
10°+
10
5
15
10
1200 Z
JULY 25, 1969
WIND SHEAR IN THE LAYER
BETWEEN 950 mb AND 700 mb
✳ MARKS THE VORTEX CENTER AT 950 mb
WIND SHEAR IN KNOTS
5°+
70°
65°
60°
55°
50°

Figure 33

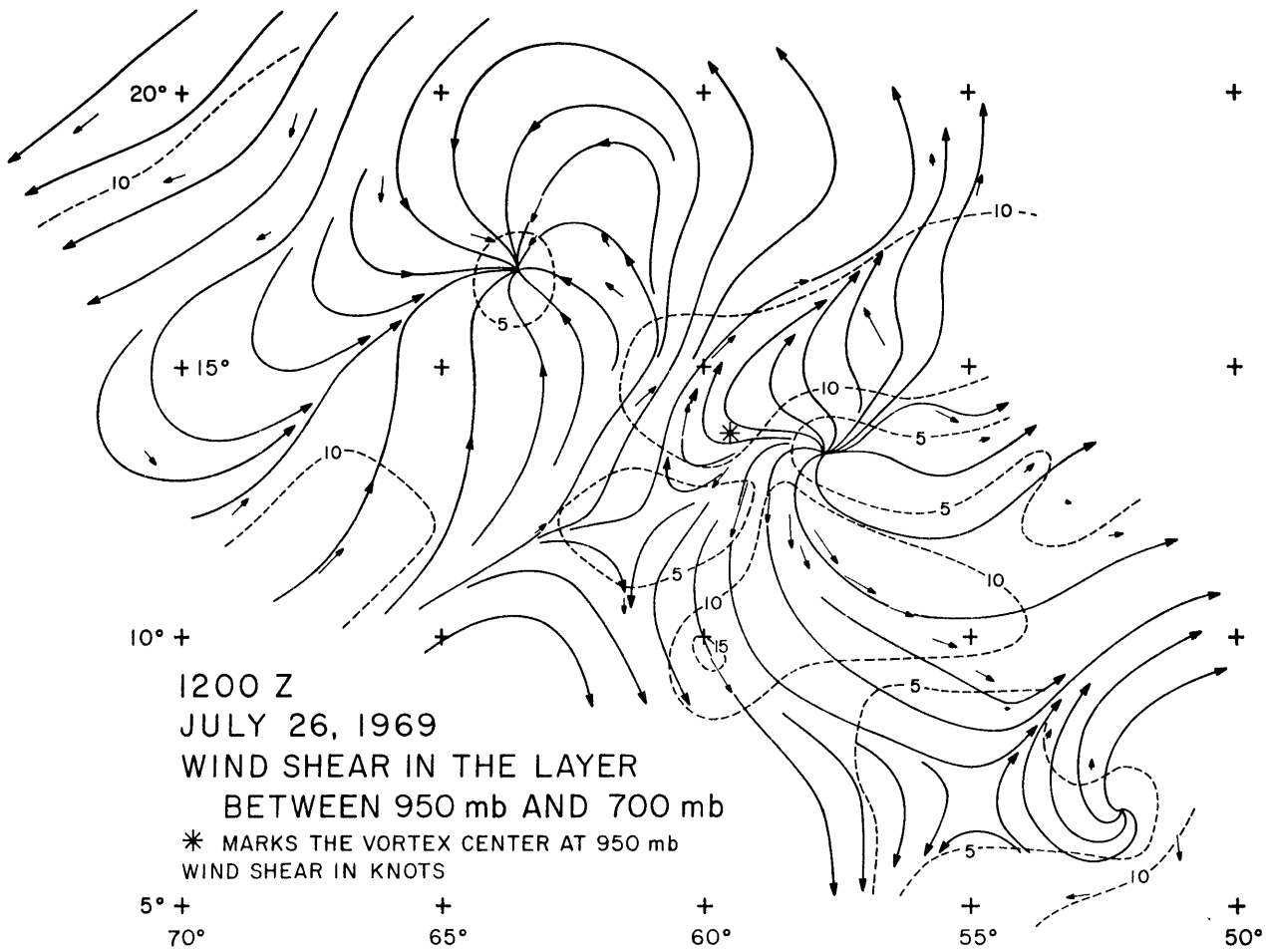
20° +
+ 15°
10° +
5° +
70°
65°
60°
55°
50°
10
5
15
1200 Z
JULY 26, 1969
WIND SHEAR IN THE LAYER
BETWEEN 950 mb AND 700 mb
✳ MARKS THE VORTEX CENTER AT 950 mb
WIND SHEAR IN KNOTS

Figure 34

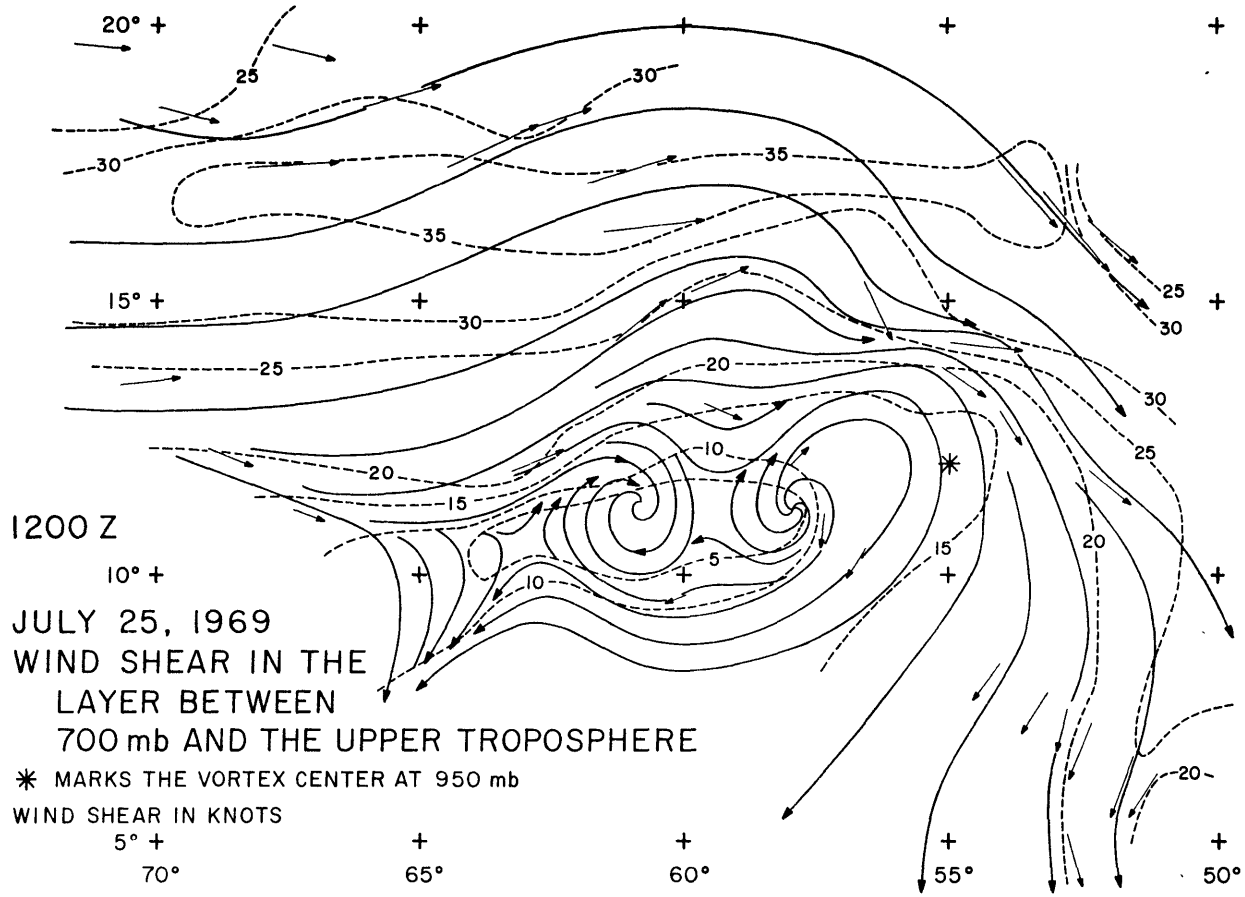
20° +
15° +
10° +
5° +
70°
65°
60°
55°
50°
25
30
35
20
15
10
5
1200 Z
JULY 25, 1969
WIND SHEAR IN THE
LAYER BETWEEN
700 mb AND THE UPPER TROPOSPHERE
✳ MARKS THE VORTEX CENTER AT 950 mb
WIND SHEAR IN KNOTS

Figure 35

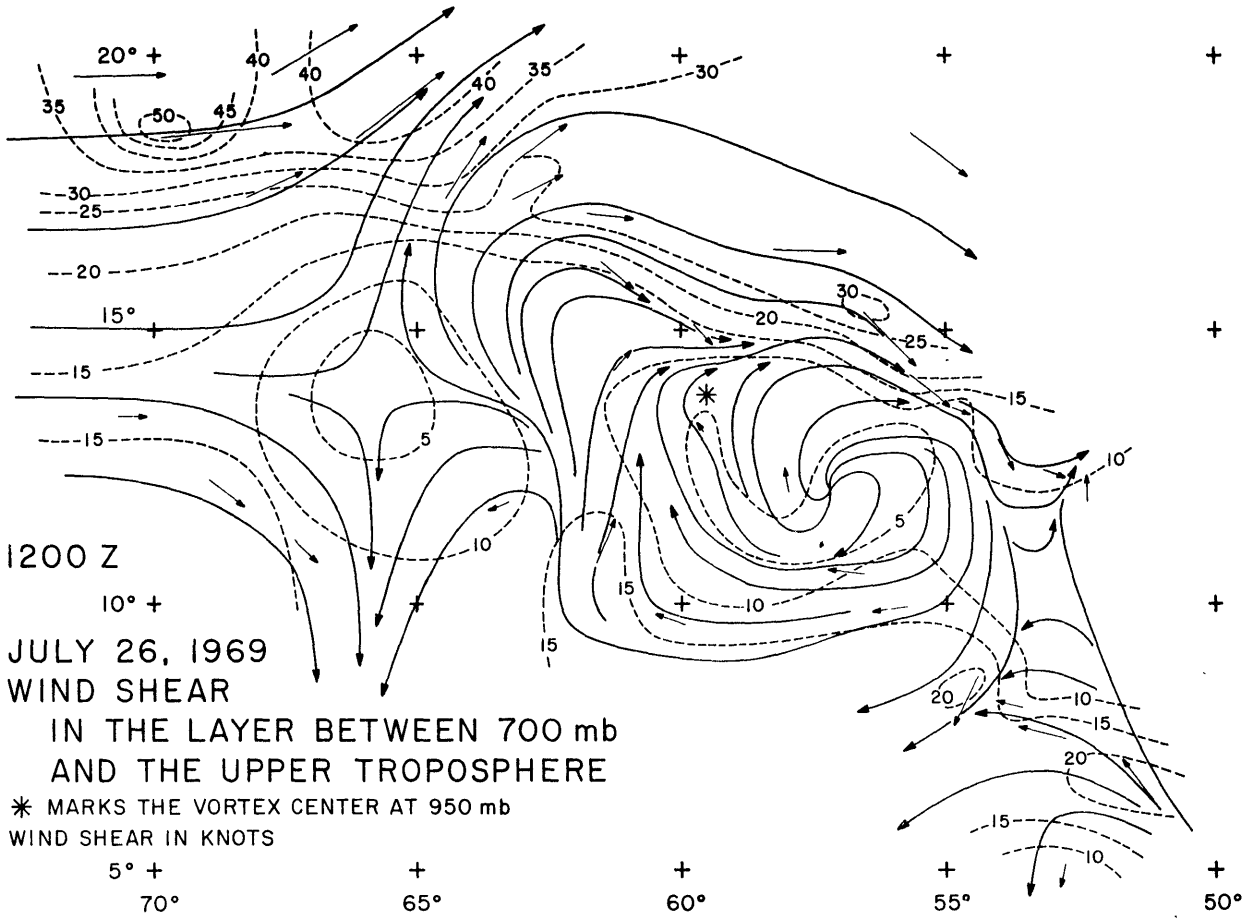
1200 Z
JULY 26, 1969
WIND SHEAR
IN THE LAYER BETWEEN 700 mb
AND THE UPPER TROPOSPHERE
✳ MARKS THE VORTEX CENTER AT 950 mb
WIND SHEAR IN KNOTS
20° +
15° +
10° +
5° +
70°
65°
60°
55°
50°

Figure 36

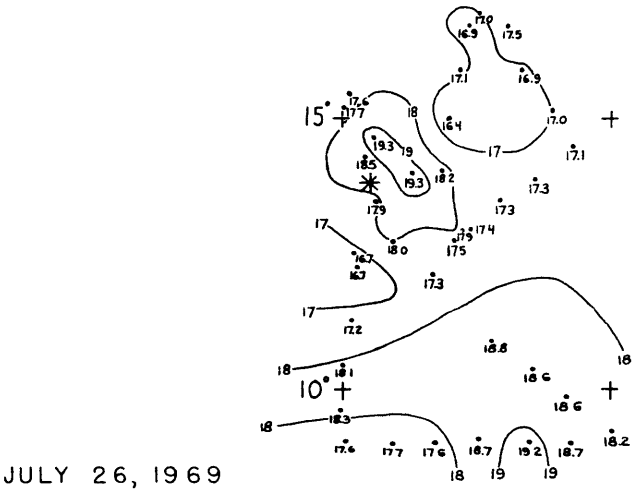
20°
15°
10°
5°
60°
55°
JULY 26, 1969
5000 FT TEMPERATURES (°C)
RFF "B" FLIGHT
* MARKS THE VORTEX CENTER AT 950 MB

Figure 37

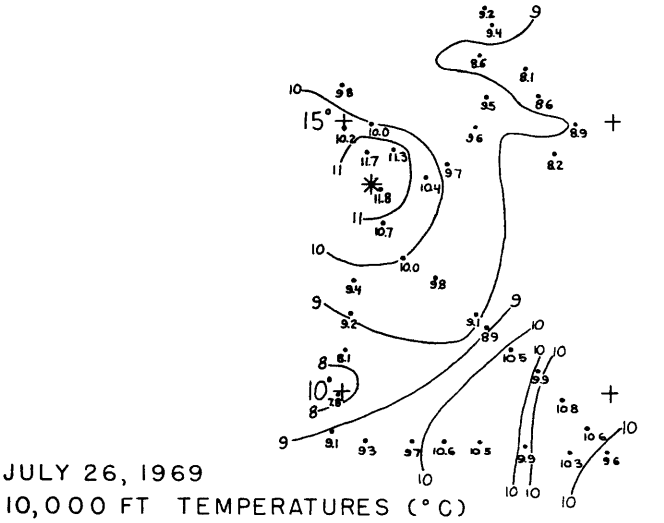

JULY 26, 1969
10,000 FT TEMPERATURES (°C)
RFF "E" FLIGHT
✳ MARKS THE VORTEX CENTER AT 950 MB

Figure 38

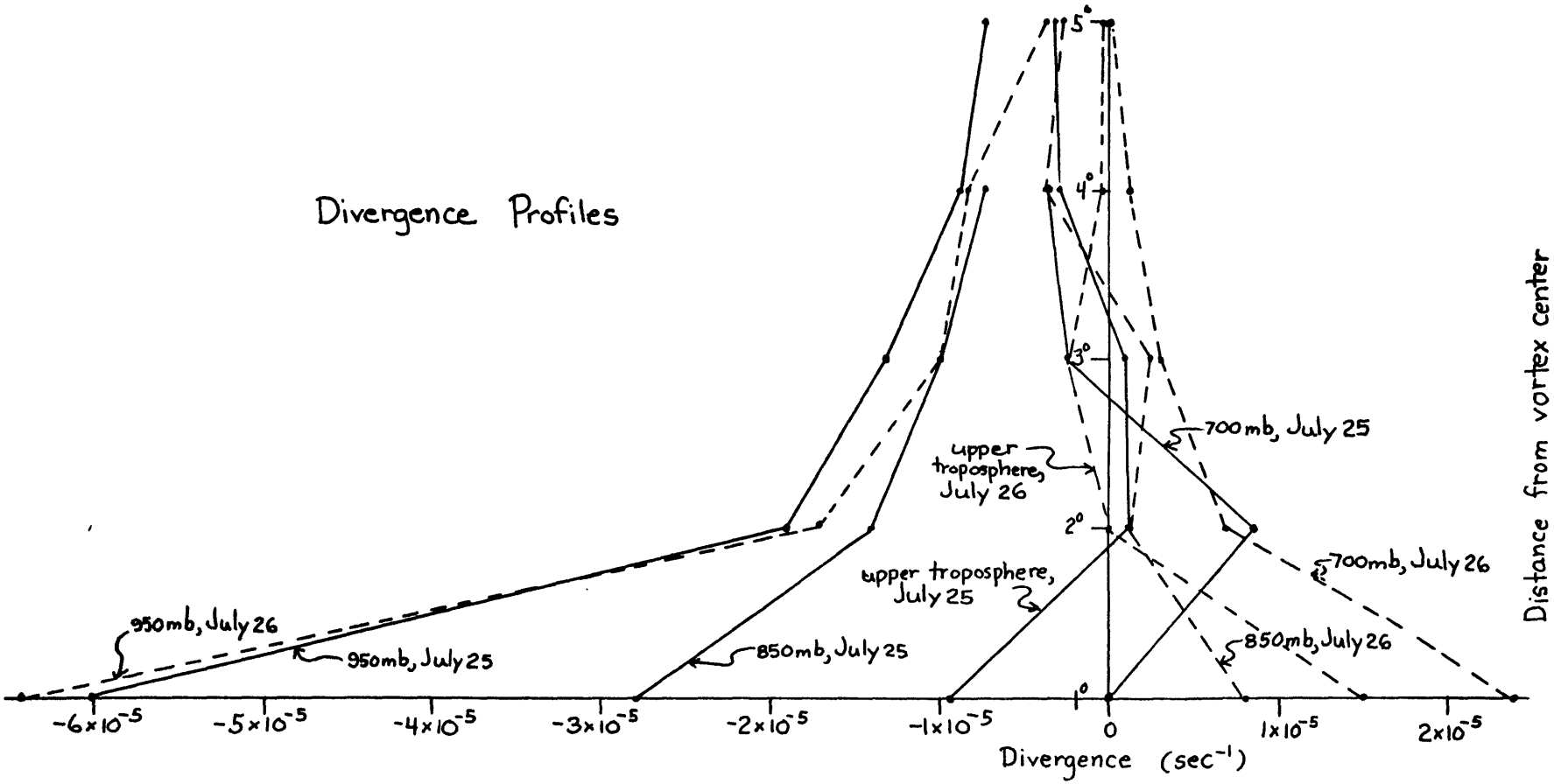
Divergence Profiles
5°
4°
3°
2°
1°
700mb, July 25
upper troposphere, July 26
700mb, July 26
upper troposphere, July 25
950mb, July 26
950mb, July 25
850mb, July 25
850mb, July 26
-6x10⁻⁵
-5x10⁻⁵
-4x10⁻⁵
-3x10⁻⁵
-2x10⁻⁵
-1x10⁻⁵
0
1x10⁻⁵
2x10⁻⁵
Divergence (sec⁻¹)
Distance from vortex center

Figure 39

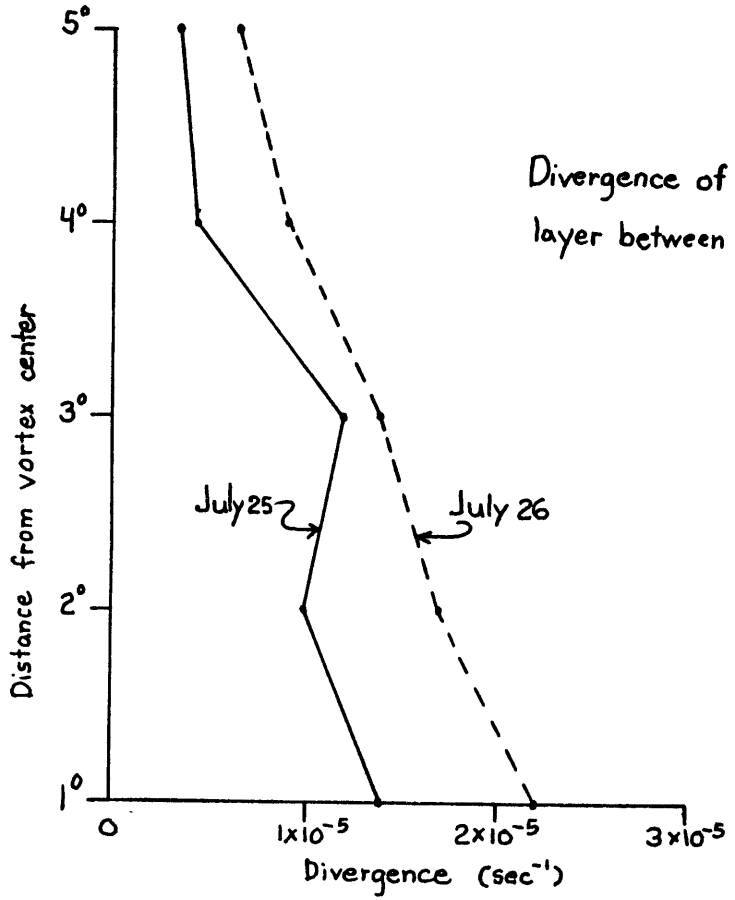
Divergence of the shear in the
layer between 950 mb and the upper troposphere
5°
4°
3°
2°
1°
Distance from vortex center
July 25
July 26
0
1x10⁻⁵
2x10⁻⁵
3x10⁻⁵
Divergence (sec⁻¹)

Figure 40

Vorticity Profiles

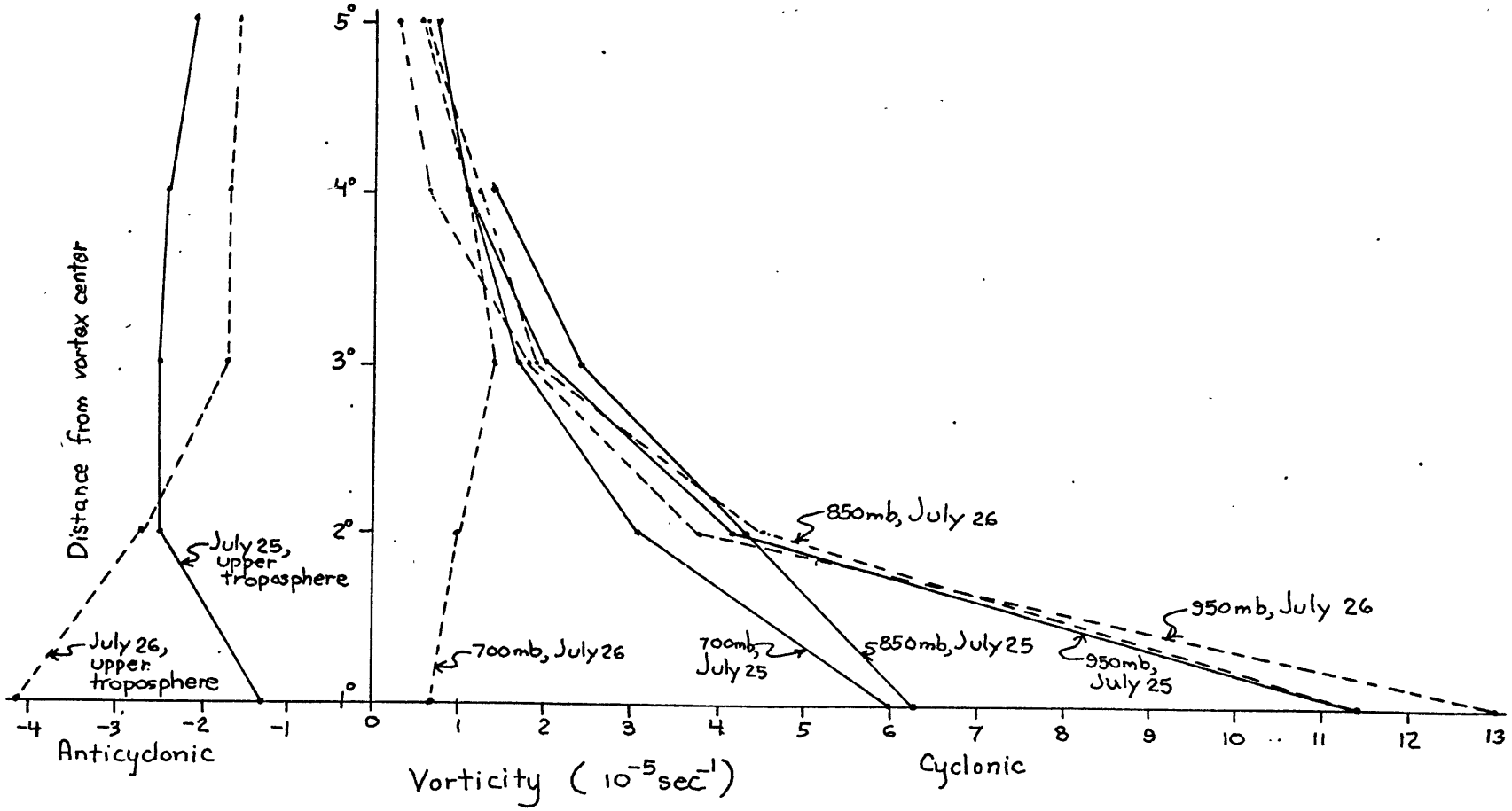

Figure 41

Vortex[1] Development Potential -- Decision Ladder

(Computations and factors apply to current through 24-hr. conditions)

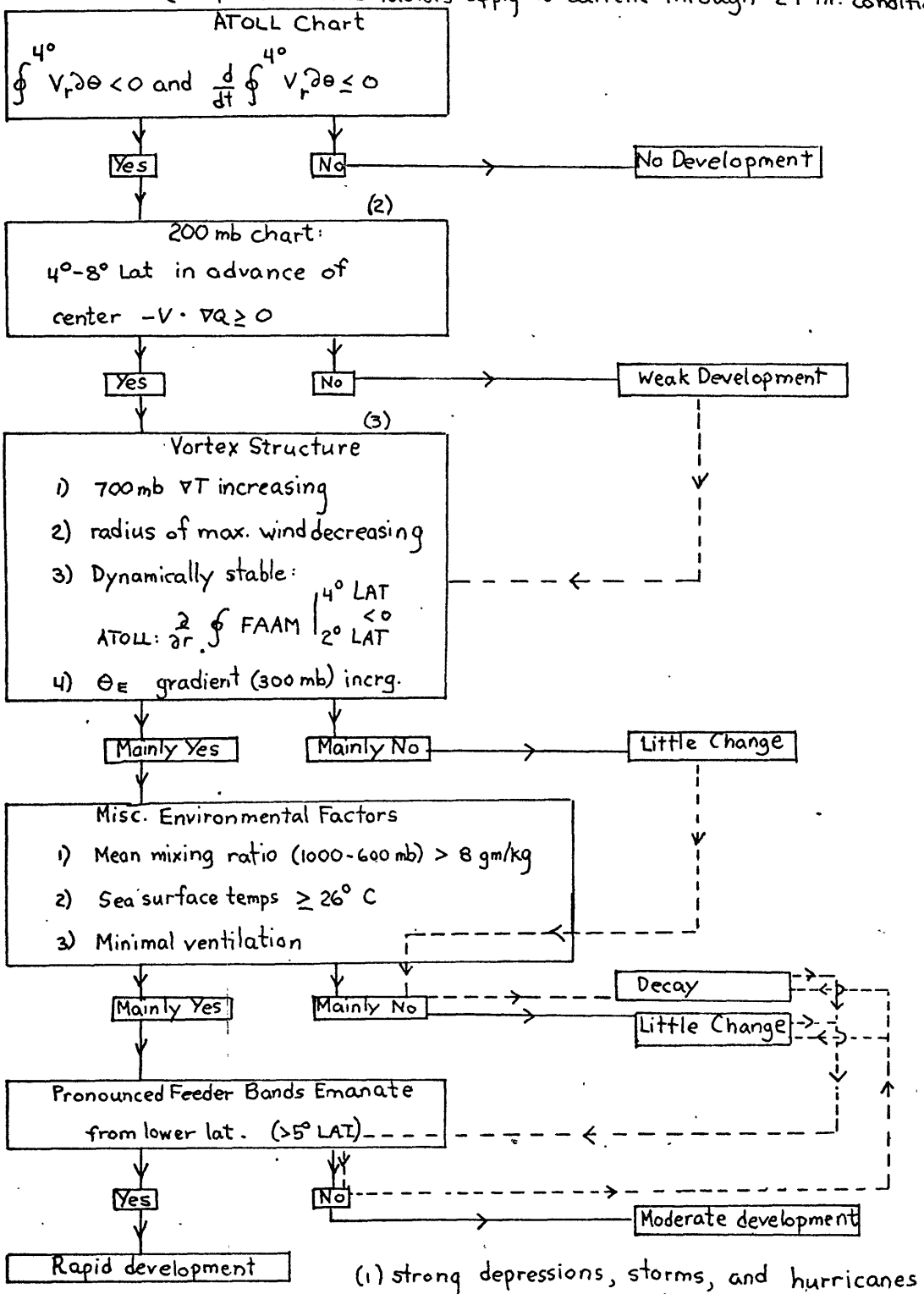

(1) strong depressions, storms, and hurricanes
(2) Q = absolute vorticity
(3) FAAM = Flux of absolute angular momentum

Figure 42

Seedling (1) Development Potential -- Decision Ladder

(Computations and factors apply to current through 24-hr. conditions)

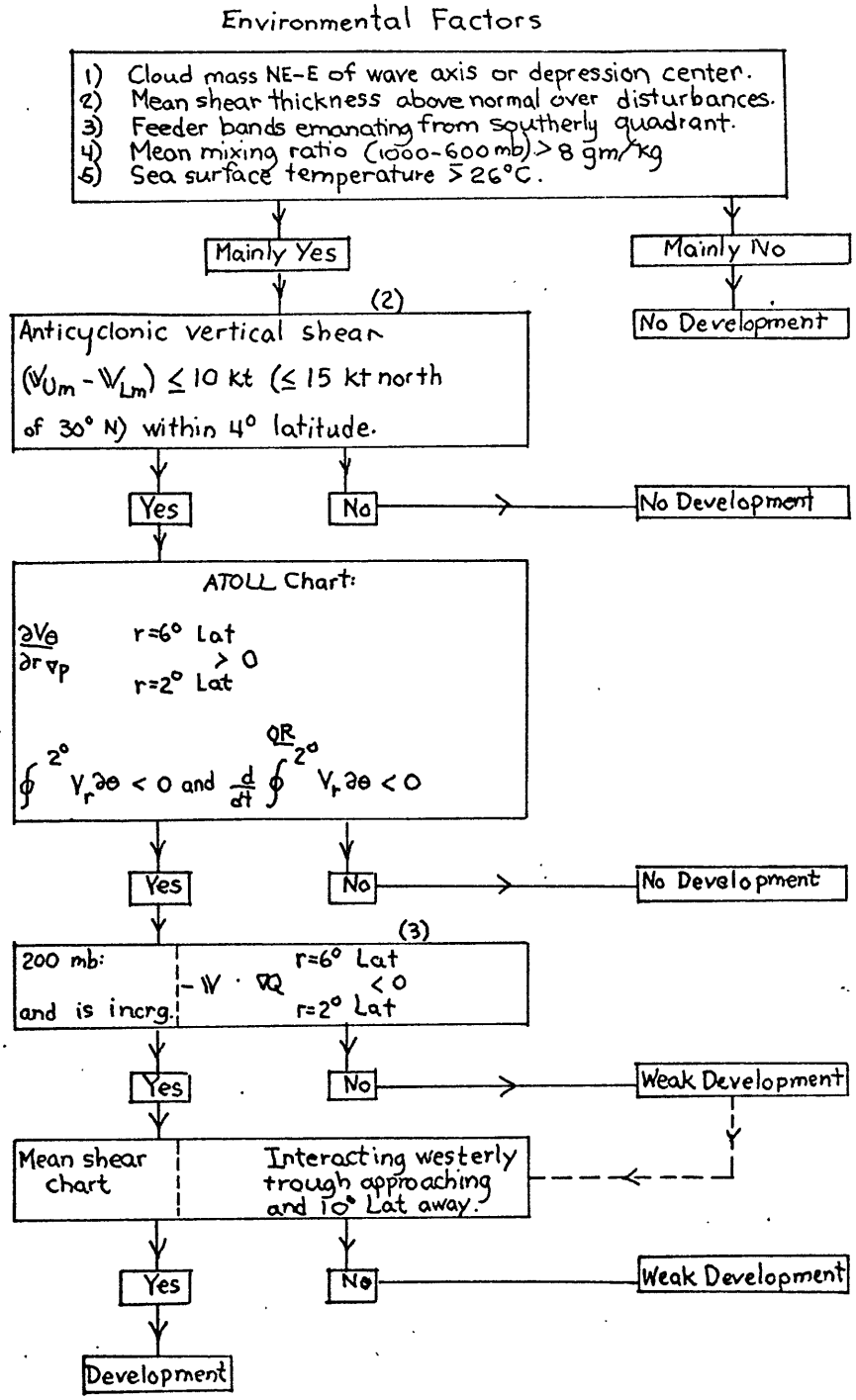

Figure 43

Acknowledgments

I thank Professor Frederick Sanders for suggesting the topic for this thesis, and providing guidance and support through its completion. I thank Rory Thompson for encouragement and helpful discussions. Ruth B. McDowell drafted figures 1 through 8, and 13 through 36.

References

Bunker, Andrew F., and Chaffee, Margaret A., "BOMEX Meteorological Data: Part I: Quantitative Cloud Measurements, Part II: Sea Surface Temperatures, Part III: Final Report," Reference No. 70-49, Technical Report, Grant GA-1700, Woods Hole Oceanographic Institution, Woods Hole, Massachusetts, Sept., 1970, 18 pp., (unpublished manuscript).

"Catalog of Meteorological Satellite Data - ESSA 9 Television Cloud Photography: July 1 - September 30, 1969," Key to Meteorological Records Documentation No. 5.323, National Oceanographic and Atmospheric Administration, Silver Springs, Md., 1971, 23 pp.

Cole, H., Griffee, L., Hill, D., Ledgerwood,J., and Marlatt, W.E., "Support Data for NASA Convair 990: Meteorological Flight V, July 2 - July 29, 1969," Projects NAS 5-11631, NAS 5-11666, Department of Atmospheric Science, Colorado State University, Fort Collins, Colorado, Dec., 1969, 135 pp.

de la Moriniere, Terry, "BOMEX Temporary Archive: Description of Available Data," NOAA Technical Report EDS 10, National Oceanic and Atmospheric Administration, Silver Springs, Md., Jan. 1972, 304 pp.

Frank, Neil L., "Atlantic Tropical Systems of 1969," Monthly Weather Review, Vol. 98, No. 4, Apr. 1970, pp. 307-314.

Friedman,H.A., Michie,J.D., and McFadden,J.D., "The NOAA Research Flight Facility's Airborne Data Collection Program in Support of the Barbados Oceanographic and Meteorological Experiment," NOAA Technical Report ERL 198-RFF 4, Research Flight Facility, Miami, Florida, Oct., 1970, 178 pp.

Gray, William M., "Global View of the Origin of Tropical Disturbances and Storms," Monthly Weather Review, Vol. 96, No. 10, Oct. 1968, pp. 669-700.

Iwanchuk, Robert, "A Study of Sea Surface Temperatures in BOMEX," unpublished term paper, Massachusetts Institute of Technology, 1972, 31 pp.

Janota, Paul, An Empirical Study of the Planetary Boundary Layer in the Vicinity of the Intertropical Convergence Zone, Ph.D. thesis, Massachusetts Institute of Technology, 1971, 279 pp.

Jordan, C.L., "Mean Soundings for the West Indies Area," Journal of Meteorology, Vol. 15, No. 1, Feb 1958, pp. 91-97.

Palmén, E., and Newton, C.W., Atmospheric Circulation Systems: Their Structure and Physical Interpretation, Academic Press, New York, 1969, 603 pp., (see p. 472).

Simpson, Robert H., 1972, (personal communication).